Deliverable D3.1
Applicability of Calorimetry to Real Waste Characterisation

Work Package

Work programme topic addressed: "Research and innovation on the overall management of radioactive waste other than geological disposal"
Supply Chain Security topic
Task3.1 Benchmark of calorimeters and standard NDA method for characterisation of large volume waste drums

EC Grant Agreement number: H2020-755371

Start date of project: June 1, 2017 Duration: 48 months
Lead beneficiary of this deliverable: CEA
Due date of deliverable: 30/04/2018

Project funded by the European Commission within the Horizon 2020 Program (2014-2020)		
Type		
R	Document, report excluding the periodic and final reports	X
DEM	Demonstrator, pilot, prototype, plan designs	
DEC	Websites, patents filling, press & media actions, videos, etc.	
OTHER	Software, technical diagram, etc.	
Dissemination level		
PU	PUBLIC, fully open, e.g. web	X
CO	CONFIDENTIAL, restricted under conditions set out in Model Grant Agreement	


V #	Date	Type of revision	Author
Draft	22/05/2018	Initial version	WP3
0.6	31/07/2018	Published version	WP3

Deliverable Contributors

Authors

Partner	Name
CEA DEN	Cédric Carasco
CEA DEN	Bertrand Perot
SCK•CEN	Bart Rogiers
WUT	Wojciech Kubinski
FZJ	Holger Tietze-Jaensch
KEP Nuclear	Andrea Francescon

Contributors

Partner	Name
KEP Nuclear	Asénath Etilé
KEP Nuclear	Christophe Mathonat

Internal Reviewers

Partner	Name
Andra	Stéphane Plumeri

Table of Contents

Table of Tables

Tables of Figures


1 Glossary

Abbreviation / Acronym	Description/meaning
ANCC	Active Neutron Coincidence Counting
ANI	Active Neutron Interrogation
CHANCE	Characterisation of conditioned nuclear waste for its Safe Disposal in Europe
ETM	Easy-To-Measure
HLW	High Level Waste
HPGe	High Purity Germanium
HRGS	High Resolution Gamma Spectrometry
ICP-MS	Inductively Coupled Plasma Mass Spectrometry
ILW	Intermediate Level Waste
KEPIC	KEP Innovation Center
LINAC	Linear Accelerator
LOD	Lower Detection Limit
LVC	Large Volume Calorimeter
MCNP	Monte Carlo N-Particle transport code
MDM	Minimum Detectable Masse
NDA	Non Destructive Assay
PGNAA	Prompt Gamma Neutron Activation Analysis
PNC	Active Neutron Counting
PNCC	Passive Neutron Coincidence Counting
PNMC	Passive Neutron Multiplicity Counting
RCA	Radio-Chemical Analysis
RN	Radionuclide
RW	Radioactive Waste
SF	Spontaneous Fission
SGS	Segmented Gamma Scanning
TGS	Tomographic Gamma Scanning

2 Executive Summary

2.1 Executive Factsheet

Who should read this deliverable? Who are the stakeholders concerned by this deliverable?	Why should s/he read this deliverable? What will s/he learn from this deliverable?	Which part of the content is most relevant for him / her?
CEA ; SCK•CEN, WP3 partners	This document will help selecting challenging waste characterisation scenarios by CEA and SCK•CEN for Task 3.2.	Section 5
CHANCE partners other than WP3.	This section is useful for partners who are not involved in WP3 to get a broad picture of mature non-destructive assay systems that are used for characterizing radioactive waste.	Section 4

Figure 1: Executive Factsheet

2.2 Executive Summary

In connection with Task 3.2 “Experimental investigation” consists in measuring plutonium and other possibly hidden RN in realistic cases with 200 L mockup waste drums at CEA Cadarache and a 200 L real unconditioned waste drum at SCK•CEN. This document presents and evaluates existing mature Non Destructive Assay (NDA) techniques that could be envisaged for characterizing the amount of plutonium and other safety relevant or declarable RN in 200 L radioactive waste drums.

Mature techniques using gamma ray and neutron measurements are first presented along with their advantages and limitations. Thereafter, calorimetry for radioactive waste assay will be presented along with its advantages and limitations.

The performances, ranges and heat deposition of gamma rays and neutron emitting radiation for the measurement of fissile material and other heat sources from possibly hidden/shielded RN in 200 L drums are evaluated by means of Monte Carlo simulations. The possibility of calorimetric detection of *e.g.* elsewise difficult-to-measure beta-emitting RN alongside significant gamma emitters in an attempts of this work package, which comprises important and yet unsatisfactorily solved scenarios for the non-destructive assay of large and possibly heterogeneous radwaste drums filled with various material embedded in concrete matrices and of various densities. Published data have also been compiled to evaluate and compare the performances of existing NDA systems.

The analyses provided in this document show that a 200 L drum filled with a concrete matrix or polyethylene reflects a real case for the characterisation of problematic waste, difficult to measure with both, High Resolution Gamma Spectrometry (HRGS) and Passive Neutron Coincidence Counting (PNCC), which are the common first choice two techniques being tested and evaluated during Task 3.2 and compared to calorimetric measurements.

Finally, first Monte Carlo simulations results of the future CHANCE calorimeter are presented.

3 Introduction

Ideally, non-destructive assay (NDA) of radioactive waste should be able to provide information concerning the type, amount and distribution of radionuclides, as well as information concerning physical and chemical state of the waste. A vast amount of literature on the characterisation of nuclear inventories already exists, and also many studies compare NDA techniques for radioactive waste characterisation, such as (Houriet), (Hsue, et al., 1997), (Dufour, et al.), (Funk, et al.), (IAEA, 2007). In the context of CHANCE WP3, the ESARDA report (Rackham, et al., 2012) is particularly relevant since it performs a quantitative comparison of the techniques in term of Minimum Detectable Mass (MDM). The present report focuses on mature NDA solutions that are already routinely used in the nuclear industry and in the laboratory practice. Nowadays, these techniques matured indeed from the experimental and developing phase managed in research laboratories and are widely standardized, certified and appropriated by commercial companies. Therefore, techniques that are still subject to active research will not be presented in this report. Examples are photo-fission (Gmar, et al., 2006), Prompt Gamma Neutron Activation Analysis (PGNAA) (Mauerhofer, et al., 2014), delayed gamma ray from neutron-induced fission (Nicol, et al., 2016), delayed gamma ray from photon-induced fission (Simon, et al., 2016) or the Associated Particle Technique (APT) (Kanawati, et al., 2013).

Most commonly used NDA is based on the measurement analysis of spontaneous or induced gamma or neutron radiation emitted by the radioactive waste. Also, a calorimetric measurement of the specific heat generated from radioactive decay can be utilized, mainly to characterize alpha and some beta emission in the radioactive waste. For high level waste, however, the sensitivity of calorimetry to gamma radiation has to be evaluated.

The first part of this report gives an overview of the main characteristics concerning mature NDA systems. The second part evaluates the techniques that are relevant for CHANCE WP3 (alpha bearing waste measurement), in the frame of Task 3.1 “Benchmark of calorimeters and standard NDA method for characterisation of large volume waste drums”. The evaluation is performed through a study of the neutron and gamma ray signals that can escape various 200 L waste drum matrices with different source configurations, and through a comparison with the published plutonium and uranium Minimum Detectable Masses (MDM) of existing systems.

4 Overview of NDA Techniques

4.1 Gamma methods

The most basic and fastest gamma NDA method consists in measuring the gamma dose rate of a waste package. The interpretation of a dose measurement for NDA requires however a very good knowledge of the nuclide vector associated to the waste, as well as its physical properties. Therefore, dose rate measurement provides poor information (concerning NDA). Similarly, gross gamma counting can be employed, but it is also a poorly informative NDA approach. The reference NDA approaches using gamma ray detection therefore employ detectors enabling gamma spectrometry.

4.1.1 Gamma spectrometry

High Resolution Gamma Spectrometry (HRGS) measurement using High Purity Germanium (HPGe), LaBr:Ce scintillation detectors or CdZnTe detectors allows identifying gamma rays associated to the waste drum's main gamma emitters. To a lesser extent, gamma detectors with a lower energy resolution such as NaI(Tl) can be employed to perform Low Resolution Gamma Spectrometry (LRGS), provided the isotopic composition of the waste is known, since gamma rays with close energy cannot be distinguished by this mean.

This approach is routinely used in every nuclear facility but its applicability to waste drums with high gamma ray activity requires screens or collimators to avoid detector or electronics saturation. In addition, for small gamma peaks, the subtraction of the Compton continuum background significantly contributes to statistical uncertainty, and therefore a high gamma activity (e.g. from ^{137}Cs or ^{60}Co) may deter the detection of secondary gamma emissions. Because gamma rays can be attenuated by waste package materials, a quantitative determination of the nuclide activity may require physical information about the waste matrix to correct for gamma ray attenuation (Pearman, 2012) (Myers, et al.). If limited information from the waste producer is available, the waste matrix can be characterized by gamma transmission or photon imaging. When the matrix size is too large or the density too high, as for instance with concrete packages, high energy and intense X rays beams produced by an electron LINAC (linear accelerator) can be employed (Estre, et al., 2015).

4.1.2 Segmented Gamma Scanning

Since gamma emitting radioisotopes are usually not distributed homogeneously within the waste package, HRGS measurement of the whole drum, performed from a single position, cannot provide accurate information concerning the radioisotopes located in the waste package. To be less sensitive to heterogeneous source distributions, one can perform Segmented Gamma Scanning (SGS) which consists in measuring thin slices of the drum at a time. This kind of measurement is usually achieved by translating and rotating the drum vertically in front of a collimated detector in order to scan only thin vertical drum segments, but other type of scans such as spiral scans are also possible (Bücherl, et al., 1998).

SGS systems are commercially available such as ANTECH Model G3200 (ANTECH) and CANBERRA's Standard Segmented Gamma Scanner (SGS) (CANBERRA).

4.1.3 Tomographic Gamma Scanning

An improvement of SGS, Tomographic Gamma Scanning (TGS), consists in performing both gamma ray emission and transmission measurements to obtain a radionuclide distribution inside the waste, taking gamma ray attenuation into account.
As shown in (Venkataraman, et al., 2007), TGS can be employed for performing NDA of 208 L radioactive waste with matrix densities up to 1 $g.cm^{-3}$ (Venkataraman, et al., 2007). However, as for HRGS and SGS, the use of TGS is limited when the gamma background is important. For instance in (Venkataraman, et al., 2007), the dose rate at contact is limited to 6 $mSv.h^{-1}$. If we assume that the nuclides are located in the middle of a 200 L concrete drum with 30 cm radius, 1332 keV and 662 keV gamma rays would be attenuated by respectively a factor 60 and 300. The 6 $mSv.h^{-1}$ dose rate would then correspond to 105 GBq of ^{60}Co or 213 GBq of ^{137}Cs. Although the dynamic range can be extended to 3 $g.cm^{-3}$ and 100 $mSv.h^{-1}$ (Venkataraman, et al., 2007), TGS and SGS might be difficult to use for inspecting high activity waste containing TBq of ^{60}Cs or ^{137}Cs which form for example a significant part of the French radioactive waste stream (ANDRA, 2017).
TGS systems are commercially available such as the WM2900 TGS developed by Canberra Industries [14] and ANTECH G3850 TGS (ANTECH).

4.1.4 Photon radiography/tomography

Radiographic devices are commonly used for imaging radioactive waste drums, in the form of mobile measurement systems (Vigil, et al.) or for in-situ operations (Estre, et al., 2015) (DOE). Providing a picture relatively simple to read by the operator, radiography can serve to identify non-conformities such as insufficient container wall thickness and the presence of void spaces or liquids (Steude, et al., 1993). Up to now, radiographic systems do not allow identifying the nature of the materials inside the waste drum, but research involving multiple energy photon beams is currently performed to enable mapping the atomic number of radiographed objects (Bonnin, et al., 2014) (Saverskiy, et al., 2015).
Most commercially available scanners based on an X-ray tube or an isotopic gamma source are however not suitable for scanning dense and thick objects, such as concrete packages. To cope with the variety of radioactive waste types, the use of a dedicated high energy Linear Accelerator (LINAC) providing high intensity photon beams is compulsory. Up to now, the use of a LINAC is however limited to few facilities like CINPHONIE in CEA Cadarache (Estre, et al., 2015).

4.2 Neutron methods

Neutron measurement can be performed in passive or active mode. It is often used in complement with, or sometimes to overcome gamma spectrometry when the detection of Pu gamma rays is impossible due to a high gamma activity of other emitters like ^{137}Cs and ^{60}Co. Passive neutron measurement mostly provides information concerning ^{240}Pu (and ^{244}Cm if present) content, whereas Active Neutron Interrogation (ANI) provides information concerning fissile isotopes ^{235}U and ^{239}Pu. The second is therefore the only possible technique to assess the fissile mass in case of gamma irradiating waste contaminated with curium. Both techniques implemented with ^{3}He detectors are fairly insensitive to the waste's gamma ray emission and therefore can be used with high activity wastes, potentially using gamma shielding like lead, which does not decrease significantly the neutron detection efficiency of the system (Carasco, et al., 2016).

Both techniques are however sensitive to the presence of neutron moderator materials (especially passive neutron counting) and absorbing elements (especially ANI) in the waste, thus requiring some additional knowledge concerning the waste matrix in order to apply the appropriate corrections. These corrections can be partially determined coupling the neutron measurement with a photon imaging system (Villani, et al., 2008) and a Prompt Gamma Neutron Activation Analysis system (Jallu, et al., 2008), at the expense of a more complex and expensive system. Some neutron transmission techniques and flux monitors (Newell, et al.) can also be used to monitor the characteristics of the matrix.

4.2.1 Passive neutron Coincidence Counting

Passive Total Neutron Counting (PTNC), consisting in counting all neutrons emitted by the drum, is of limited use since it requires additional information to separate the count rate contributions of Spontaneous Fissions (SF) and (α,n) reactions. In the presence of α emitters, Passive Neutron Coincidence Counting (PNCC), which consists in measuring the rate of coincident neutron pairs (doublets) (Reilly, et al., 1991), is therefore required to estimate a drum's plutonium content. By measuring coincidences with higher multiplicity level, Passive Neutron Multiplicity Counting (PNMC) allows to recover the measurement of the neutron detection efficiency, the α neutron emission rate and the fission multiplication factor provided some hypothesis are fulfilled (Reilly, et al., 1991) but, being a more complex measurement, PNMC is less employed than PNCC and requires long measurement times to obtain sufficient triplet counting statistics. For this reason, PNMC is generally restricted to safeguards applications.

The accuracy of passive neutron counting is limited by the neutron count rate associated to (α,n) reactions which, in extreme cases, increases significantly the random coincidence rate and thus the statistical precision of the measurement. On the other hand, given the much higher fission rate of the even isotopes of curium, see Figure 2, the presence of even small amounts of curium makes the interpretation of the coincidence rate measurement in terms of effective ^{240}Pu mass difficult.

PNCC systems able to measure 200 L drums are commercially available, such as the JCC21 system proposed by Mirion Technology (previously Canberra) (Davidson, et al.) or the ANTECH Model 4100-440 Passive Neutron Drum monitor (Tolchard, et al., 2003). Several research institutes have also designed their own PNCC allowing effective ^{240}Pu detection limits between 1 mg to 100 mg (Bücherl, et al., 2001).

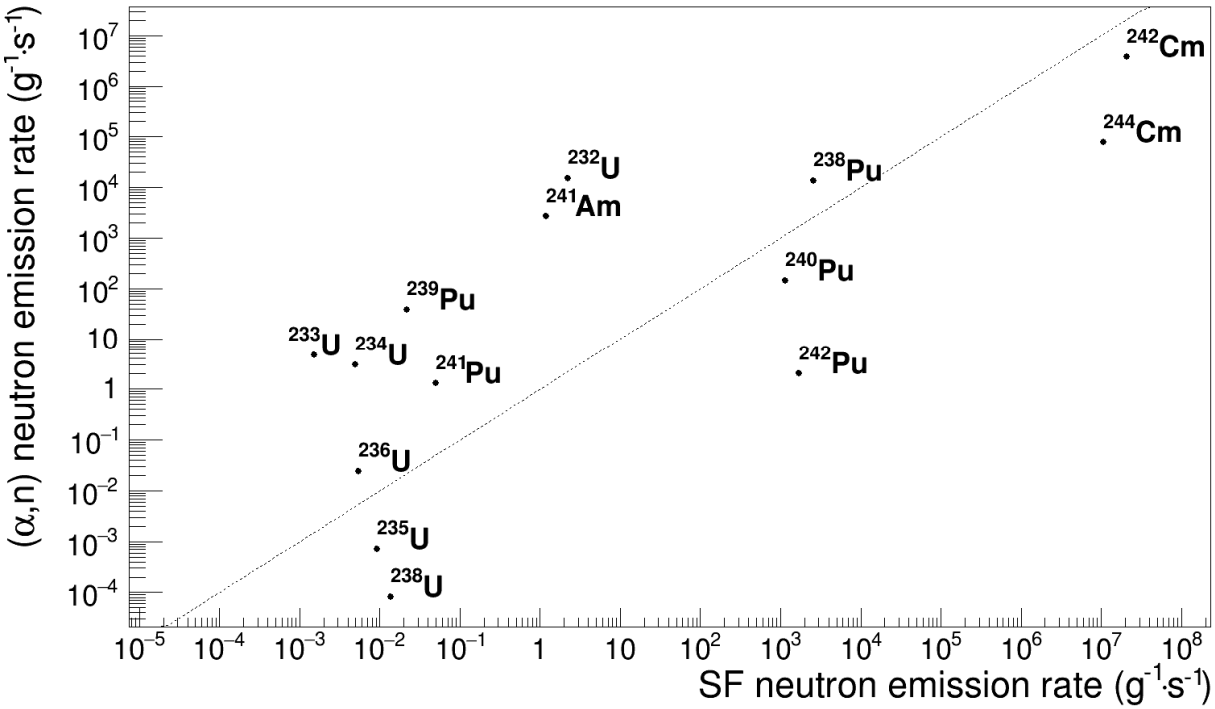

Figure 2: (α,n) neutron emission rate for oxides versus spontaneous fission neutrons emission rate for isotopes of interest concerning radioactive waste characterisation. The dotted line represents the identity function "y=x" and allows separating isotopes which are emitting more (α,n) neutrons than spontaneous fission.

4.2.2 Active neutron interrogation

Active Neutron Interrogation (ANI) allows determining directly the amount of fissile material such as ^{239}Pu and ^{235}U, which can only be determined indirectly by PNCC because of their small SF emission rate. ANI usually consists in interrogating the waste with neutrons produced by a pulsed neutron generator, following the Differential Die-Away (DDA) method (Jordan, et al., 2007). When performing DDA, interrogating neutrons are thermalized in the measurement cell (graphite and/or polyethylene walls), induce fissions in the fissile nuclides, fast fission prompt neutrons from thermal neutron induced fissions being detected between the generator neutron pulses. The signal due to the thermal interrogating neutrons is cut by cadmium sheets surrounding the neutron detectors.

Being a very sensitive method, with detection limits reaching a few mg of fissile material in dense matrices that would strongly cut the gamma ray signal, ANI is however not adapted for measuring matrices containing thermal neutron absorbing elements such as cadmium or boron, as well as hydrogen-rich materials like concrete. Hydrogen has a smaller absorption cross section than the former, but is present with a high concentration in concrete.

ANI has been developed by research institutes (Passard, et al., 2001), (Favalli, et al., 2009) and is used in specific facilities such as the spent fuel reprocessing plant at AREVA NC/La Hague to measure high level metallic residues (hulls and nozzles after spent fuel dissolution) (Eleon, et al., 2014). Commercially available systems such as the Canberra (Mirion Technology) Integrated Waste Assay System (IWAS) (Mirion Technology) which combines multiple assay techniques and the ANTECH Active Totals Counting Differential Die-away Model 4100-440 (Mason, et al., 2003) allow for ANI on 200 L drums.

4.3 Calorimetry for nuclear assay

Calorimetry is an experimental technique employed for the measurement of the thermal power generated by heat-producing substances (Mason, 1982). Calorimetry is exploited in a variety of fields including scientific research, medicine, industry, military research and biology.

Calorimetry has been successfully applied to the characterisation of nuclear materials that generates heat by alpha and beta particle decay in the range of thermal powers spanning from 1 mW to 135 W. It is mainly used for the assay of Plutonium and ^{241}Am (either as a single isotope or mixed with Plutonium). According to (ASTM, 2016), the typical range of applicability for plutonium, corresponds to ~0.1 g to ~5 g depending on the isotopic composition. Calorimetry measurement was also successfully employed in the assessment of the amount of tritium in radioactive waste packages. Tritium assay has always been challenging as neither a destructive analysis on the waste nor a sampling of radioactive matter inside the package (strongly dependent on the physical state of tritium) can be envisaged (Galliez, et al., 2016). In addition, direct nuclear counting is also not viable because of the low energy of beta particles of tritium, which can be stopped by few microns of metal. Whereas calorimetry measures the heat produced by the interaction of beta particles with the matter, and the ^{3}H mass of the sample can be inferred by knowing the specific power of tritium (324 mW/g). The typical range of applicability of calorimetry measurement in the assay of tritium extends from ~1 mg to ~400 g.

The measurement of the heat generated by a nuclear sample through calorimetry combined with a measurement of the nuclear isotopic mass ratios of the samples by another Non Destructive Assay (NDA) technique (e.g. High Resolution Gamma Spectrometry) provides a convenient and accurate measure of the total radioactive mass of the sample. Presently, calorimetry represents the most accurate and precise NDA measurement of the mass of nuclear materials, if the isotopic vector is known, thus it has generated a great interest for what concern the characterisation of radioactive nuclear wastes and for safeguards purposes.

Calorimetry measurement technology is characterised by the following advantages compared to other NDA techniques (Bracken, et al., 2002):

- Very high precision, ranging from ~0.5% for low power items (≤0.2 W) to ~0.1% for items dissipating more than 1 W. If the isotopic composition of the item can be accurately determined with another NDA technique, the precision of the calorimetric measurement is comparable to chemical analysis, making calorimetry the most precise NDA technique for nuclear materials.
- The calorimetric analysis involves the entire mass, so that the result is not the extrapolation from a limited specimen. Thanks to this, the result is independent of nuclear material distribution within the sample. This feature is very important when the distribution of the sample is not known in advance and it cannot be extrapolated. Note that gamma or neutron radiation, dependent on the energy and matrix composition, might escape from the drum and even the calorimeter. Such losses of energy should be checked for and, if necessary, corrected for.
- It is not possible to shield the power generation. Once a steady state condition is reached, the whole power generated by the item under test is completely evacuated by the measurement chamber, regardless of the packaging of the item.
- Calorimetry, on the one hand, measures the summated heat deposition of all radioactive nuclides present. In that sense, none of the radioactive material can be missed, except for small amounts below the (sensitive) lower detection limit. On the other hand, calorimetry is not viable to discriminate various RN, unless prior knowledge from other means can be utilized.

- The measurement result is independent from material matrix composition and geometry (only assay time is affected). Thanks to this, it is not necessary to characterize the matrix in order to measure the radioactive sample.
- Without phase changes and chemical reactions, answer is bias free and not affected by self-attenuation effects. The evaluation of chemical reaction bias will be evaluated later on during the project.
- The calibration of the instrument is standardized and can be verified when necessary.

On the other side, the calorimetric method is affected by the following limitations:

- The measurement accuracy can be degraded in case of materials with inhomogeneous isotopic composition, because of the uncertainty in the determination of the effective specific power. In general, the accuracy of the calorimetric measurement is related to the ability to determine the isotopic composition of the sample.
- The calorimetric assay features longer measurement time compared to other NDA techniques. Typical measurement times are in the order of several hours but can increase up to several days for large samples with very low thermal power rates. Attention must be paid to the fact that even if the packaging of the source does not affect the measurement accuracy, it can still affect the measurement time.
- It usually requires very large equipment for accurate measurement results. Because of the relatively low power rates of nuclear samples and the large volume under test, usually the overall dimensions of standard equipment can be important an possibly limiting.
- If heat is produced by reactions others than nuclear, this cannot be discriminated by the calorimeter and this can bias the measurements.

In this section calorimetry was briefly presented, especially how it can contribute to dedicated issues of nuclear waste characterisation regarding its advantages and limitations. A complete document written by Andrea Francescon presents the state of the art of calorimetry Annex 2. The author carried out an overview of the existing calorimeters; the main designs of calorimeters and specific parts of the calorimetric system (essential to precise heat-flow measurements) are detailed with their advantages and drawbacks.

4.3.1 Application of calorimetry experiments

Calorimetry is not likely as stand-alone NDA. It rather supplements gamma and neutron spectrometry (mainly PTNC, ANI and PNCC, cf. Chapter 4.2), especially for declarable radionuclides (RN) with no or only too weak gamma signals to be detected. Calorimetry is sensitive to all RN inside a waste drum, as all radiation emitted turns into heat, eventually (*i.e.* some radiation might also escape the drum and calorimeter). However, its stronghold is also its weakness as calorimetry detects all heat sources, exceeding its lower detection limit (LOD), of course, but does this without discriminating RN or isotope or location in the drum. Yet, another stronghold is its capability of measuring large volume compounds and, if need be, of heterogeneous content.

As the CHANCE project is focused on conditioned waste only, some pre-knowledge of the waste composition and history may well be assumed, *f.i.* non-radioactive heat sources or sinks are generally negligible, and the results of preceding gamma and possibly neutron assay are known.

If representative sampling is possible and viable then, of course, the whole experimental toolset of a full-range radio-chemical analysis (RCA) can be applied (Figure 3). In many cases of nuclear waste management, however, sampling and RCA is not (at first) possible.

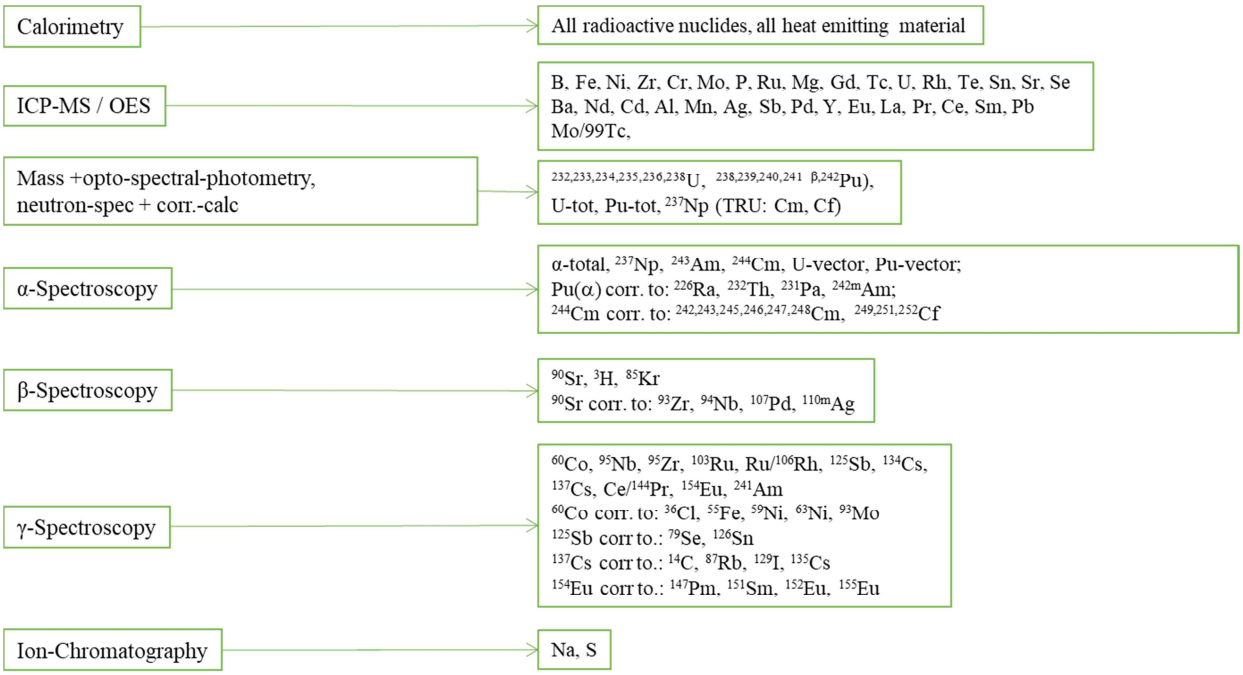

Figure 3: RCA methods for the determination of radionuclides and elements (activities or masses per volume or waste compound); neutron-spectrometry comprises mainly PTNC and AN or PNCC

So, essentially the experimental task of calorimetric NDA is either to establish or rule out the additional existence of RN that are not detectable by either gamma or neutron spectrometry. Thus the task is determining the upper limit for the activity or mass of assumed beta- or alpha radiation heat source or the possibility of hidden/shielded gamma or neutron source, such as a shielded ^{60}Co or ^{99}Mo/^{99}Tc or even a ^{252}Cf source that are used for medical purposes or as a reactor ignition source.

The ultimate objective for the characterisation of RN is to meet the declaration requirements for the final disposal of the radioactive waste (RW) compound, which varies from country to country and differs for different repositories, too. However, there is a general tendency of the authorities to request more and more RN and chemo-toxic content and matrix material to be characterized and declared, despite the fact that metrological assay provides easy-to-measure (ETM) results for a hand-full of RN, only. The remaining RN are usually correlated to ETM-key-nuclides (^{60}Co, ^{125}Sb, ^{134}Cs, ^{137}Cs, ^{154}Eu), and the uncertainties, detection limits and maximum missed activities are thus correlated, too. Table 1 comprises the RN that are to be declared for medium-active compacted and vitrified waste compounds to be disposed of in Germany. Whereas for high-level vitrified waste containers this RN-list required for Germany is older and contains significantly less declarable RN, though the same crucial key nuclides are determined (^{60} Co, ^{125}Sb, ^{134}Cs, ^{137}Cs, ^{154}Eu, ^{235}U, ^{238}U, ^{239}Pu, ^{241}Pu, ^{244}Cm, ^{237}Np, ^{241}Am, ^{243}Am). All others are derived from numerical correlations which are verified by the process performance and qualification.

	Radionuclide
Declarable RN	^{3}H, ^{14}C, ^{36}Cl, ^{41}Ca, ^{54}Mn, ^{55}Fe, ^{59}Ni, ^{63}Ni, ^{58}Co, ^{60}Co, ^{79}Se, ^{85}Kr, ^{90}Sr/^{90}Y, ^{93}Zr, ^{95}Zr, ^{94}Nb, ^{93}Mo, ^{99}Tc, ^{103}Ru, ^{106}Ru/^{106}Rh, ^{107}Pd, ^{110m}Ag, ^{125}Sb, ^{126}Sn, ^{129}I, ^{134}Cs, ^{135}Cs, ^{137}Cs, ^{144}Ce/^{144}Pr, ^{147}Pm, ^{151}Sm, ^{152}Eu, ^{154}Eu, ^{155}Eu, ^{226}Ra, ^{232}Th, ^{231}Pa, ^{232}U, ^{233}U, ^{234}U, ^{235}U, ^{236}U, ^{238}U, ^{237}Np, ^{238}Pu, ^{239}Pu, ^{240}Pu, ^{241}Pu, ^{242}Pu, ^{241}Am, ^{242m}Am, ^{243}Am, ^{242}Cm, ^{243}Cm, ^{244}Cm, ^{245}Cm, ^{246}Cm, ^{247}Cm, ^{248}Cm, ^{249}Cf, ^{251}Cf, ^{252}Cf
Additionally declarable RN	U_{total} , Pu_{total} , α_{total} , β_{total}
Additionally declarable RN (repository-dependent from long-term safety assessment)	^{108m}Ag, ^{227}Ac, ^{229}Th, ^{230}Th, ^{243}Pu, ^{244}Pu

Table 1: Declarable RN in compacted or vitrified ILW (for Germany) (Kugel, et al., 2017). The "blue" RN are β-only emitters without significant heat deposition, "orange" RN deposit measurable heat.

Therefore, the RN list of Table 1 may be considered a token for the declaration task, and to which degree calorimetry is expected to add value to the results. Namely for historical and large volume RW-compounds calorimetry is expected a stronghold. A number of declarable RN amongst the listed (Table 1) ones cannot be measured easily by gamma- or neutron-spectrometry. Namely the RNs (^{3}H, ^{90}Sr/^{90}Y, ^{106}Ru/^{106}Rh, ^{238}Pu, ^{243}Am, ^{244}Cm) that deposit a measurable radiation heat (*cf.* Table 2) and are difficult to detect by other NDA surveys. Moreover, sealed radioactive sources deposit their radiation heat while the shielding prevents gamma radiation to emerge. These are the candidates to be addressed using calorimetry, and biased knowledge from the preconditioning process helps to rule out potential content of other sources of heat.

Isotope	Specific power [mW/g]	Transition / branching ratio	Energy [keV]
^{3}H	324	β / 100%	5.7
^{14}C	1.3	β / 100%	49,5
^{36}Cl	0.06	β / 100%	298
^{60}Co	649	β / 4% - γ / 96%	97 (β) / 2504 (γ)
(Sr)/^{90}Y	3 E6	β / 100%	933
Mo/^{99}Tc	0.006	β / 100%	55,2
Ru/^{106}Rh	30 E9	β / 87% - γ / 13%	206 (β) / 1413 (γ)
^{134}Cs	1256	β / 10% - γ / 90%	164 (β) / 1554 (γ)
^{137}Cs	125	β / 29% - γ / 71%	244 (β) / 597 (γ)
^{238}Pu	568	α / 100%	5579 (α) / 1.9 (γ)
^{241}Pu	3.3	α / 2% - β / 98%	0.12 (α) / 5.2 (β)
^{241}Am	115	α / 99%	5581 (α)
^{244}Cm	2829	α / 100%	5892 (α)

Table 2: Specific power and branching ratio for some selected radionuclides. *(NEA, 2018)*
For the red colored ones, calorimetry appears a viable method, the black ones are better measured by gamma-spec, the green ones are likely to remain undetected by calorimetry. For β emitters, the energy indicates the mean β energy.

The measurable heat flux [W] or thermal power W_{RN} [W] deposited is the simple product of the specific thermal radiation power deposition P_{RN} [W/g] multiplied with the mass m_{RN} of the radionuclide:

$$W = m\,P \quad \text{or} \quad W_j = \sum_i m_{ij} P_{ij} \qquad (1)$$

Where j denotes the different radionuclides RN_j, i runs over the isotopes $RN_j(i)$ and m_i denotes the mass fractions, respectively. P_i is their associated specific power. W is the experimentally accessible variable.

Uncertainty considerations derive directly from equation (1), statistical considerations, uncertainty propagation and from the measurable variables associated with the specific experimental set-up. Assessment and evaluation of the uncertainties will be subject of a specific report (D3.4) that will be addressed later after the experiments.
The nuclear characterisation task asks for m_{ij}, thus resolving equation (1) for m_{ij} which requires additional information about i and j, i.e. the radionuclide m_j and in many cases the nuclide vector m_i, as well.
In its application for the characterisation of conditioned radioactive waste drums calorimetry is complementary and supplementary to mainly gamma- and neutron spectrometry. Calculating the resulting heat-load should normally match the calorimetric results unless significant heat sources are hidden in the compound. This can be detected but the heating RN(s) cannot be identified. However solving equation 1 for the additional unknown heater allows for an upper limit of the spurious mass or activity associated to a specific RN, and considering the associated uncertainty would establish an upper limit or max. missed activity or mass, respectively.

5 Connection with CHANCE Task 3.2: U/Pu measurement in 200 L drums

As outlined above, not all declarable beta-emitters of Table 1 (red and blue color mark) can be measured with calorimetry, obviously only those with a significant heat stamp (red color mark). Elsewise, the CHANCE experiments are selected under the aforementioned criteria. The WP3 working group is working on the following cases to study within task 3.2:

1.) Pu pins or unirradiated MOX fuel inserted at different positions in a 200L drum with concrete and/or sand matrix (SCK•CEN, mock-up drum)
2.) Unconditioned waste containing Pu in a 200L drum (SCK•CEN, real drum)

These cases should enable us to demonstrate, in general, that the KEP calorimeter LVC CHANCE provides sufficiently precise calorimetric data (total heat flux) on 200L drums.

Plutonium, curium and americium are the main alpha contributors. Regarding nondestructive inspection, in the case of americium, the relevance of calorimetry is obvious since americium is measured using gamma ray spectrometry and is thus very sensitive to the waste drum matrix. Curium and plutonium on the other hand can be measured using passive and active neutron measurement. However, the measurement of plutonium with these techniques is more difficult than curium, since curium spontaneous fission neutron emissions are four orders of magnitude larger than plutonium (~10^7 neutrons/g/s of ^{244}Cm or ^{242}Cm, versus ~10^3 neutrons/g/s of ^{238}Pu or ^{242}Pu). Therefore, the following studies focus on plutonium measurement.

Case-1): SCK•CEN will produce or re-use a 220L drum filled with quartz-sand (probably comparable to the sketch in Figure 6), or a cement-based matrix, with a system of putting PuO_2 pins or unirradiated MOX fuel (with known fractions of ^{238}Pu, ^{239}Pu, ^{240}Pu, ^{241}Pu, ^{242}Pu and a small amount of ^{241}Am) in place.
Monte-Carlo simulations for this set-up (or at least something close to it) are well underway [cf. section 5.5] and the Pu-pin(s) will be the only heat source(s) in this experimental arrangement. The thermal power of the Pu-inset is known, thus this experiment is straightforward, as no obstacles are expected.
To mimic the presence of beta emitters, the most viable option at this point seems to be the use of a battery powered tunable (up to 3 W) electrical heat source (provided by KEP), which can be inserted inside the calorimeter, together with any of the other considered setups. MCNP simulations are initiated and the results will be available beforehand to tune and optimize the experiment.

Case-2): Eventually, a final real field test should be done on a real MAW waste drum to prove the capability, optimum application range and merits of the LVC CHANCE calorimeter. Details of this experiment are to be defined later, when the specific drum data will be known and evaluated before the experiment.

These 200 L drum experiments, using different Pu sources, source geometries and matrix compositions, will serve to compare neutron and gamma measurement techniques with calorimetric measurement. The experiments target the optimum application range of the large drum calorimeter LVC CHANCE, and are designed to:

1.) Demonstrate heat emitting alpha-sources can be measured in typical heterogeneous waste drums with e.g. a concrete matrix.

2.) Vary source position within the mock-up drums, which should allow assessing the effects of heterogeneous source distributions on HRGS and PNCC, while the calorimeter results should be more robust towards heterogeneity.
3.) Demonstrate detection of hidden beta sources is feasible, and can lead to proper RN-declaration required before disposal. If such hidden beta-sources can be detected from measurements, rather than being declared on the basis of history records or numerical correlation, it will provide a major step forward for RN-characterisation quality control.
4.) Demonstrate that tests on real (unconditioned) waste drums lead to similar results as for the mock-up drums in terms of applicability and usefulness of calorimetry.
5.) Allow for a thorough uncertainty assessment that will follow-up each of these experiments and will be part of the data assessment and evaluation. The sources of uncertainties will be described and assessed in the course of the experiments.

In this context, the present following sections (5.1, 5.2, 5.3) serve to evaluate the capabilities, and especially the limitations of neutron and gamma measurements to measure nuclear material in 200 L drums. Since ANI is a reference tool for detecting fissile materials, it is also included here, in the frame of task 3.1, even if it is not included in the CHANCE experimental benchmark (task 3.2).

5.1 Passive neutron/gamma measurement

In order to evaluate neutron and gamma approaches regarding the challenge of measuring fissile material in 200 L drums, Monte Carlo simulations using the MCNP code (Pelowitz, 2005) have been performed to quantify the impact of matrix composition and density with regard to the amount of signal that can exit a 200 L drum containing plutonium.
The calculations, described in Annex 8.1, consider the case of a 200 L drum filled with bitumen, stainless steel, polyethylene, concrete or graphite of various densities. Neutrons and gamma rays are emitted from the drum center to simulate the emission of a point-like plutonium source loaded in the middle of the drum. The amount of gamma rays and neutrons that escape the drum is recorded with an isotopic plutonium composition being {^{238}Pu; ^{239}Pu; ^{240}Pu; ^{241}Pu; ^{242}Pu} = {1.7 %; 56.0 %; 24.1 %; 12.8 %; 5.4 %}, which correspond to a PWR-type fuel (Carlson, et al.).
Figure 4 allows comparing different types of matrices and densities relative to the amount of gamma ray or neutron signal that can escape a 200 L drum. The densities are varied between 0.2 $g \cdot cm^{-3}$ and the respective material's true density in order to simulate matrices partially or completely filled. Figure 4 shows that to first order, the gamma ray attenuation is mainly determined by the matrix density, but is poorly affected by the matrix type. For example, for density 0.4 $g \cdot cm^{-3}$, for all matrices, the gamma ray emission rate exiting the drum is between 400 and 550 $s^{-1} \cdot g^{-1}$. As shown in Figure 5, such a feature is caused by the fact that, between 100 keV and 1 MeV, where Compton scattering dominates, for all the elements that compose the matrices, gamma ray mass attenuation coefficients (μ/ρ in $cm^2 \cdot g^{-1}$) are similar. Thus, to first order, the gamma ray attenuation of plutonium characteristics rays is independent of the matrix composition but is mostly sensitive to the matrix density.
Figure 4 illustrates the fact that neutron attenuation is also very sensitive to the amount of hydrogen in the matrix. Thus, passive measurement cannot be envisaged for matrices with high hydrogen concentration unless some prior knowledge is provided concerning the matrix composition and density. For other types of waste, as long as the absence of hydrogen is guaranteed, passive neutron measurement is however a valuable option since it poorly depends on the matrix composition and density, as long as the latter stays below ~1 $g \cdot cm^{-3}$.
In connection with Task 3.2, this study suggests to use a polyethylene, bitumen or concrete filled 200 L drum to test HRGS and PNCC and compare their performances with a calorimetric measurement.

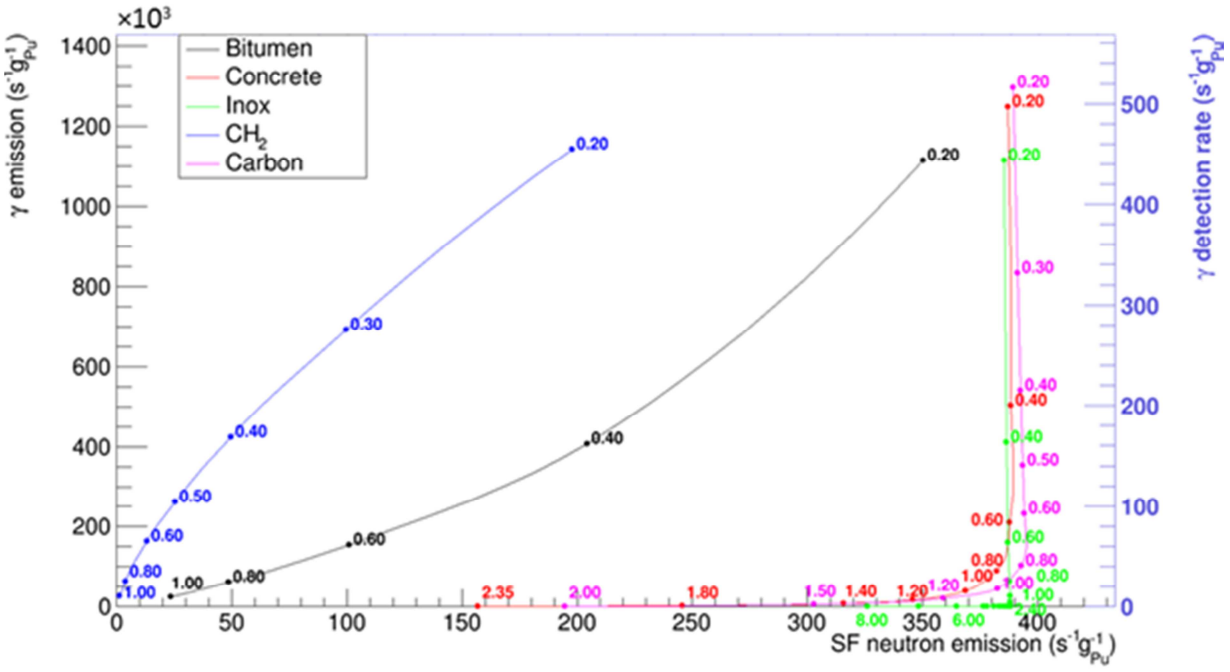

Figure 4: Rate of plutonium gamma rays exiting a 200 L drum versus rate of neutrons exiting a 200 L drum for various drum matrices and densities (black axis). The corresponding detection count rates expected for a High Purity Germanium with a 100% relative efficiency (relative to a 3"×3" NaI(Tl) at 1.33 MeV) are also indicated (blue axis). The figures indicated in color give the density in g·cm^{-3} of the matrix having the same color code.

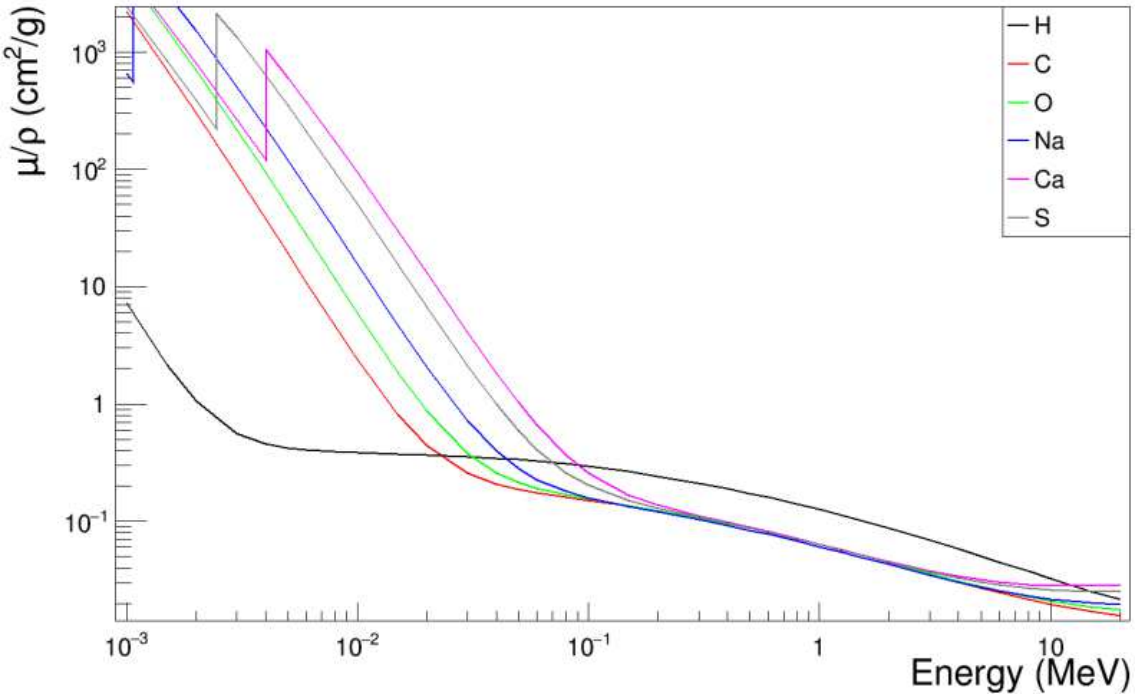

Figure 5: Gamma ray mass attenuation coefficients of the main elements composing the Figure 4 matrices.

5.2 Effects of source distribution

5.2.1 Experimental case setup

For assessing the effects of the source distribution within a drum, we base ourselves on the geometry provided by Bickel *et al.* (Bickel, et al., 1999), as shown in Figure 6, with a minimum distance of one centimeter between the sources and the inner surface of the drum, and a drum thickness of one millimeter. This geometry includes potential positions for plutonium sources at 7 radial and 3 axial locations, and all combinations thereof. For this preliminary analysis, we consider the following cases:

- A single source in the center of the drum ("most conservative", *i.e.* with this assumption, we get a maximum possible activity),
- A single source close to the top and the outer side of the drum ("least conservative", *i.e.* with this assumption, we get a minimum possible activity), and
- A combination of 21 sources, filling all possible locations within the drum ("homogeneous").

These three cases will provide us with an idea on the most and least conservative heterogeneous source distributions (in terms of calibration for activity concentration estimation based on the gamma or neutron emission), as well as an indication on the homogeneous case. These will therefore also allow assessing the usefulness of calorimetry, with respect to PNCC and HRGS, when the source distribution is unknown, as calorimetry is normally less affected by such heterogeneity.

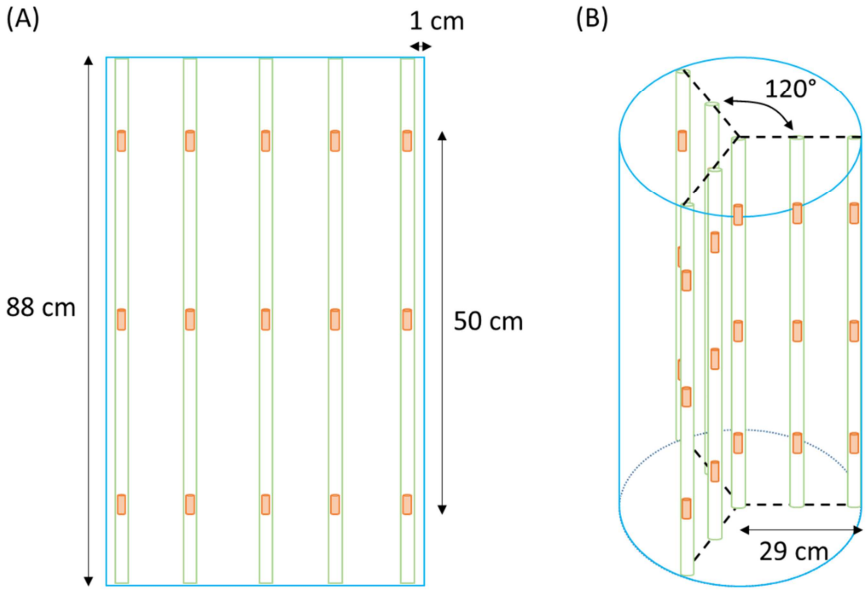

Figure 6: Possible source positions considered here, based on the geometry provided by Beckel et al. (1999).

5.2.2 Modelling approach

The same approach as the one used before to estimate the gamma and neutron emission rates in Section 5.1 was applied here, with a few minor differences in terms of implementation in the numerical model:

- **Compositions**: The same matrix and drum compositions were used here, but additionally, sand was also considered, as it might be a practical alternative to a cement-based matrix to use with existing mock-up drums. For the plutonium, we used a typical reactor-grade composition (Framatome ANP, 2002), (Massih, 2006), (Konno, et al., 1999).

- **Sources**: For the gamma source, the same peaks were considered. For the neutron source, a spontaneous fission source was considered instead of explicit specification of the energy distribution, but this leads to very comparable results.
- **Particle flux**: The MCNP type 1 tally was used to get a direct estimate of the number of particles crossing the outer surface of the drum.

Only the plutonium sources are considered currently in the models. The skeleton that holds them in place is not taken into account for now.

5.2.3 Results

The results of the three considered cases are provided in Figure 7, Figure 8 and Figure 9. Figure 7 basically corresponds to the results presented before, but is slightly different because of the considered geometry and source definition. Also here, it is very clear that most considered matrices are challenging for HRGS at their true density, while for PNCC, bitumen and polyethylene are more challenging because of their hydrogen content.

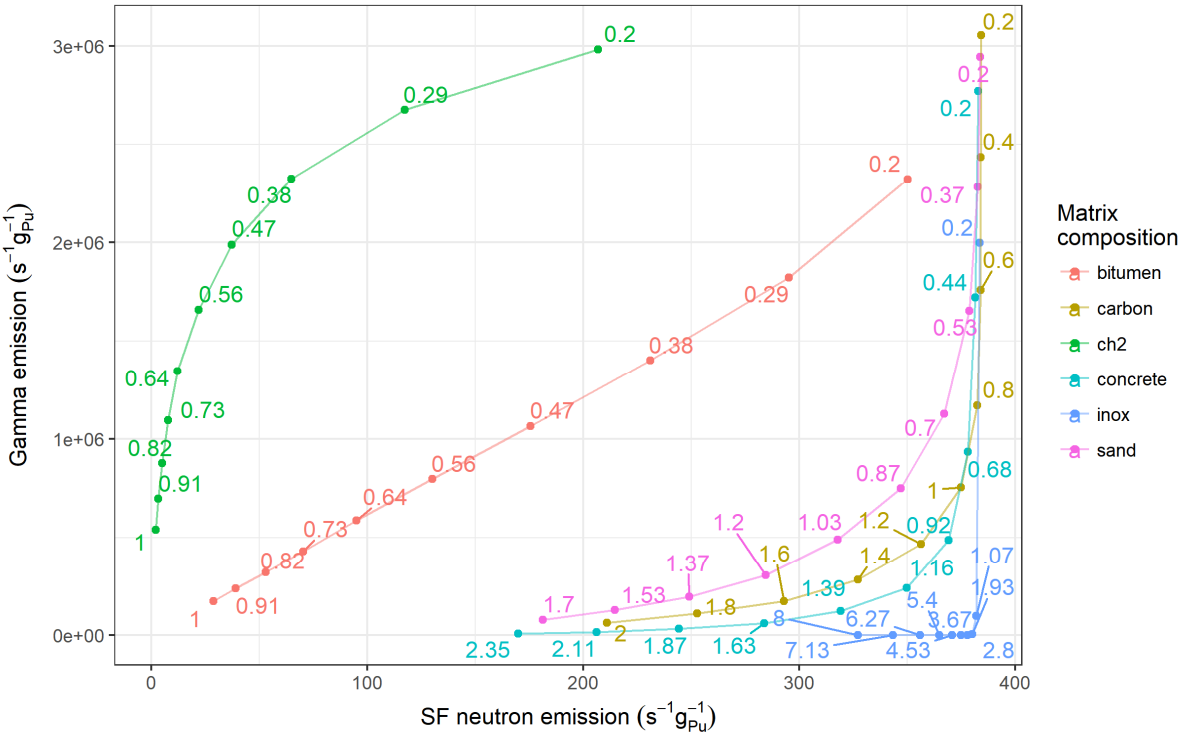

Figure 7: Gamma versus neutron emission rates for the most conservative case, in function of matrix composition and density (g/cm^3).

In Figure 8, for the least conservative case, results are very different, as there is only a small amount of material between the source and the outer surface of the drum. In this case, obtaining reasonable gamma and neutron emission rates seems not to be a problem at all.

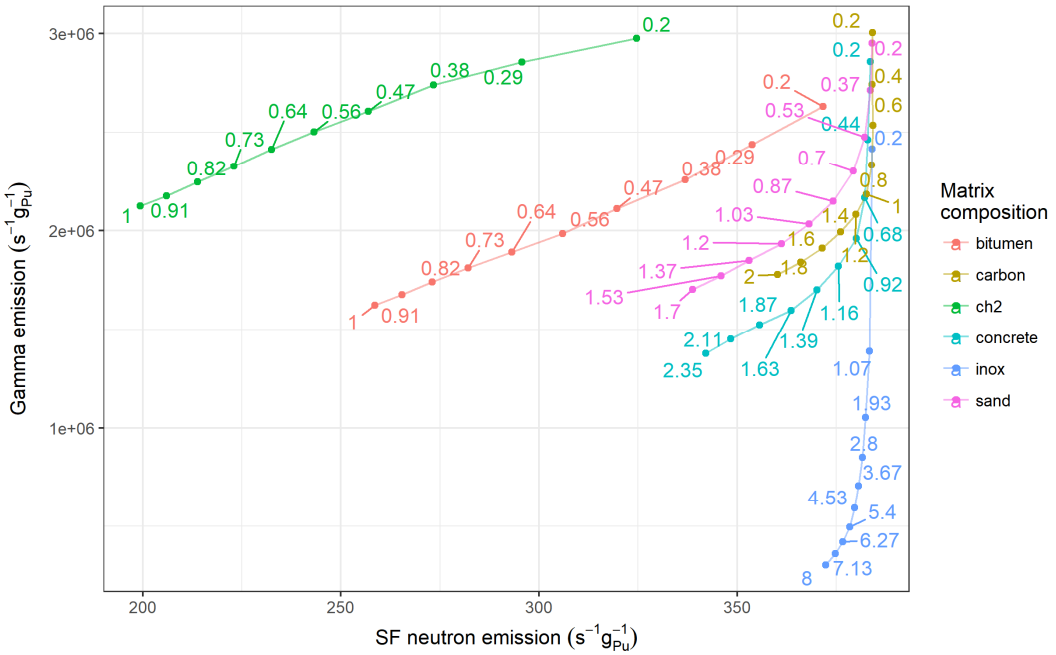

Figure 8: Gamma versus neutron emission rates for the least conservative case, in function of matrix composition and density (g/cm³).

The results for the homogeneous case, presented in Figure 9, are of course somewhere in between, and only very high densities might be a problem for the gamma emission rate there.

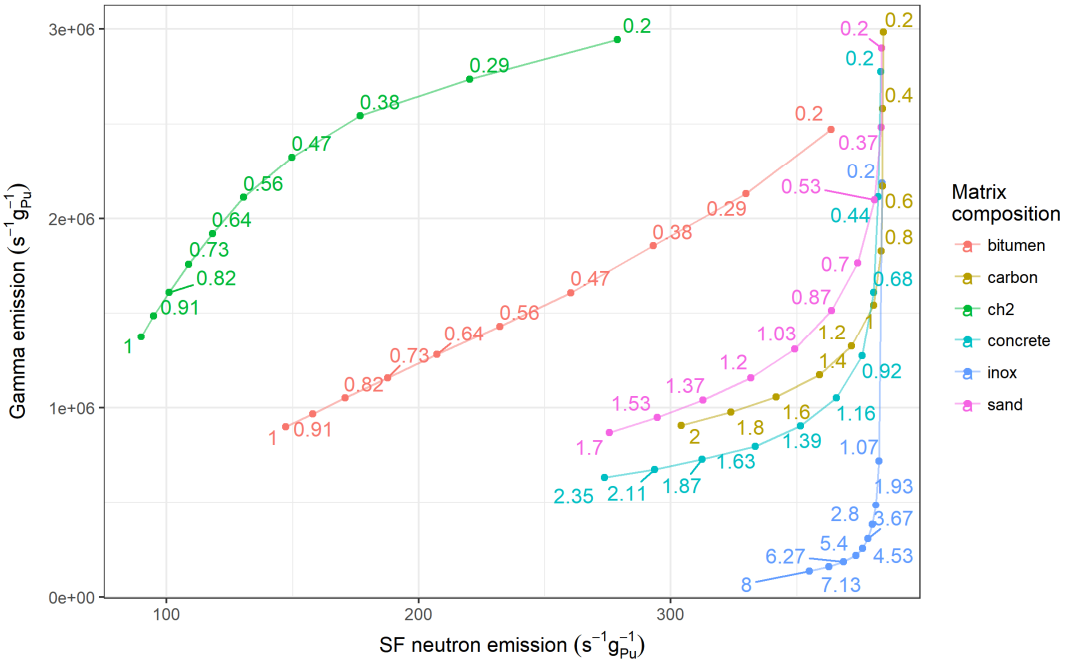

Figure 9: Gamma versus neutron emission rates for the homogeneous case, in function of matrix composition and density (g/cm³).

Erreur ! Source du renvoi introuvable. Figure 10 provides a comparison between the different considered geometries. It reveals clearly that the uncertainty related to the exact position of sources in a drum can be large. Also, it seems to suggest that the ratio of gamma versus neutron emission rates is more or less constant for bitumen, and the effect of source position is comparable to that of the matrix

density. This means that where for the other matrices, if the density is more or less known, the ratio of gamma versus neutron emission rates can provide information on the source position, for bitumen it cannot. In this respect, bitumen, or at least the exact composition considered here, is problematic for the combination HRGS – PNCC, and calorimetry might bring additional information.

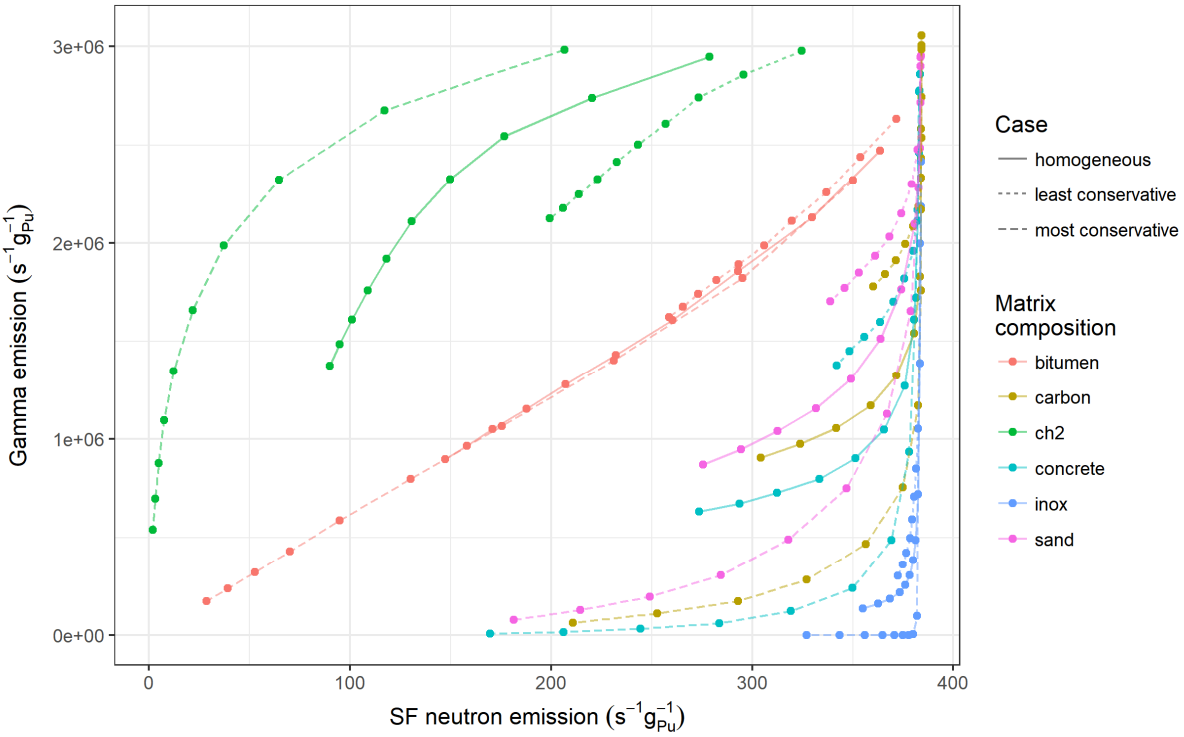

Figure 10: Comparison of the gamma versus neutron emission results, in function of matrix composition and the considered spatial distribution cases. See Figure 7, Figure 8 and Figure 9 for the actual considered densities.

The ratio of the least conservative and the homogeneous cases, with the most conservative case, are provided in Figure 11 for the gamma and Figure 12 for the neutron emission rates. This clearly shows the magnitude of the uncertainties. For the gamma emission, we can easily reach a difference of a factor 10 to 20, with respect to the most conservative case. For concrete, this is a factor 100 to 200, so an uncertainty of about two orders of magnitude. This clearly indicates that HRGS comes with large uncertainties when the source position is not exactly known, whereas the results from calorimetry might almost be unaffected by the source position in this case. First simulations of the calorimeter (described in paragraph 5.5.3.1.2) show that for gamma sources, energy detection varies from 48% to 79% depending on the source position, which is clearly less than the one or two orders of magnitude obtained here (although only the most conservative and homogeneous cases where looked at). For the neutron emission, the uncertainty is smaller for concrete, with a maximum of a factor 2 difference with the most conservative case. For the bitumen and polyethylene it goes up to a factor 10 and a factor 100. Also here, calorimetry is expected to reduce uncertainties drastically, even in the case of concrete. First simulations of the calorimeter (described in paragraph 5.5.3.2.2) show that for neutron sources, energy detection varies from 78% to 94% depending on the source position, which is again much better than the result obtained here (although only the most conservative and homogeneous cases where looked at).

As mentioned above, these uncertainties can be partly reduced by combining HRGS and PNCC measurements, as the ratio of gamma versus neutron emission rates provides some information about the source position/distribution. As bitumen seems to result in a more or less constant ratio, reducing

uncertainties by combining the measurement methods is not possible, and these results also reflect the uncertainty in that case.

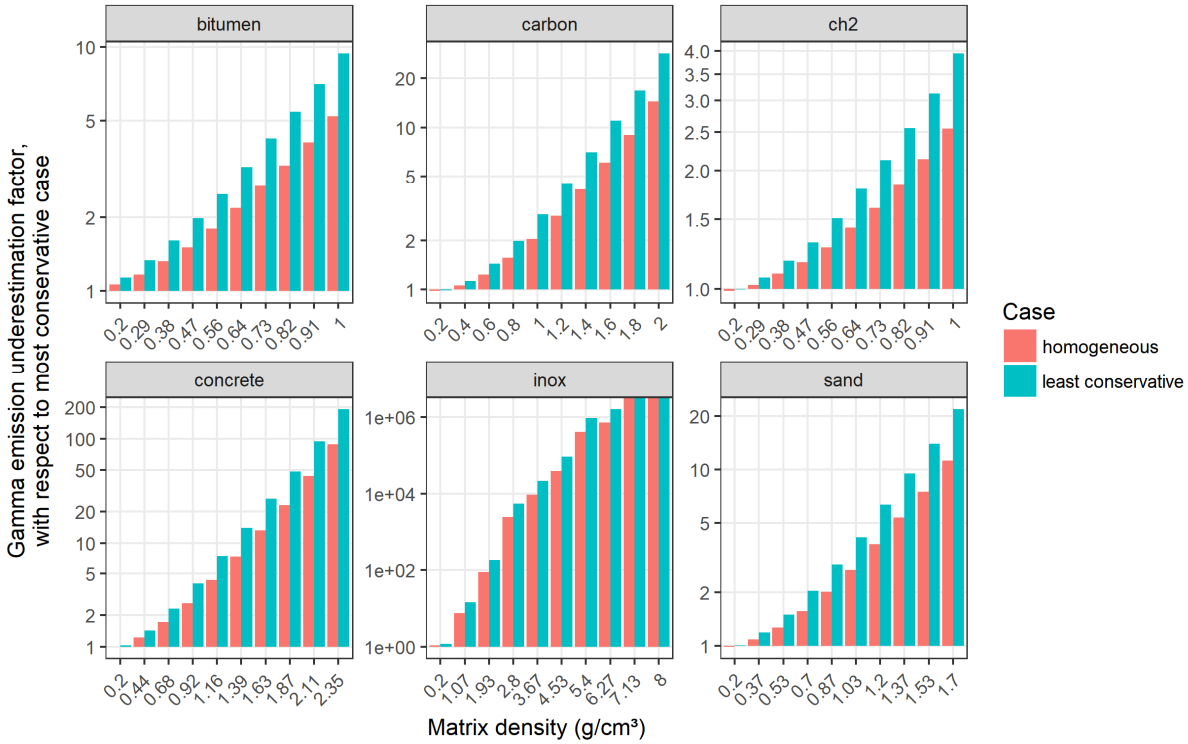

Figure 11: Ratio of the least conservative and homogeneous cases to the most conservative case, for the gamma emission rate.

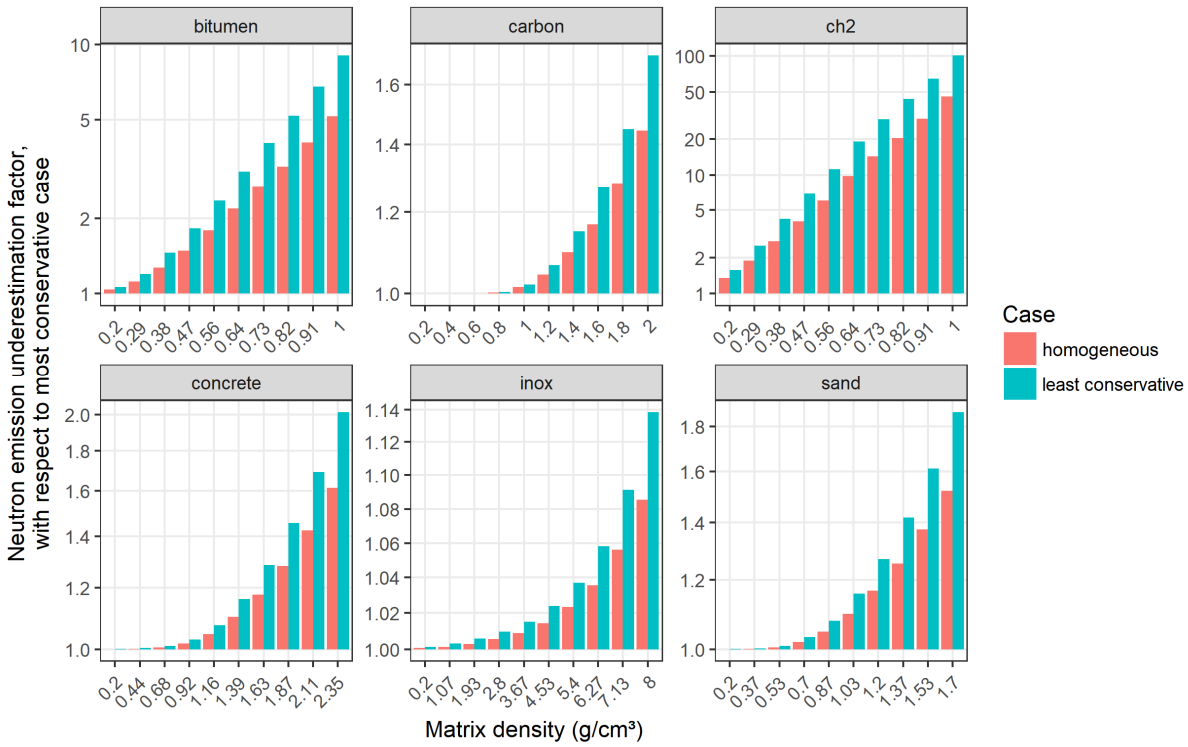

Figure 12: Ratio of the least conservative and homogeneous cases to the most conservative case, for the neutron emission rate.

5.3 Performances comparisons

To evaluate and compare the capability to measure plutonium and uranium with existing HRGS, SGS, TGS, PNCC systems, the Minimum Detectable Mass (MDM) in 200 L drums for ^{240}Pu, ^{239}Pu and ^{235}U that can be found in the literature have been used to build Figure 13. Accompanying each point of Figure 13 is the reference from which the data have been extracted, the nature of the measured nucleus and the measurement time. The text color code serves to identify the matrix composition.

The data indicated in Figure 13 are only rough indications of the performances of the measurement systems since they are not all straightforwardly comparable due to different counting time, but also due to differences of nuclear material distribution inside the waste matrix. Indeed, the nuclear material can be distributed homogeneously inside the matrix or at a fixed position in the periphery or in the center of the matrix, which, in this latter case, can increase, for example in the case of ANI, the MDM up to a factor 3 compared to the homogeneous case for a drum filled with concrete (Jallu, et al., 2011).

A simplified version of Figure 13 is presented in Figure 29 without the references and the indication of U and Pu, since the MDM associated to ^{235}U and ^{239}Pu points is comparable and because the nature of the measured nuclei is straightforward.

The correspondence between the matrix label used in this report and the matrix labels employed in the quoted references is indicated in Table 3 . Matrices indicated as being of “mixed” nature cover the “mixed” type matrix as indicated in (Rackham, et al., 2012) but also matrices indicated as being heterogeneous in other references. Only data from references providing the matrix density or for which a density can be reasonably guessed have been selected. More information concerning the labelling of the data points is given in Annex 8.3.

The HRGS and PNCC data shown in Figure 13 are of particular interest for Task 3.2, since these two types of measurements will be tested along with a newly developed calorimeter for measuring plutonium with mockup drums in challenging configurations.

Having Task 3.3 perspective in mind, Figure 13 shows that a 200 L drum filled with ~2 g·cm^{-3} concrete represents a challenging configuration for both HRGS and PNCC, since, compared to other matrices, the MDM is the highest for both type of measurement. Therefore, from this bibliographic study, the construction of a concrete mockup drum is recommended for Task 3.2.

Waste matrix name in Figure 13	Waste matrix as identified in the references
Combustible	Combustible, Combustible/PVC (Rackham, et al., 2012).
Metal	Metal, Lead (Rackham, et al., 2012), (Wilson, et al., 2010).
Mixed	Mixed, Heterogeneous (Alvarez, et al., 2006).
Debris	Debris
Concrete	Concrete, Cemented waste (Alvarez, et al., 2006).
Organic	Neoprene (Alvarez, et al., 2006), plastics (Wilson, et al., 2010), Solvents (Simpson, et al., 2013), wet soil and sludge (Mirion Technology).

Table 3: Link between the matrices label employed in Figure 13 and the labels originally employed in the references from which the MDM data have been extracted.

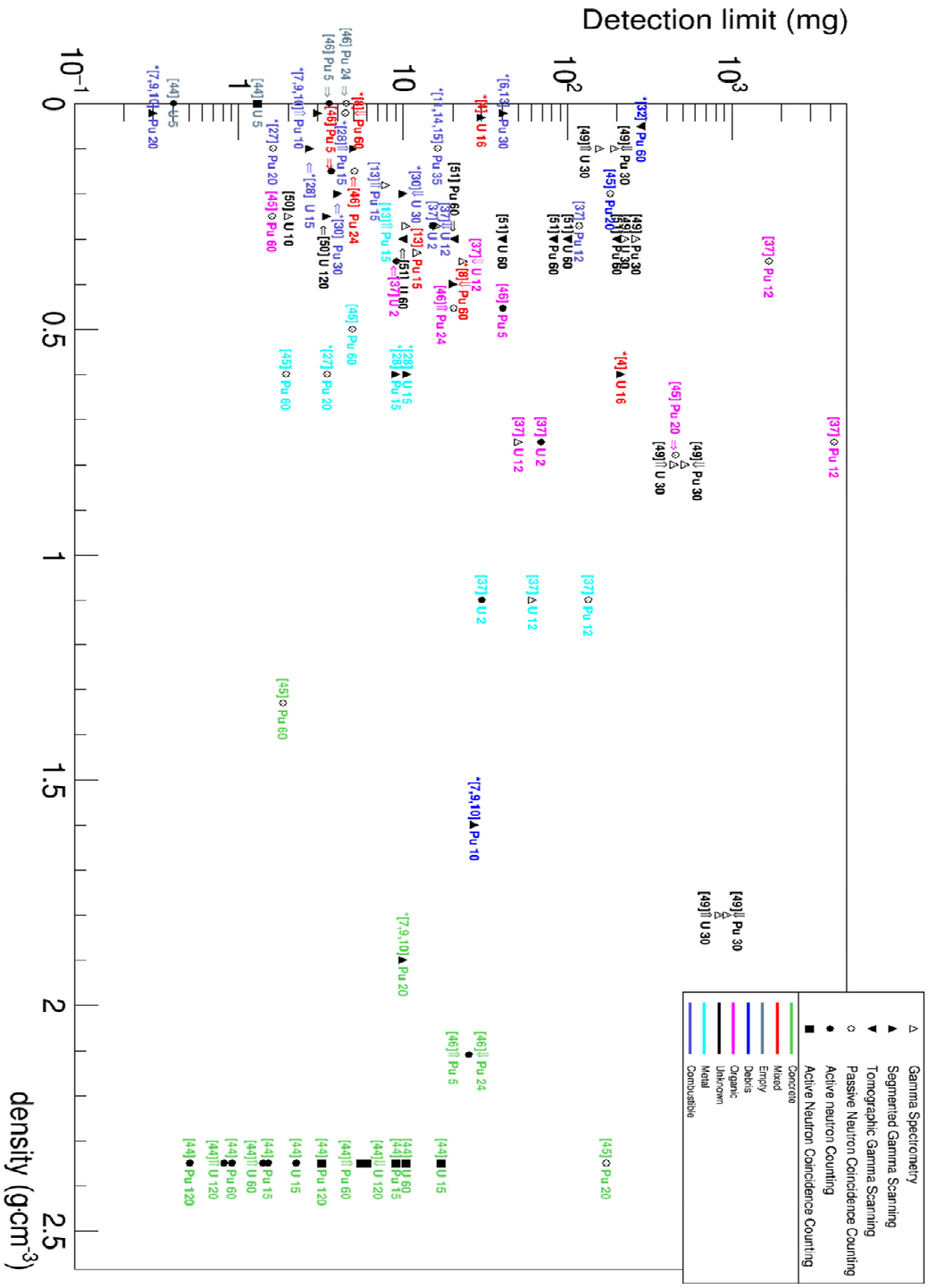

*Figure 13: ^{240}Pu, ^{239}Pu and ^{235}U MDM that can be achieved with different measurement techniques. For gamma measurements and active neutron measurements, Pu or U refers respectively to ^{239}Pu and ^{235}U and for passive neutron measurements Pu refers to ^{240}Pu.The reference from where the data have been taken is indicated in brackets. References proceeded by * refer to references from (Rackham, et al., 2012).The measurement time in minute is indicated after 'U' or 'Pu'.*

5.4 Discussions

Monte Carlo simulations on 200 L drums show that the gamma signal associated to plutonium is mainly affected by the matrix density, the nature of the matrix being of second importance with regard to gamma ray attenuation, since the energy of plutonium gamma rays used for NDA is greater than 100

keV. Similarly, as long as hydrogen concentration in the matrix is small, which usually is the case for materials other than polyethylene, bitumen or concrete, the composition of the matrix has only a limited impact on the passive neutron signal, for a density below ~1 $g \cdot cm^{-3}$. For active neutron interrogation however, information concerning both the matrix density and nature (presence of absorbing elements) is crucial to convert neutron counting measurement into mass of fissile material.

Additionally, the first assessment on the effect of a heterogeneous source distribution illustrates clearly that uncertainties related to gamma radiation easily span one to two orders of magnitude. Similar uncertainties can be obtained for neutron radiation, but for concrete it seems only to go up to a factor two. Calorimetry is however more robust towards heterogeneity, and would in such cases be very useful for reducing uncertainty.

Also, the capability to detect nuclear material placed inside a 200 L drum have been investigated through a bibliographic study for High Resolution Gamma ray Spectrometry (HRGS), Segmented Gamma Scanning (SGS), Tomographic Gamma Scanning (TGS), Passive Neutron Coincidence Counting (PNCC), Active Neutron Counting (ANC) and Active Neutron Coincidence Counting (ANCC).

These investigations suggest that a 200 L drum filled with concrete, polyethylene or bitumen are good candidates for challenging HRGS and PNCC, which are the two techniques that will be tested with calorimetry within Task 3.2.

5.5 MCNP CHANCE Calorimeter modelling

As mentioned in previous paragraphs, calorimetry is known as one of the best non-destructive assay techniques for radionuclide mass determination. However, this method is not bias-free. Source position, material density distribution, chemical reactions, phase changes and also radiation leakage can influence the final result. In order to evaluate how the leakage changes the result and how the radiation behaves within the volume of the calorimeter (i.e. how the energy is deposited inside the system and to estimate the amount of escaping flux) Monte Carlo simulations of the future CHANCE calorimeter were realized, using the MCNP code and ENDFB-7.1 cross sections library. In this paragraph the modelling of the CHANCE calorimeter (also referred to as LVC CHANCE) and the first preliminary MCNP results will be presented.

5.5.1 Model description

Based on the conceptual design by the KEPIC (KEP Innovation Center) engineers (presented on Figure 14), the model has been simplified towards the relevant parts for the particle transport simulations.

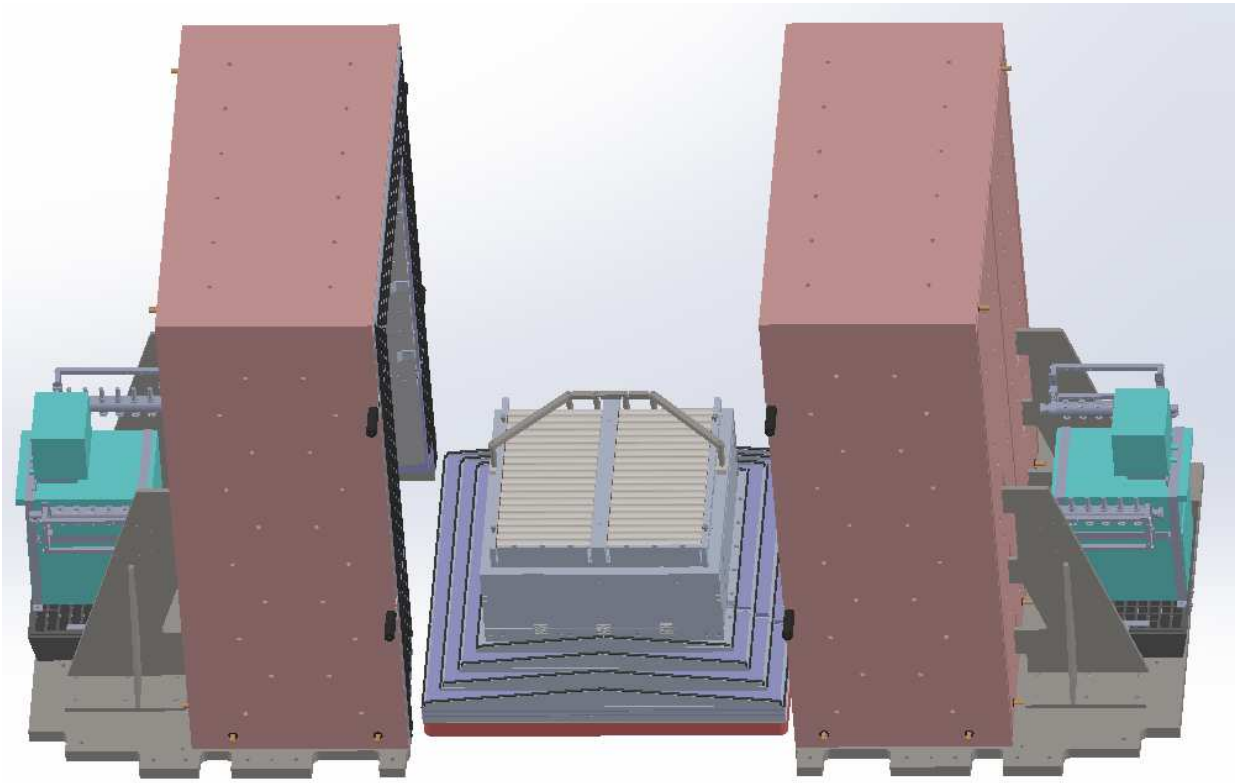

Figure 14: 3D view of the CHANCE Calorimeter

The MCNP model presented on Figure 15 consists of different layers: at the very inside of the model there is a sample (in this case a drum filled with sand and an assembly with radioactive material). Sand composition is presented in Annex 8.4 (US Department of HomeLand Security , 2011). Next layer is the octagon-shaped structure with the heat flux detectors on each wall, inside the measurement chamber, which is filled with air. Then, there is one homogenization layer, then one insulation layer and so on, up to the fourth homogenization layer. Underneath the measurement chamber there is a reference chamber (or ghost chamber) with a phantom aluminium block, which compensates for the influence of the ambient environment (*e.g.* temperature changes). The outer aluminium layer (or cold plate) is kept at a constant temperature.

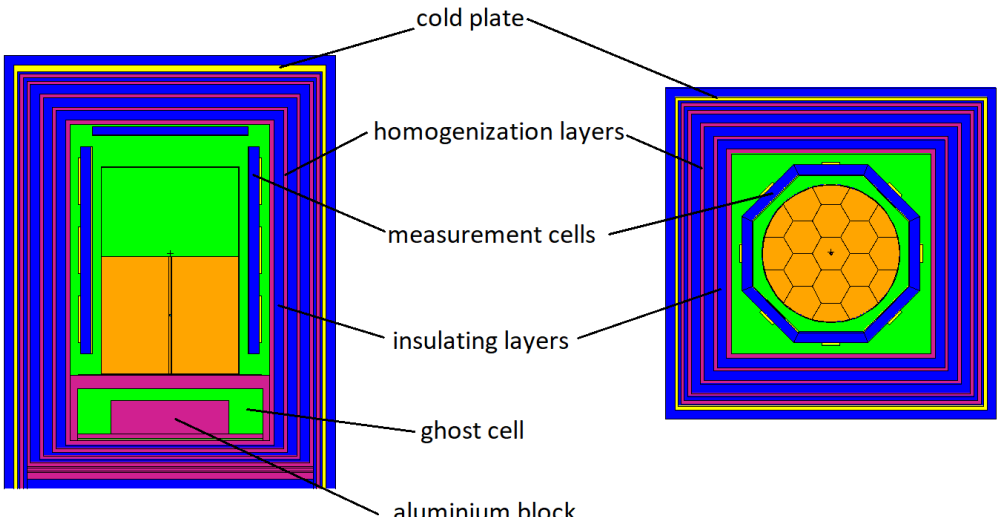

Figure 15: MCNP geometry 2D views. Left: xz plan view. Right: xy plan view.

5.5.2 Simulations

5.5.2.1 Source description (most conservative and homogeneous)

Two kinds of sources were used in the simulations. A first one, hereafter called the “most conservative” source, was filled with an assembly of pins with containers containing radioactive material (as presented on Figure 6). The drum was filled with the assembly up to 50 cm and the remaining part was filled with air. The space between the pins was filled with sand. In this study, the most conservative source was limited to only one pin in the centre of the assembly with only one container in the middle of the pin. This configuration corresponds roughly to as the “most conservative” one in section 5.2.1. In this scenario the particles, on average, need the longest possible path to leave the system.

A second kind of source, hereafter called the “homogeneous" source (which roughly corresponds to the “homogeneous” configuration mentioned in Section 5.2.1), was a drum filled up to 50 cm only with sand (for the composition *cf.* Annex 8.4), and air in the remaining part, and particle starting points were sampled inside the whole section filled with sand. The amount of escaping radiation is of course higher in this case, as the particles can appear nearby the wall of the drum as well. Figure 16 shows the difference between particles sampling in both kinds of source configurations.

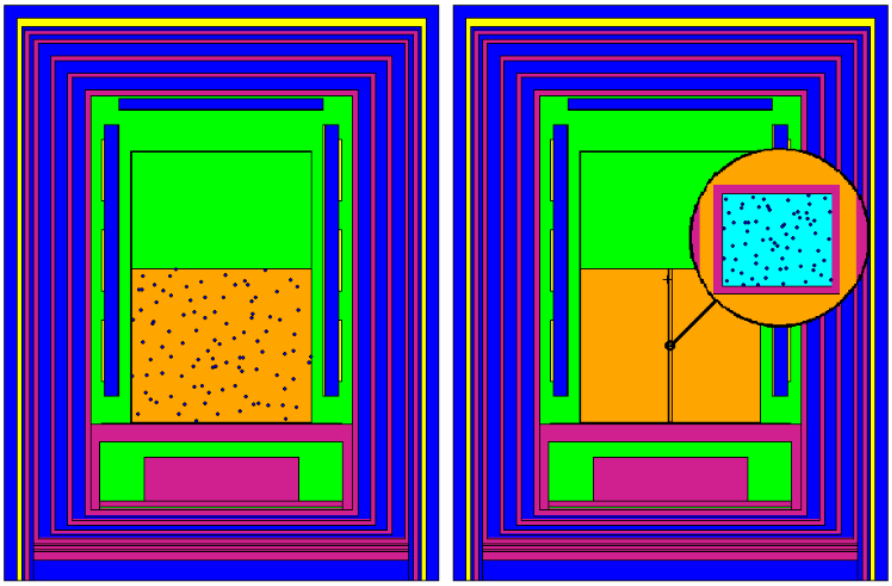

Figure 16 : Homogeneous (left) and most conservative (right) source configurations.

5.5.2.2 Stability test

The number of particles needed for reliable simulations was evaluated by plotting the statistical error of the energy deposition as a function of the number of particles used in each simulation. As the maximal error in the system was determined and the statistical error is different for each part of the calorimeter (as a different number of particles achieve each part), for the stability test, energy deposition was taken into account the outmost layer only. For this layer, the smallest number of particles was detected, so the statistical error was largest there. In addition, the simulated value (normalized by the most reliable result *i.e.* with the minimum error) was plotted also as a function of the number of particles used in each simulation. The results are presented on Figure 17 and ***Figure 18***. One can see that for 10^6 particles the result is statistically reliable with a relative error inferior to 1% for both, neutron and gamma radiation

tally results. Thus the number of particles has been scaled-up to 10^6 and used in all the simulations and resulting viewgraphs for comparison.

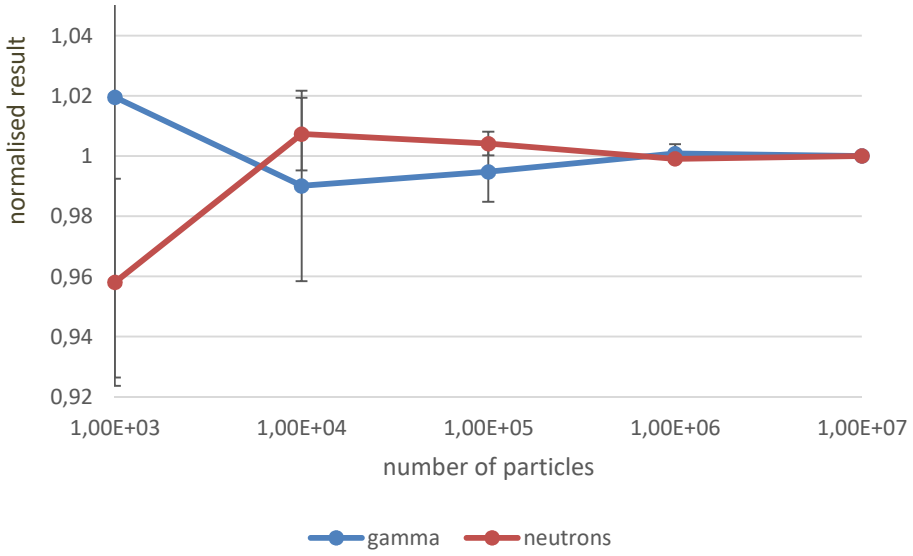

Figure 17: Deposited energy stability test results, as a function of the number of particles, relative to the most accurate value.

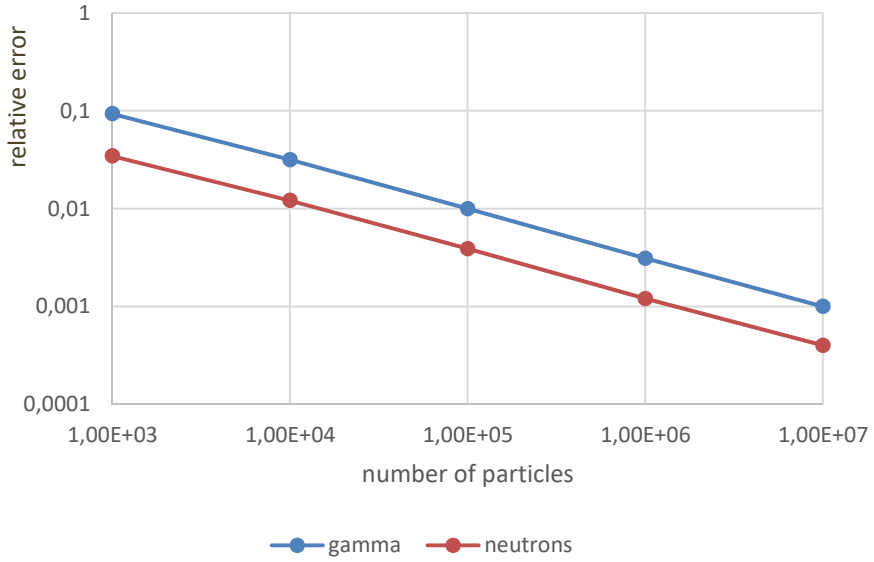

Figure 18: Deposited energy stability test relative errors, as a function of the number of particles.

5.5.3 Results

5.5.3.1 Gamma radiation

5.5.3.1.1 Particle flux study

To evaluate how the gamma flux behaves within the drum and the calorimeter, a tally 4 with the mesh option was used. The tally 4 determines the mean flux in each cell of a defined grid (mesh option). The result shows the number of particles per cm^2, per source particle. The flux was checked along the x axis

at z = 74 cm (at height of the source position) and y = 0 and along the z axis at x and y equal to 0. In the charts, a logarithmic scale was used. A generic mono-energetic gamma source of 2.5 MeV was used. The results shown in Figure 19 and Figure 20 are those obtained along the x-axis for the most conservative and homogeneous source models.

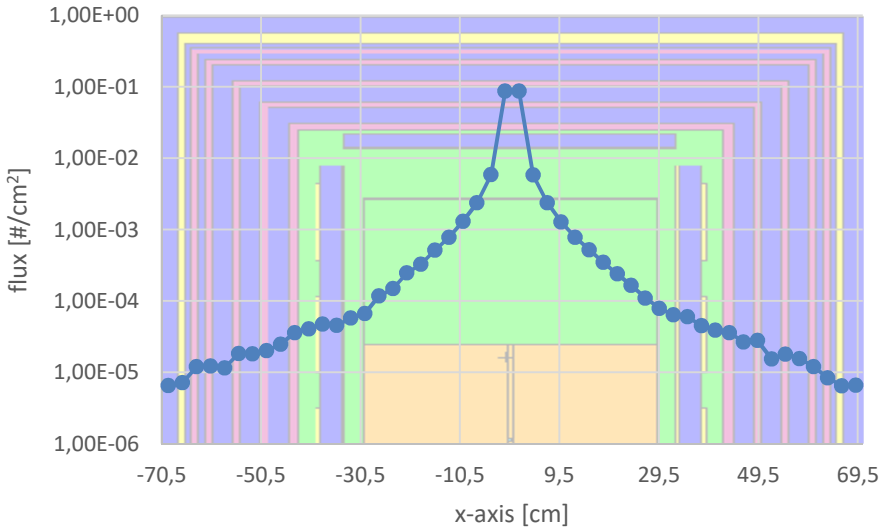

Figure 19: Gamma particle flux, most conservative source – profile at (y;z) = (0;74) cm

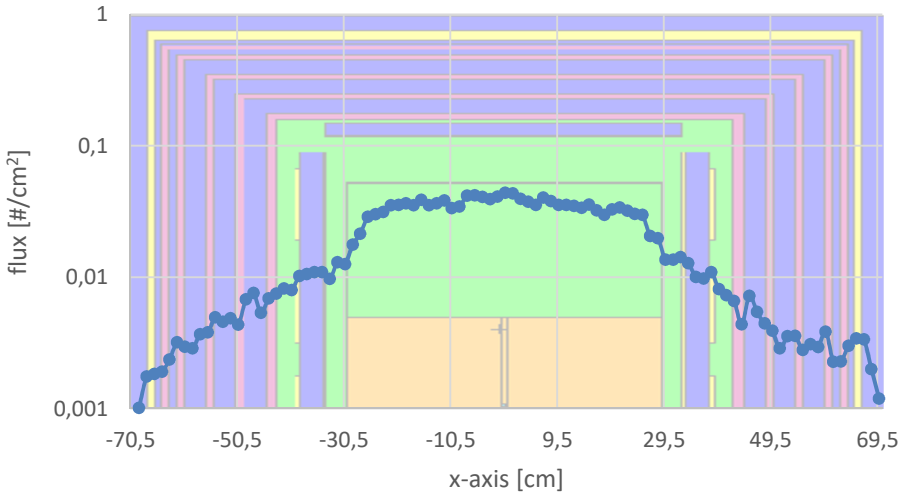

Figure 20: gamma particle flux, homogeneous source – profile at (y;z) = (0;74) cm

As one can see in these charts the flux goes down very fast inside the drum (and a bit slower within the range of the calorimeter walls). Moreover, a percentage of the radiation energy is not deposited inside the system (up to $10^{-5}cm^{-2}$ in case of the most conservative source and $10^{-3}cm^{-2}$ in case of the homogeneous one).

Figure 21 shows the results obtained along the z-axis for the homogeneous (left) and most conservative (right) source models.

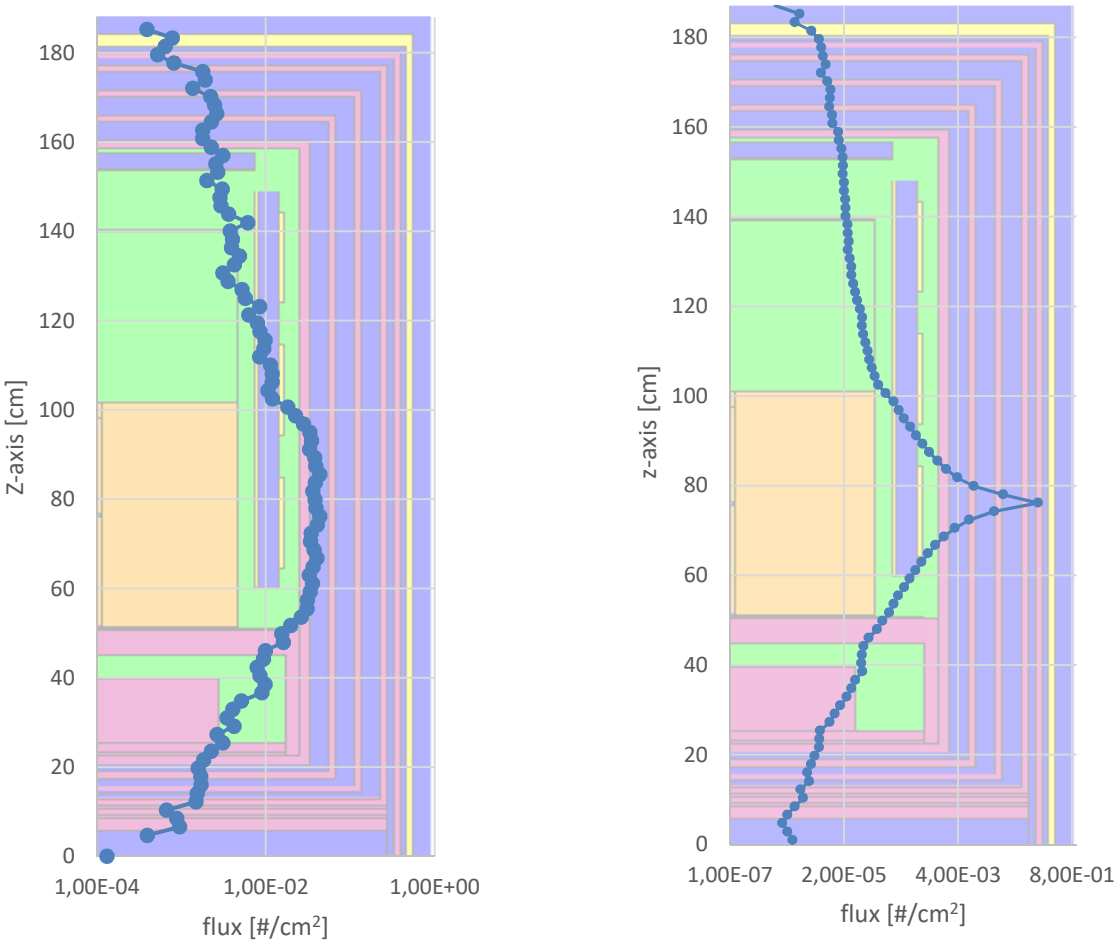

Figure 21 : gamma particle flux, homogeneous (left) and most conservative (right) sources – profile at (x;y) = (0;74) cm

One can see that a part of the radiation goes through the aluminum block and ghost cell (reference part). Heating of this part can cause an additional bias. This phenomenon is visible for both the most conservative and homogeneous source.

5.5.3.1.2 Energy deposition study

Complementary to the flux behaviour, it is important to evaluate the effect of the radiation on the calorimeter elements. To evaluate this, the energy deposition in each part (cell) was calculated using tally 6 (it determines energy deposition per one gram of material in a cell).

Table 4 and Table 5 provide the obtained results (given per source particle).

Layer	Energy [MeV/g]*	Energy [MeV]**	Energy deposition [%]	Rel. Error [%]
Drum	1.38315E-05	**1.97E+00**	**78.95**	0.11
thermal block	1.17162E-07	5.91E-02	2.37	0.12
homogenization layer 1	1.56868E-07	4.88E-02	1.95	0.14
homogenization layer 2	1.13239E-07	4.19E-02	1.68	0.15
homogenization layer 3	8.27864E-08	3.60E-02	1.44	0.16
homogenization layer 4	6.26212E-08	3.07E-02	1.23	0.18
cold plate	4.58141E-08	2.97E-02	1.19	0.20
measurement plates	5.93441E-07	**1.80E-02**	**0.72**	0.15
ghost chamber	3.09834E-07	**8.78E-03**	**0.35**	0.81
aluminum block	1.78418E-07	**6.01E-03**	**0.24**	0.46
reference plates	4.70379E-07	**4.67E-03**	**0.19**	0.36
insulation layer 1	2.09893E-07	4.87E-04	0.02	0.14
measurement cells	5.68344E-07	**4.71E-04**	**0.02**	0.15
insulation layer 2	1.50879E-07	4.19E-04	0.02	0.16
insulation layer 3	1.09898E-07	3.60E-04	0.01	0.17
insulation layer 6	4.33793E-08	2.25E-04	0.01	0.21
measurement chamber	1.57044E-09	**2.04E-04**	**0.01**	0.13
insulation layer 4	8.06395E-08	1.17E-04	0.00	0.19
insulation layer 5	6.37206E-08	6.69E-05	0.00	0.20
bottom measurement plate	2.60122E-07	3.43E-05	0.00	0.38
	sum total	**2.26E+00**	**90.4**	**0.6**
	sum detected	**1.97E+00**	**78.9**	**0.6**

Table 4: Energy deposition for the most conservative gamma source

*average energy deposited in one gram of the material in the layer per 2.5 MeV photon
**average total energy deposited in the layer per 2.5 MeV photon

The heat depositions in the layers were divided into three components: energy that was detected by the measurement elements (colored in green), energy that will reduce the final result (colored in red) and parts with negligible influence on the power measurement (not colored). We define final result as:
energy deposited in the drum + energy deposited in the measurement cells - energy deposited in the reference parts.
The sums presented in Table 4 shows that for the most conservative source, the total energy deposition is about 90%, and final detected energy is around 79%. One can see that about 10% of the radiations escape the calorimeter.

Layer	Energy [MeV/g]*	Energy [MeV]**	Energy deposition [%]	Rel. Error [%]
drum	1.80E-05	1.19E+00	47.55	0.29
thermal block	1.19E-06	2.78E-01	11.10	0.24
homogenization layer 1	6.59E-07	9.49E-02	3.79	0.26
homogenization layer 2	4.88E-07	8.36E-02	3.35	0.28
homogenization layer 3	3.67E-07	7.38E-02	2.95	0.30
homogenization layer 4	2.21E-07	6.61E-02	2.64	0.37
cold plate	2.89E-07	6.56E-02	2.62	0.33
measurement plates	2.69E-06	3.78E-02	1.51	0.27
ghost chamber	1.23E-06	1.62E-02	0.65	0.91
aluminum block	7.41E-07	1.16E-02	0.46	0.97
reference plates	1.98E-06	9.11E-03	0.36	0.86
insulation layer 1	2.37E-06	9.09E-04	0.04	0.31
measurement cells	8.38E-07	9.00E-04	0.04	0.27
insulation layer 2	6.12E-07	7.88E-04	0.03	0.29
insulation layer 3	4.58E-07	6.95E-04	0.03	0.31
insulation layer 6	2.09E-07	5.04E-04	0.02	0.38
measurement chamber	6.66E-09	4.00E-04	0.02	0.27
insulation layer 4	3.47E-07	2.33E-04	0.01	0.34
insulation layer 5	2.85E-07	1.39E-04	0.01	0.36
bottom measurement plate	1.13E-06	6.91E-05	0.00	0.81
	sum total	**1.93E+00**	**77.2**	**0.7**
	sum detected	**1.19E+00**	**47.6**	**0.7**

Table 5: Energy deposition for a homogeneous gamma source

*average energy deposited in one gram of the material in the layer per 2.5 MeV photon
**average total energy deposited in the layer per 2.5 MeV photon

For the homogeneous model one can see a decrease in the calculated values. Only 77% of the radiation was deposited inside the system, (and 23% escaped). Only 48% of the radiation energy would be detected.

5.5.3.1.3 Real source simulation: example of ^{60}Co

Next simulations were performed using a real case gamma source, *i.e.* ^{60}Co emitting two gamma-rays at 1.332 MeV and 1.173 MeV almost every time it decays (99.88%). Simulations were realized for both, homogeneous and the most conservative source models, the results are presented in Table 6.

	homogeneous source			The most conservative source		
Layer	**energy [MeV/g]***	**power [mW/g]****	**Energy deposition [%]**	**energy [MeV/g]***	**power [mW/g]****	**Energy deposition [%]**
Drum	**1.57E+00**	**1.05E+04**	**72.27**	**2.18E+00**	**1.46E+04**	**87.24**
thermal block	1.70E-01	1.14E+03	6.77	5.85E-02	3.93E+02	2.35
homogenization layer 1	1.00E-01	6.71E+02	3.99	3.47E-02	2.33E+02	1.39
homogenization layer 2	8.15E-02	5.47E+02	3.25	2.83E-02	1.90E+02	1.13
homogenization layer 3	6.63E-02	4.45E+02	2.65	2.30E-02	1.54E+02	0.92
homogenization layer 4	5.32E-02	3.57E+02	2.12	1.83E-02	1.23E+02	0.73
cold plate	4.65E-02	3.12E+02	1.86	1.61E-02	1.08E+02	0.64
measurement plates	**4.55E-02**	**3.05E+02**	**1.82**	**1.45E-02**	**9.74E+01**	**0.58**
aluminum block	**1.29E-02**	**8.68E+01**	**0.52**	**5.75E-03**	**3.86E+01**	**0.23**
reference plates	**1.09E-02**	**7.32E+01**	**0.44**	**3.75E-03**	**2.51E+01**	**0.15**
bottom measurement plate	1.03E-02	6.89E+01	0.41	3.69E-03	2.48E+01	0.15
measurement cells	**1.13E-03**	**7.61E+00**	**0.05**	**3.50E-04**	**2.35E+00**	**0.01**
insulation layer 1	1.01E-03	6.78E+00	0.04	3.38E-04	2.27E+00	0.01
insulation layer 2	8.23E-04	5.53E+00	0.03	2.74E-04	1.84E+00	0.01
insulation layer 3	6.65E-04	4.46E+00	0.03	2.23E-04	1.50E+00	0.01
measurement chamber	**4.94E-04**	**3.32E+00**	**0.02**	**1.54E-04**	**1.04E+00**	**0.01**
insulation layer 6	3.31E-04	2.22E+00	0.01	1.10E-04	7.38E-01	0.00
insulation layer 4	2.06E-04	1.38E+00	0.01	6.89E-05	4.62E-01	0.00
insulation layer 5	1.10E-04	7.40E-01	0.00	3.68E-05	2.47E-01	0.00
ghost chamber	**6.20E-05**	**4.16E-01**	**0.00**	**2.08E-05**	**1.40E-01**	**0.00**
sum total	**2.17E+00**	**1.46E+04**	**86.59**	**2.38E+00**	**1.60E+04**	**95.59**
sum detected	**1.59E+00**	**1.07E+04**	**73.19**	**2.18E+00**	**1.46E+04**	**87.46**

Table 6: Energy deposition of a ^{60}Co source in the calorimeter

* energy deposited in one gram of the material in the layer
**calculated power of one gram of the radioactive material

In this case, the relative error was also below 1% for each part (cell) of the calorimeter. One can see that about 4% of the radiation escaped the calorimeter and 87% would be detected in case of the most conservative source configuration. About 13% of the radiation escaped the system and ca. 73% would be detected in case of homogeneous source.

5.5.3.1.4 Energy deposition pattern

In order to evaluate the energy deposition in each layer of the calorimeter simulations were carried out with a 1 MeV mono-energetic gamma source emitted from the center of the empty drum. The layers are labelled from inside outwards: 0 – drum; 2,4,6,8 – homogenization layers; 10 – cold plate.
The results are presented in Figure 22 and Figure 23.

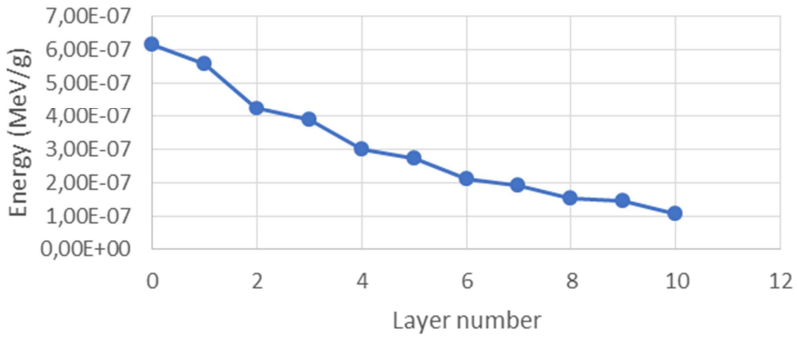

Figure 22: Gamma radiation energy deposition in layers

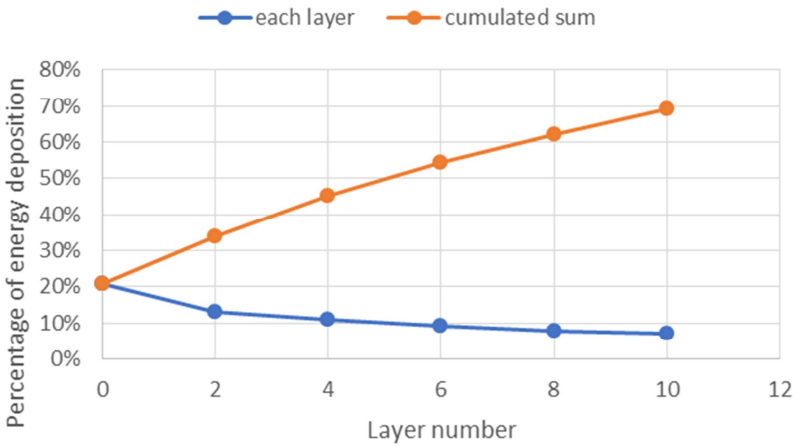

Figure 23: Distribution of gamma radiation energy deposition

One can see that only about 70% of the radiation was deposited inside the calorimeter. Therefore, further simulations were performed to evaluate the energy deposition as a function of the gamma source energy. The results are presented in Figure 24. For gamma radiation with energy levels above 0.2 MeV there is a significant decrease of the total energy deposited in the calorimeter. For lower energies, energy deposition is above 75% but for energies of about 5 MeV and more it drops to about 60% or less.

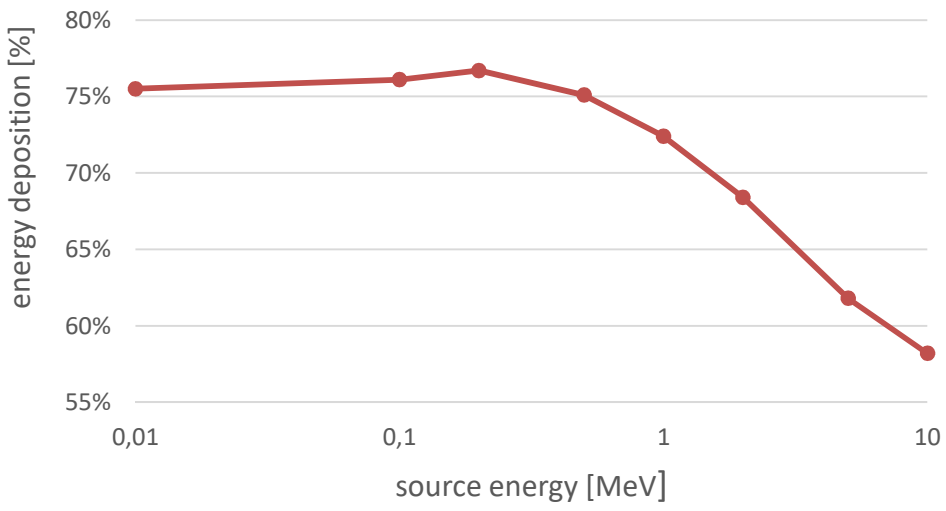

Figure 24: Gamma radiation energy deposition as a function of the source energy

5.5.3.2 Neutron radiation

5.5.3.2.1 Particle flux study

Analogous to the gamma source simulations, homogeneous and most conservative neutron source models were used. A generic mono-energetic neutron source of 5.2 MeV was used. Results obtained along the x-axis are presented in Figure 25 for the most conservative source and in Figure 26 for the homogeneous source. Analogically to the gamma simulations, tally 4 was used to determine the fluxes.

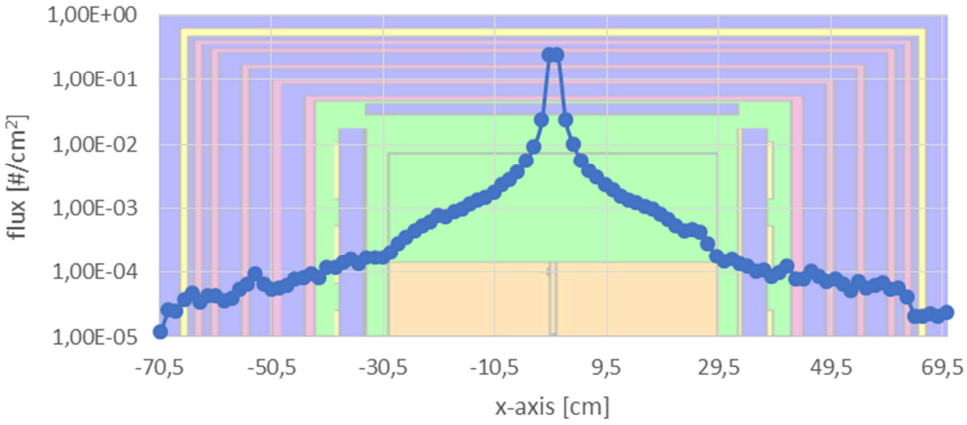

Figure 25: Neutron particle flux, most conservative source – profile at (y;z) =(0;74) cm.

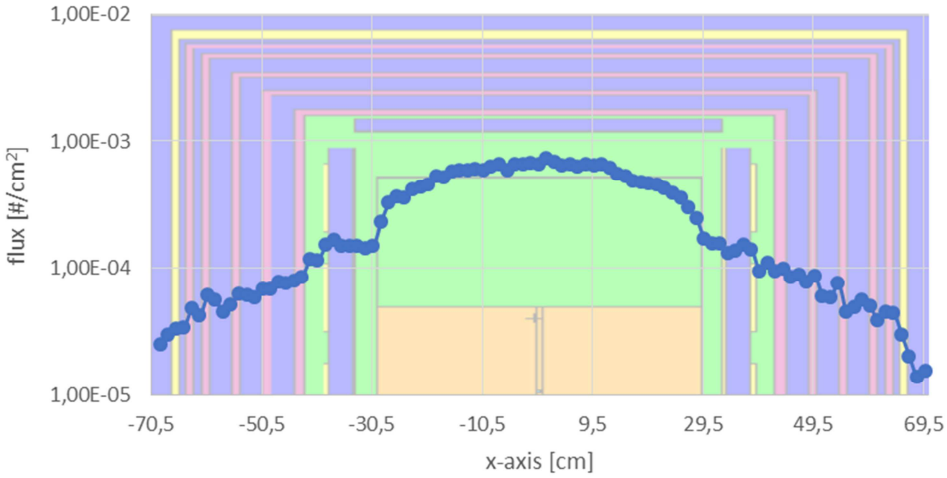

Figure 26: Neutron particle flux, homogeneous source – profile at (y;z) =(0;74) cm.

For neutrons, radiation flux escaping the calorimeter was around $1 \cdot 10^{-5} cm^{-2}$ in case of the most conservative source and $3 \cdot 10^{-5} cm^{-2}$ in case of the homogeneous source.

Results obtained along the z-axis are presented in Figure 27 (on the left for the homogeneous source and on the right for the most conservative source).

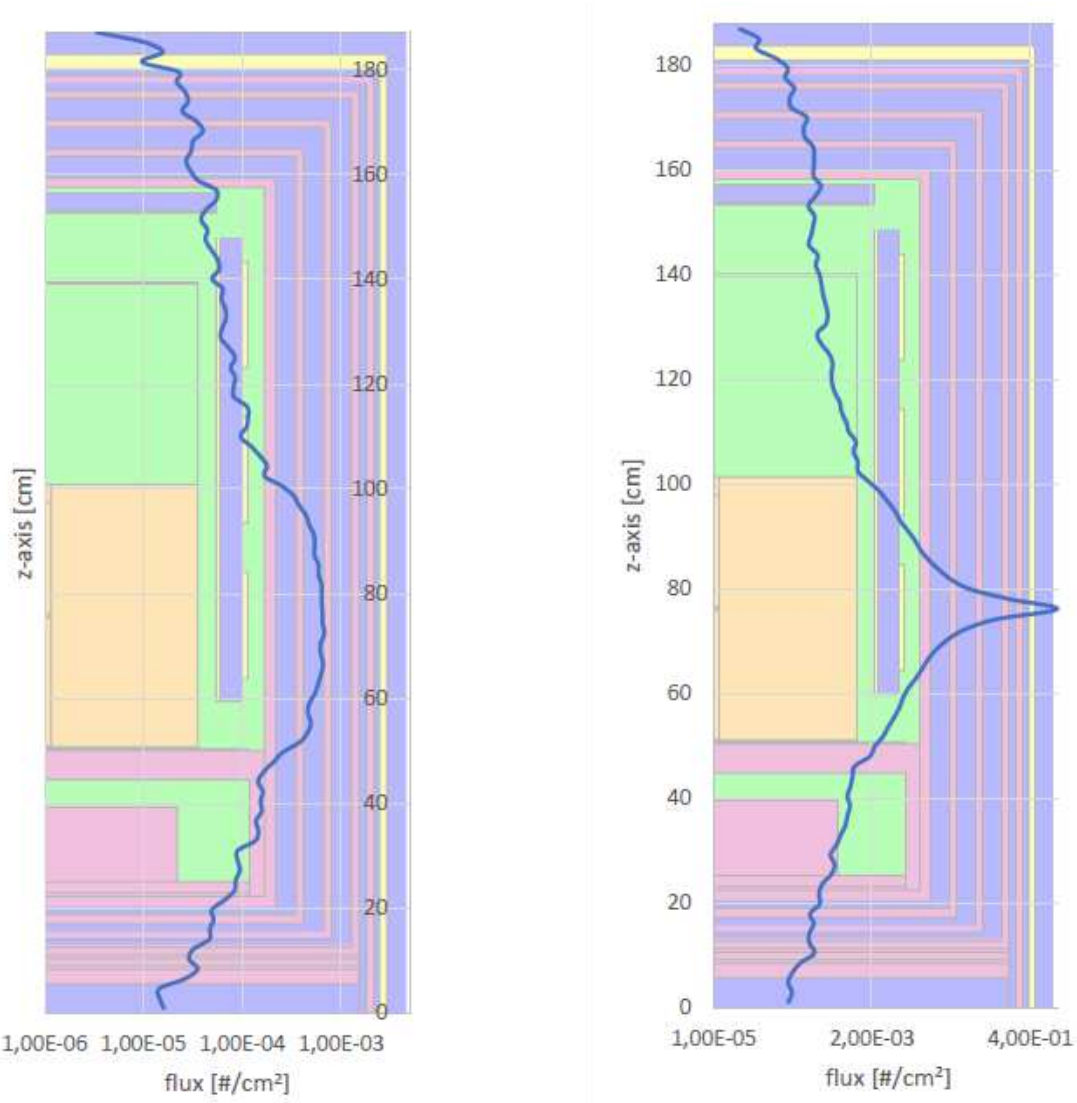

Figure 27: Neutron particle flux along the z-axis – sprofile at (x;y) =(0;0). Left: homogeneous source. Right: most conservative source.

For the neutron radiation we get the same situation as for the gamma radiation. Part of the flux goes through the reference elements which causes additional bias.

5.5.3.2.2 Energy deposition study

Complementary to the flux behaviour, the effect of the radiation on the calorimeter elements was evaluated using tally 6.
Table 7 and Table 8 show the obtained results (given per source particle) for the most conservative and homogeneous sources.

Layer	Energy [MeV/g]*	Energy [MeV]**	Energy deposition [%]	Rel. Error [%]
drum	3.44E-05	**4.90E+00**	**94.32**	0.40
thermal block	9.61E-08	4.85E-02	0.93	0.44
homogenization layer 1	5.96E-08	1.85E-02	0.36	0.46
homogenization layer 2	4.52E-08	1.67E-02	0.32	0.48
homogenization layer 3	3.45E-08	1.50E-02	0.29	0.50
homogenization layer 4	2.61E-08	1.28E-02	0.25	0.52
cold plate	1.83E-08	1.19E-02	0.23	0.52
insulation layer 1	3.63E-06	8.43E-03	0.16	0.46
insulation layer 2	2.82E-06	7.83E-03	0.15	0.48
insulation layer 3	2.15E-06	7.05E-03	0.14	0.50
measurement cells	6.80E-06	**5.64E-03**	**0.11**	0.70
measurement plates	1.59E-07	**4.82E-03**	**0.09**	0.30
insulation layer 6	7.59E-07	3.94E-03	0.08	0.45
aluminum block	1.36E-07	**3.86E-03**	**0.07**	0.71
bottom measurement plate	8.24E-08	2.78E-03	0.05	0.90
insulation layer 4	1.62E-06	2.35E-03	0.05	0.56
insulation layer 5	1.27E-06	1.33E-03	0.03	0.59
reference plates	1.29E-07	**1.28E-03**	**0.02**	0.40
measurement chamber	3.55E-09	**4.60E-04**	**0.01**	0.32
ghost chamber	8.50E-07	**1.18E-04**	**0.00**	0.65
	sum total	**5.08E+00**	**97.7**	**0.4**
	sum detected	**4.91E+00**	**94.4**	**0.4**

Table 7: Energy deposition for the most conservative neutron source

*energy deposited in one gram of the material in the layer
**total energy deposited in the layer

Layer	Energy [MeV/g]*	Energy [MeV]**	Energy deposition [%]	Rel. Error [%]
drum	1.36638E-05	4.06E+00	78.00	0.25
thermal block	2.43121E-07	2.55E-01	4.91	0.26
homogenization layer 1	1.47645E-07	9.54E-02	1.84	0.28
homogenization layer 2	1.13048E-07	8.71E-02	1.67	0.29
homogenization layer 3	8.62351E-08	7.80E-02	1.50	0.30
homogenization layer 4	6.71208E-08	6.85E-02	1.32	0.32
cold plate	4.83609E-08	6.51E-02	1.25	0.32
insulation layer 1	7.76448E-06	3.75E-02	0.72	0.30
insulation layer 2	5.98318E-06	3.46E-02	0.67	0.31
insulation layer 3	4.61537E-06	3.14E-02	0.60	0.32
measurement plates	4.35649E-07	2.75E-02	0.53	0.28
measurement cells	1.56974E-05	2.71E-02	0.52	0.31
insulation layer 6	1.76158E-06	1.90E-02	0.37	0.27
ghost chamber	3.13533E-07	1.85E-02	0.36	1.38
aluminium block	1.96387E-07	1.38E-02	0.26	0.89
insulation layer 4	3.54571E-06	1.07E-02	0.21	0.36
reference plates	3.44502E-07	7.11E-03	0.14	0.75
insulation layer 5	2.80884E-06	6.14E-03	0.12	0.39
measurement chamber	7.53913E-09	2.04E-03	0.04	0.25
bottom measurement plate	1.58456E-06	4.35E-04	0.01	0.66
	sum total	**4.94E+00**	**95.0**	**0.1**
	sum detected	**4.07E+00**	**78.3**	**0.1**

Table 8: Energy deposition for a homogeneous neutrons source

*energy deposited in one gram of the material in the layer
**total energy deposited in the layer

From Table 7 and Table 8 one can see that for the most conservative source configuration, only 2% of the energy escaped the system and 94% was detected, whereas for the homogeneous one, 5% of the radiation escaped and 78% was detected.

5.5.3.3 Real case Pu sample simulations

For the first simulations of a real case, the simplest scenario was chosen. In this case the model consisted of one pin in the centre of the drum with one container in the middle of the pin, *i.e.* the most conservative source configuration. The container was filled with a radioactive material (blue part on Figure 16). The isotopic composition of the radioactive material is presented in Table 9.

Isotope	Fraction [%]	Normalised [%]	Specific power [mW/g]	Specific power contribution [mW/g]
^{238}Pu	1.35	1.30	568.00	7.372
^{239}Pu	66.54	63.86	1.93	1.232
^{240}Pu	23.22	22.28	7.10	1.582
^{241}Pu	4.46	4.28	3.30	0.141
^{242}Pu	4.43	4.25	0.10	0.004
^{241}Am	4.2 % of Pu	4.03	115.00	4.635
			Total	**15.0**

Table 9 : isotopic Pu/Am composition of the container inside the center pin

As a first approximation, ^{241}Pu being mainly a beta emitter (98%) it was omitted in this simulation (it'll be taken into account in the next simulations).

From the results of deposited energy, calculations were done in order to determine the specific power. The calculated specific power obtained with MCNPx is (14.4 ± 0.2) mW/g compared to the 15.0 mW/g from literature (ENDF/B-VII-1, 2011); as a first conclusion, the gap between the two values is due the ^{241}Pu contribution omission (about 0.14 mW/g).

Particle	source	Deposited energy [%]	Relative error [%]	Detected energy [%]	Relative error [%]
gamma	Most conservative	**90.4**	0.6	**78.9**	0.6
	Homogenous	**77.2**	0.7	**47.6**	0.7
neutron	Most conservative	**97.7**	0.4	**94.4**	0.4
	Homogenous	**95.0**	0.1	**78.3**	0.1
Alpha	Most conservative	**100.00**	0.00003	**100.00**	0.00003
	homogenous	**100.00**	0.00003	**100.00**	0.00003

Table 10: Summary of gamma and neutron energy deposition simulations in the CHANCE calorimeter

5.5.4 Summary and conclusion

Table 10 resumes simulation results for gamma and neutron energy deposition in the calorimeter.

Depending on the source configuration and particle types, 2% up to about 25% of the energy escaped the system and 50% up to 95% was detected. The amount of deposited energy in the reference element was no bigger than 1.5%. This deposited energy is not measured by the Peltier elements, and the final result would be reduced by this value. The maximum bias caused by this phenomenon also wouldn't be bigger than 3%. Also, as shown in Figure 24, the percentage of the total deposited energy depends on the source energy, so for low energy emitters these biases would be smaller and for higher energies it would increase. More and other kinds of simulations will be carried out in future to study this in greater detail, and simulations representing the actual conditions of the experiments that will be performed will be added in due time as well.

6 Overall conclusion

In this document, we presented and evaluated existing mature NDA techniques that can be used for characterizing plutonium and other radioactive nuclides in 200 L radioactive waste drums. After providing an overview of the techniques, we focused mainly on demonstrating the limitations of HRGS and PNCC, as these are the NDA techniques that will be applied for complementing, and comparing with, the calorimetry in the experimental part of the work package.

MCNP simulations were performed for quantifying the percentage of particles (mainly gamma and neutrons) that would leave a waste drum, for a generic and specific source and matrix compositions. The results suggest that the most interesting cases would be polyethylene, bitumen and concrete matrices. Due to the limitations of the experimental program, however, only the latter will probably be available to perform experiments with; possibly supplemented by a sand matrix, which behaves in a similar way, but is somewhat less restrictive on escaping radiation. While escaping radiation can be largely hampered with these matrices, the heat flux is unaffected, thus demonstrating the usefulness and complementarity of calorimetry in these cases and in general.

Further simulations with heterogeneous and homogeneous distribution of activities within the drums showed that the neutron and gamma measurements are very sensitive to the source distribution, leading to uncertainties that can reach two orders of magnitude, depending on the matrix composition. In case of gamma emission, the two orders of magnitude are obtained for concrete, while for neutron emission it is only a factor of two, leading to a factor four in the neutron coincidence rate measurement. The first MCNP simulations of the calorimeter suggest that the uncertainty related to the energy deposition, based on uncertainty on the distribution of activities within a drum, is much smaller than the two orders of magnitude. Therefore, we also demonstrated the usefulness of calorimetry in cases with unknown distribution of activities within drum.

Furthermore, published data were compiled and presented to evaluate and compare the performances of existing NDA systems. This also suggested using concrete as a matrix for the experimental part.

All of these results provide multiple lines of evidence that calorimetry is useful, targeted, and can quite likely reduce uncertainties considerably, in particular in the case of a concrete matrix and/or heterogeneous distribution of activities within a drum. Therefore, we suggest here that the experimental program should:

1. focus primarily on concrete as a matrix
2. preferably include different measurements of the same drum and matrix, where the source position is altered,
3. include a variation of captured and partially escaping gamma background,
4. investigate the feasibility and sensitivity of calorimetry for (hidden) beta-sources, which shall be surrogated using an electric heating device.

All experiments will be supported by appropriate MC simulation efforts.

7 Bibliography

Alvarez E. [et al.] PANWAS: A Passive/Active Neutron Waste Assay for the Radfiological Characterization of Waste Packages at the Nucleco Facility at Casaccia [Conference] // WM'06 Conference. - Tucson, USA : [s.n.], 2006.

ANDRA Catalogue descriptif des familles 2015, Inventaire national des matières et déchets radioactifs [Book]. - 2015.

ANDRA Inventaire national des matières et déchets radioactifs [Online]. - ANDRA, 2017. - 12 september 2017. - https://www.andra.fr/download/site-principal/document/editions/350.pdf.

ANTECH ANTECH G3200-340 Segmented Gamma Scanner [Online]. - 13 september 2017. - http://www.antech-inc.com/wpcms/wp-content/uploads/DS.G3200-340.SGS_.3.4.A4.pdf?bb0488.

ANTECH G3850 Tomographic Gamma Scanner [Online]. - 13 september 2017. - http://www.antech-inc.com/wpcms/wp-content/uploads/G3850-data-sheet-1.9.pdf?bb0488.

ANTECH Webpage: http://www.antech-inc.com/ [Article].

ASTM ASTM C1458-16, Standard Test Method for Non-destructive Assay of Plutonium, Tritium and 24Am by Calorimetric Assay [Report]. - West Conshohocken, United States : ASTM International, 2016.

Berthet A. Utilisation du plutonium dans les REP [Article] // Techniques de l'ingénieur,. - 10 avril 1999. - BN3120 V1.

Bickel M. [et al.] New standars for the measurements of plutonium in radwaste. [Conference] // Proceedings of the symposium on safeguards and nuclear material management, 21st Annual meeting, ESARDA. - 1999. - pp. 4-6.

Boldeman J. W. and Hines M. G. Prompt Neutron Emission Probabilities Following Spontaneous and Thermal Neutron Fission [Journal] // Nucl. Sc. and Engineering. - 1985. - Vol. 91. - pp. 114-116.

Bonnin A. [et al.] Concept of effective atomic number and effective mass density in dual-energy X-ray computed tomography [Journal] // Nucl. Instr. and Meth. in Phys. Res. B . - 2014. - Vol. 318. - pp. 223-231.

Boucher L. Non Destructive Controls Of Radioactive Waste At CEA [Conference] // 8 th International Summer School on Nuclear Decomissionning and Waste Management. - Ispra, Italy : [s.n.], 2016.

Bracken D.S. [et al.] Application guide to safeguards calorimetry, Los Alamos National Laboratory Manual LA-138867-M [Report]. - 2002.

Bracken D.S. and et al. Design and Performance of a Vacuum-Bottle Solid-State Calorimeter [Article] // 38th Annual meeting of the Institute of Nuclear Material Management. - Phoenix, Arizona (US) : [s.n.], 20-24 July 1997.

Bracken D.S. and et al. Performance testing of a Large Volume Calorimeter [Article] // 45th Annual Meeting of the Institute of Nuclear Material Management. - Orlando, Florida (US) : [s.n.], July 2004.

Bracken D.S. Performance of a Large Volume Calorimeter, proceedings of the 45th Annual meeting of the Institute of Nuclear Material management [Article]. - Orlando FL : [s.n.], July 2004. - pp. 28-22.

Bücherl T. and Gostomski Ch. Lierse von Comparison of Neutron Determining Systems and Measuring Procedures for Radioactive Waste Packages, ENTRAP Report WG-A-02 [Online]. - 2001. - 12 september 2017. - http://www.en-trap.eu/doc/neutronsynopsis.pdf.

Bücherl T., Kaciniel E. and Lierse Ch. Synopsis Of Gamma Scanning Systems, Comparison of Gamma Determining Systems and Measuring Procedures for Radioactive Waste Packages [Report]. - [s.l.] : European Network of Testing Facilities for the Quality Checking of Radioactive Waste Packages, 1998.

Bükki-Deme A. and et al. First results with the upgraded TLK tritium calorimeter IGC-V0.5 [Article] // Fusion Engineering and Design. - 2013. - Vol. 88. - pp. 2865-2869 .

Büukki-Deme A. and et al. Current status of tritium calorimetry at TLK [Article] // Fusion Science and Technology. - 2015. - Vol. 67. - pp. 282-285.

Calvet E. Nouveau microcalorimètre diffèrentiel et à compensation [Article] // C. R. Hebd. Séances Acad. Sci.. - 1948. - Vol. 226. - pp. 1702-1704.

CANBERRA CANBERRA's Standard Segmented Gamma Scanner [Online]. - 13 september 2017. - http://www.canberra.com/products/waste_safeguard_systems/pdf/SSGS-SS-C38548.pdf.

Carasco C. [et al.] Beryllium characterization in powders containing plutonium by photoneutron activation analysis using a 124Sb gamma source [Journal] // Journal of Radioanalytical and Nucl. Chem.. - 2016. - Vol. 309. - pp. 967-971.

Carlson J. [et al.] Plutonium Isotopics - Non-Proliferation And Safeguards Issues [Report]. - [s.l.] : Australian Safeguards Office, Canberra ACT, Australia - IAEA-SM-351/64.

Carlson J. [et al.] Plutonium Isotopics - Non-Proliferation And Safeguards Issues [Article] // Australian Safeguards Office. - Canberra ACT, Australia : [s.n.], 1997. - IAEA-SM-351/64.

Croft S. and et al. Nuclear Calorimetry – Dispelling the Myths [Article] // Proceeding from the Waste Management Conference. - Phoenix AZ, USA : [s.n.], 7-11 March 2010.

Davidson D. R., Martin E. R. and Nuclear Applied Systems Division Canberra Results of Low Level Waste Analysis of Plutonium with a Passive Neutron Coincidence Counter, Applied Systems Division Canberra Nuclear [Online]. - 12 september 2017. - http://www.canberra.com/literature/waste_special_systems/tech_papers/asme.pdf.

DOE Waste Inspection Tomography (WIT), Innovative Technology Summary Reports, OST/TMS ID 259 [Report]. - [s.l.] : DOE.

Dörr L. and et al. High resolution vacuum calorimeter [Article] // Fusion Science and technology. - July/Aug 2005. - Vol. 48.

Dufour J.L., B.Autrusson and Funk P. Waste Drums Measurements [Report]. - [s.l.] : Scientific documentation from the Institut de Radioprotection et de Sûreté Nucléaire-Radioactive Material Security Department (IRSN).

Eleon C. [et al.] Status of the nuclear measurement stations for the process control of spent fuel reprocessing at AREVA NC/La Hague [Conference] // Advancements in Nuclear Instrumentation Measurement Methods and their Applications (ANIMMA). - Lisbonne, Portugal : [s.n.], 2014.

ENDF/B-VII-1 [Online]. - 2011. - http://www.oecd-nea.org/janisweb/search/endf?inc=RDD&lib=ENDF%2FB-VII.1&z=26&a=55.

Ensslin N. [et al.] Application Guide to Neutron Multiplicity Counting, Los Alamos Report LA-13422-M [Report]. - [s.l.] : LANL, 1998.

Estre N. [et al.] High-Energy X-Ray Imaging Applied to Nondestructive Characterization of Large Nuclear Waste Drums [Journal] // IEEE Trans. On Nucl. Sc.. - 2015. - Vol. 62. - pp. 3104-3109.

Favalli A. [et al.] Pulsed Neutron Facility for Research in Illicit Trafficking and Nuclear Safeguards [Journal] // IEEE Transactions on Nuclear Science. - 2009. - Vol. 56. - pp. 1292-1296.

Fernando K., Wong R. and Taylor B. Validation Of Gamma Spectroscopy Systems For Free Release Measurements [Conference] // Annual Meeting of the International Network of Laboratories for Nuclear Waste Characterization (LABONET). - Vienna, Austria : [s.n.], 2013.

Fiarman S. and Perry R.B. Attributes measurements by calorimetry in 15 to 30 minutes [Article] // Proceedings of the 28th Annual Meeting of the Institute of Nuclear Material Management. - Newport Beach, CA, USA, : [s.n.], 12 July 1987.

Framatome ANP MOX Fuel Design Report. BAW-10238 (NP) Revision 0. 43-10238NP-00 [Report]. - 2002.

Funk P. and Autrusson B. Characterisation Of The Content Of A Radioactive Waste Drum: Example Of Techniques Used In France For Plutonium Measurement [Report]. - [s.l.] : Scientific documentation from the Institut de Radioprotection et de Sûreté Nucléaire-Radioactive Material Security Department.

Galliez K [et al.] Large Volument Calorimeter LVC 1380 for the tritium peasurement in radioactive waste packages [Conference] // Proceedings of the 11th International Conference on Tritium Science and Technology. - Charleston, USA : [s.n.], 2016.

Galliez K. and et al. Characterization of low level wastes: a new design for calorimetric measurement [Article] // Proceedings of ANIMMA 2017 Advancements in Nuclear Instrumentation Measurement Methods and their Applications. - Liege, Belgium : [s.n.], 19-23 June 2017.

Gmar M. [et al.] Photofission tomography of nuclear waste packages [Journal] // Nucl. Instr. And Meth. In Phys. Res. A. - 2006. - Vol. 562. - pp. 1089-1092.

Hafemeister D. Physics of Societal Issues Calculations on National Security, Environment, and Energy [Article]. - New York : Springer-Verlag, 2014.

Hemmerich J.L., Loos J.-C. and Milverton P. Advances in temperature derivative control and calorimetry [Article] // Review of Scientific Instruments. - 1996. - 11 : Vol. 67.

Hemmerich J.L., Serio L. and Milverton P. High resolution tritium calorimetry based on inertial temperature control [Article] // Review of Scientific Instruments. - 1994. - Vol. 65.

Houriet J.Ph. Monitoring des déchets radioactifs: Mise à jour 1984, Rapport Technique 84-10 [Report]. - Würenlingen : Institut fédéral de recherches en matière de réacteurs.

Hsue S. -T. [et al.] Guide to Nondestructive Assay Standards: Preparation Criteria, Availability, and Practical Considerations, LA-13340-MS report [Report]. - [s.l.] : Los Alamos National Laboratory, 1997.

IAEA Strategy and Methodology for Radioactive Waste Characterization, IAEA report IAEA-TECDOC-1537 [Report]. - Vienna : [s.n.], 2007.

Jallu F. and Loche F. Improvement of non-destructive fissile mass assays in α low-level waste drums: A matrix correction method based on neutron capture gamma-rays and a neutron generator [Journal] // Nucl. Instr. and Meth. in Phys. Res. B. - 2008. - Vol. 266. - pp. 3674-3690.

Jallu F., Passard C. and Brackx E. Application of active and passive neutron non destructive assay methods [Journal] // Nucl. Instr. and Meth. in Phys. Res. B. - 2011. - Vol. 269. - pp. 1956-1962.

Jordan K. A. and Gozani T. Pulsed Neutron Differential Die Away Analysis for Detection of Nuclear Materials [Journal] // Nucl. Instr. and Meth. B. - 2007. - Vol. 261. - pp. 365-368.

Kanawati W. El, Pérot B. and Carasco C. Monte Carlo Simulation of high-level radioactive waste characterization with the associated particle technique [Journal] // Nucl. Instr. And Meth. In Phys. Res. A. - 2013. - 61-73 : Vol. 705.

Kasperki P.W. and et al. The large volume calorimeter for measuring the “pressure cooker” shipping container [Report]. - [s.l.] : Department of Energy, United States , 1991.

Kirkpatrick J.M. [et al.] A Mobile Automated Tomographic Gamma Scanning System [Conference] // WM2013 Conference. - Phoenix, USA : [s.n.], 2013.

Konno K. and Hirosawa T. Melting temperature of simulated high-burnup mixed oxide fuels for fast reactors [Article] // Journal of nuclear science and technology. - 1999. - Vol. 36(7). - pp. 596-604.

Kugel K. and Möller K. Endlagerungs bedingungen Konrad [Report]. - 2017. - https://www.endlager-konrad.de/SharedDocs/Downloads/Konrad/DE/fachunterlagen/endlagerungsbedingungen_konrad.pdf?__blob=publicationFile&v=7.

Likes R. Calorimetric assay instruments [Article] // Passive Non-Destructive Assay of Nuclear Materials. - [s.l.] : Reilly, Doug, Ensslin, Norbert, Smith Jr., Hastings (Eds.), 1991. - NUREG/CR-5550 .

Mason J.A. [et al.] A Tomographic Segmented Gamma Scanner For The Measurement Of Decommissioning Wastes [Conference] // Proceedings of ICEM ’03, The 9th International Conference on Radioactive Waste Management and Environmental Remediation . - 2003.

Mason J.A. [et al.] An Automated Non-Destructive Assay System For The Measurement And Characterization Of Radioactive Waste [Conference] // Proceedings of ICEM ‘03: The 9th International Conference on Radioactive Waste Management and Environmental Remediation. - Oxford, England : [s.n.], 2003.

Mason J.A. and et al. Design and operation of a large volume twin-cell heat-transfer calorimeter for the measurement of both tritium and plutonium samples [Article] // Proceedings of the 50th Annual Meeting of the Institute of Nuclear Materials Management. - Tucson, Arizona, USA : [s.n.], 12-16 July 2009.

Mason J.A. and et al. Design and performance of a sensitive multi-mode calorimeter for single cell isothermal or single and twin cell heat-flow measurements of Plutonium and Tritium [Article] // Proceedings of WM2014 Conference in Waste Management. - Phoenix, Arizona : [s.n.], 2014.

Mason J.A. Isothermal Calorimeters Applied to the Measurement of Plutonium Residues for Plant Post Operational Clean-out [Article] // Proceedings of the 9th International Conference on Environmental Remediation and Radioactive Waste Management ICEM03. - Oxford, England : Examination School, 2003.

Mason J.A. The use of calorimetry for plutonium assay, A report submitted to the United Kingdom Atomic Energy Authority Safeguards R&D Project, [Report]. - 1982.

Massih A.R Models for MOX fuel behaviour. SKI Report 2006:10. ISSN 1104-1374. iRSN SKI-R/06/10-SE. [Report]. - 2006.

Mathonat C., Jossens G. and Bachelet F. Nuclear waste measurement calorimeter for very large drums with 385 litres sample volume [Article] // Fusion Science and Technology. - 2015. - Vol. 67(2).

Mauerhofer E. [et al.] Quantitative comparison between PGNAA measurements and MCNP calculations in view of the characterization of radioactive wastes in Germany and France [Journal] // AIP Conference Proceedings. - 2013. - Vol. 432. - p. 1525.

Mauerhofer E. and Havenith A. The MEDINA facility for the assay of the chemotoxic inventory of radioactive waste packages [Journal] // J Radioanal Nucl Chem. - 2014. - Vol. 302. - pp. 483-488.

McConn R.J. [et al.] Compendium of material composition data for radiation transport modeling [Report]. - 2011.

Mirion Technology Integrated Waste Assay System (IWAS) data sheet [Online]. - 12 september 2017. - http://www.canberra.com/products/waste_safeguard_systems/pdf/IWAS-SS-C9756.pdf.

Mirion Technology Auto Q2, Low Level Waste Assay [Online]. - 12 september 2017. - http://www.canberra.com/products/waste_safeguard_systems/pdf/AQ2-SS-C20837.pdf.

Myers S. C. [et al.] Systematic Bias Estimates Of The Snap™ Analytical Technique In Measurement Trials Of Known Pu Standards In Mockup Drums At Los Alamos National Laboratory, LA-UR-01-5728 [Report]. - [s.l.] : LANL.

NEA OECD-NEA [Online]. - 2018. - www.oecd-nea.org/janisweb/search/endf.

Newell Matthew R. and Jones Stephanie Performance of WIPP certifiable mobile waste characterization NDA measurements on tru waste drums at LLNL [Online]. - 8 january 2018. - http://pajaritoscientific.com/pdf/TECH_6TH_NDA_IPAN_AT_LLNL.pdf.

Nicol T. [et al.] Feasibility study of 235U and 239Pu characterization in radioactive waste drums using neutron-induced fission delayed gamma rays [Journal] // Nucl. Instr. And Meth. In Phys. Res. A. - 2016. - 85-94 : Vol. 832.

Passard C. [et al.] PROMETHEE: An Alpha Low Level Waste Assay System Using Passive and Active Neutron Measurement Methods [Journal] // Radioactive Waste Management And Disposal. - 2001. - Vol. 140. - pp. 303-314.

Pearman I. Application Of ISOCS In The Measurement Of Bulk Plutonium Contaminated Waste During Decommissioning [Conference] // IRPA13 SECC. - Glasgow, Scotland : [s.n.], 2012.

Pelowitz D. B. MCNPXTM user's manual, Version 2.5.0, LA-CP-05-0369 [Report]. - [s.l.] : LANL, 2005.

Rackham J., Weber A.L. and Chard P. Performance Values for Non-Destructive Assay (NDA) Technique Applied to Wastes: Evaluation by the ESARDA NDA Working Group, ESARDA Bulletin [Journal] // Bulletin. - 2012. - Vol. 48. - pp. 25-78.

Ramthun H. Recent developments in calorimetric measurements of radioactivity, [Article] // Nuclear Instruments and Methods. - 1973. - Vol. 112. - pp. 265-272.

Reilly D. [et al.] Passive Non-Destructive Assay of Nuclear Materials, NUREG/ CR-5550, LA-UR-90-732 [Report]. - [s.l.] : LANL, 1991.

Sarge S.M., Höhne G.W.H. and Hemminger W. Calorimetry: fundamentals, instrumentation and applications [Article]. - New York : Wiley, 2014.

Saverskiy A. Y., Dinca DC. and Rommel J. M. Cargo and Container X-Ray Inspection with Intra-Pulse Multi-Energy Method for Material Discrimination [Journal] // Physics Procedia. - 2015. - Vol. 66. - pp. 232-241.

Simon E. [et al.] Feasibility study of fissile mass quantification by photofission delayed gamma rays in radioactive waste packages using MCNPX [Journal] // Nucl. Instr. And Meth. In Phys. Res. A . - 2016. - Vol. 840. - pp. 28-35.

Simpson A. [et al.] Passive Neutron Non-Destructive Assay for Remediation of Radiological Waste at Hanford [Conference] // WM2013 Conference. - Phoenix, USA : [s.n.], 2013.

Steude J. [et al.] Nondestructive Evaluation Of Radioactive Waste Drums Containing Miscellaneous Waste Forms [Journal] // Review of Progress in Quantitative Nondestructive Evaluation. - 1993. - Vol. 12. - pp. 2289-2296.

Technology KEP LVC-1380 calorimter from KEP technology [Online]. - 12 september 2017. - http://www.kep-nuclear.fr/instrumentation-et-mesure/lvc-1380/.

Technology Mirion WM2900 TGS [Online]. - 12 september 2017. - http://www.canberra.com/products/waste_safeguard_systems/pdf/WM2900-TGS-SS-C40780.pdf.

Thornton et al. Performance evaluation of a thermopile based small sample calorimeter in PERLA [Article] // 23rd Annual meeting symposium on safeguards and nuclear material management. - Oud Sint-Jan, Bruges, Belgium : [s.n.], 8-10 May 2001.

Tian A. Utilisation de la méthode calorimétrique en dynamique chimique : emploi d'un micro-calorimètre à compensation [Article] // Bull. Soc. Chim. Fr.. - 1923. - 33 : Vol. Ser. 4. - pp. 427-429.

Tolchard A.C., Looman M.R. and Mason J.A. A Very High Efficiency Neutron Counter for the measurement of plutonium in decommissioning wastes [Conference] // Proceedings of the 9th International Condeference on Environmental Remediation and Radioactive Waste Management. - Oxford, England : [s.n.], 2003.

US Department of HomeLand Security Compendium of Material composition Data for Radiation Transport Modeling, PIET-43741-TM-963, PNNL-15870 Rev. 1 [Report]. - [s.l.] : US Department of HomeLand Security, 2011.

Venkataraman R. [et al.] An integrated Tomographic Gamma Scanning system for non-destructive assay of radioactive waste [Journal] // Nucl. Instr. and Meth. in Phys. Res. A. - 2007. - Vol. 579. - pp. 375-379.

Verbeke J. M., Hagmann C. and Wright D. Simulation of Neutron and Gamma Ray Emission from Fission and Photofission, UCRL-AR-228518 [Report]. - [s.l.] : Lawrence Livermore National Laboratory, 2009.

Vigil J. [et al.] Los Alamos National Laboratory's Mobile Real Time Radiography System [Conference] // 5th Nondestructive Assay and Nondestructive Examination Waste Characterization Conference.

Villani M.F. [et al.] Passive and Active Neutron Matrix Correction for Heterogeneous Distributions Utilizing the Neutron Imaging Technique [Conference] // WM2008 Conference. - Phoenix, USA : [s.n.], 2008.

Wilson M., Rackham J. and Sharpe J. TRU/LLW Segregation using Passive Neutron Coincidence Counting - 10072 [Conference] // WM2010 Conference. - Phoenix, Arizona : [s.n.], 2010.

8 Annex 1

8.1 Detail of the calculations performed to obtain Figure 4

To study the neutron/gamma attenuation in 200 L drums, Monte Carlo simulations have been performed to assess the amount of gamma/neutron signal that can exit 200 L drums containing plutonium.
The calculation considers the case of a 200 L drum filled with bitumen, stainless steel, polyethylene, concrete or graphite of various densities. Neutrons and gamma rays are emitted from the drum center to simulate the emission of a point-like plutonium source loaded in the middle of the drum. The amount of radiations that escape the drum is recorded. The isotopic composition of the simulated plutonium load is {^{238}Pu; ^{239}Pu; ^{240}Pu; ^{241}Pu; ^{242}Pu} = {1.7 %; 56.0 %; 24.1 %; 12.8 %; 5.4 %}, which correspond to a PWR-type fuel (Carlson, et al.).

The energy E of the source neutrons is sampled from the Watt distribution $Ce^{-E/a}\sinh(bE)^{1/2}$ associated to ^{240}Pu with parameters a=0.799 MeV and b=4.903 MeV^{-1} (Pelowitz, 2005), the neutron emission being calculated taking into account the neutron emission of the plutonium isotopes indicated in Table 11. To build the gamma-ray spectrum of the simulated plutonium source, only the two main gamma-ray signatures above 60 keV of the main plutonium gamma emitters are considered (Reilly, et al., 1991), their relative emission being weighted according to the isotopic composition of the source. These gamma rays are presented in Table 12.

^{238}Pu	^{239}Pu	^{240}Pu	^{241}Pu	^{242}Pu
2587	0.02	1026	0.05	1717

Table 11: Spontaneous fission neutron emission for the plutonium isotopes considered in this study, in $s^{-1}.g^{-1}$ (Reilly, et al., 1991).

^{238}Pu		^{239}Pu		^{240}Pu		^{241}Pu	
152.7 keV	$5.90\cdot10^{6}$	129.3 keV	$1.44\cdot10^{5}$	160.3 keV	$3.37\cdot10^{4}$	148.6 keV	$7.15\cdot10^{6}$
766.4 keV	$1.39\cdot10^{5}$	413.7 keV	$3.42\cdot10^{4}$	642.5 keV	$1.04\cdot10^{3}$	208.0 keV	$2.04\cdot10^{7}$

Table 12: Principal nondestructive analysis gamma-ray signatures used for measuring plutonium with the corresponding activities in $\gamma s^{-1}.g^{-1}$ (Reilly, et al., 1991).

The MCNP type-2 tally, which estimates a particle flux over a surface, is used to evaluate the amount of radiation exiting the drum. Since neutrons measurement cells are usually coated with cadmium to favor the detection of fast neutrons, only neutrons with an energy above 0.4 eV are considered, since neutrons with less energy have a much stronger probability to be captured by cadmium as shown in Figure 28.

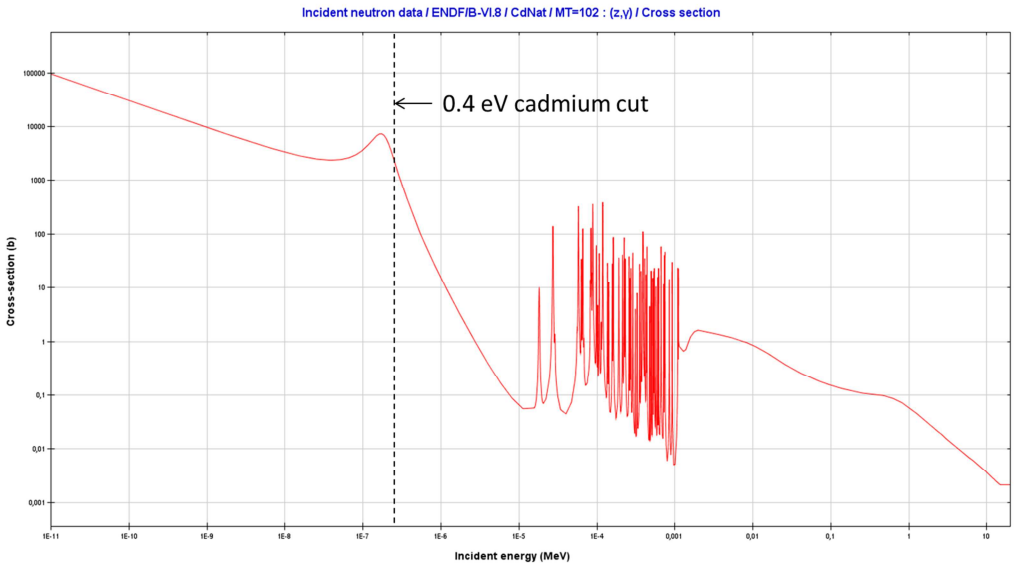

Figure 28: Neutron capture cross section for cadmium presented in log-log scale (top) and lin-log scale (bottom).

The number of neutrons exiting the drum is

$$N_n(s^{-1} \cdot g_{Pu}^{-1}) = S \times \Phi_n \times \sum_{i=\{238,239,240,241,242\}} f_i E_i^n$$

With Φ_n (cm^{-2}) the neutron flux per source neutron calculated with MCNP over a sphere surrounding the drum with a MCNP type-2 tally, f_i the fraction of the plutonium isotope i, E_i^n the neutron emission of plutonium isotope i indicated in Table 11 and S the sphere surface.

Using the gamma fluxes $\Phi_i^{\gamma_0}$ and $\Phi_i^{\gamma_1}$ (cm^{-2}) calculated with MCNP over a sphere surrounding the drum for the two energies indicated in Table 12 for plutonium isotope i, the number of gamma rays exiting the drum being usable for gamma-ray spectrometry is

$$N_\gamma(s^{-1} \cdot g_{Pu}^{-1}) = S \times \sum_{i=\{238,239,240,241,242\}} f_i\left(\Phi_i^{\gamma_0} E_i^{\gamma_0} + \Phi_i^{\gamma_1} E_i^{\gamma_1}\right)$$

With $E_i^{\gamma_0}$ and $E_i^{\gamma_1}$ the gamma emission of the two gamma rays indicated in Table 12 for plutonium isotope i.

The measured useful gamma ray count rate per gram plutonium is estimated as

$$C_\gamma = \varepsilon_\gamma \times N_\gamma \times \frac{s}{S}$$

ε_γ being the gamma ray detection efficiency. Results shown in Figure 4 assume an overall gamma ray detection efficiency ε_γ=0.5 corresponding to the average detection efficiency between 100 keV and 700 keV of a 100% relative efficiency high Purity Germanium detector with a detection surface s=10 cm^2 (Mauerhofer, et al., 2014). The N_γ versus N_n and C_γ plots which are presented in Figure 4 allows comparing different type of matrices and densities. The densities are varied to simulate more or less compact matrices, from 0.2 g·cm^{-3} up to the asymptotic case of a drum filled completely with a matrix at its nominal density.

8.2 Simplified version of Figure 13

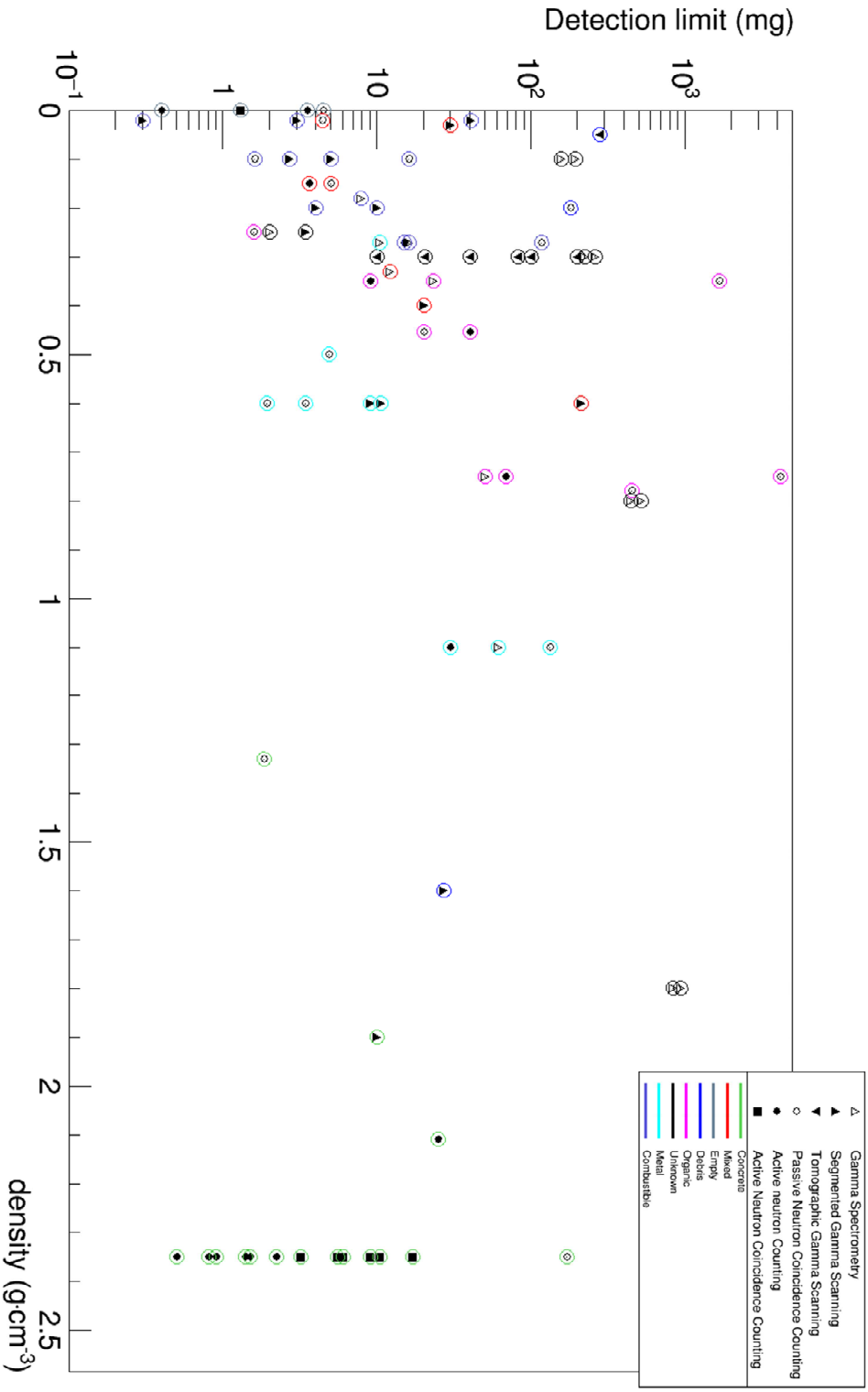

Figure 29: ^{240}Pu, ^{239}Pu and ^{235}U Minimum Detectable Masses that can be achieved with different measurement techniques.

8.3 Additional information concerning the data presented in Figure 13

In references (Mirion Technology), (Fernando, et al., 2013) and (Mason, et al., 2003) which concern gamma measurements, the nature of the matrix is not indicated. This lack of information is however not a concern, since, as explained in 5.1, the matrix nature is not a crucial issue regarding plutonium gamma ray measurements.

The waste drum mockups used in (Jallu, et al., 2011) are composed of cotton, cardboard, plastic, metals, paper, and are placed in the central well of the drum before being filled with concrete. Concrete being the main material composing the waste, the matrix related to (Jallu, et al., 2011) measurements is therefore labeled as "Concrete".

The mockup drums labeled as "heterogeneous" in (Alvarez, et al., 2006) are only labeled "heterogeneous" in Table III of (Alvarez, et al., 2006) and could be the "Diverse active waste (DAW) – Mixed waste containing mainly paper and some plastic" indicated in Table I of (Alvarez, et al., 2006). These mockup drums are therefore labeled "Mixed" in this report.

Since, in (Simpson, et al., 2013), data related to the measurement system 'B' are almost the same as for system 'A', only data related to the system 'A' of (Simpson, et al., 2013) have been used. Also, the density of the debris waste used in (Simpson, et al., 2013) ranging from 0.08 to 0.32 $g \cdot cm^{-3}$ density, an average of 0.2 $g \cdot cm^{-3}$ has been taken for the "debris" label wastes. Concerning the "solvent" waste indicated in (Simpson, et al., 2013), no density being indicated, the density of acetone (0.782 $g \cdot cm^{-3}$) is assumed, whereas a density of 2.35 $g \cdot cm^{-3}$ is assumed for the "Concrete drum".

The data related to "wet soil" and "sludge" in (Mirion Technology) are classified here as being of organic nature since these matrixes contain hydrogen.

This document has been produced under Grant Agreement H2020-755371.

8.4 Composition of the sand assumed for the simulation

The following atom fraction composition of sand was (US Department of HomeLand Security , 2011).

277 Sand

Formula = - Molecular weight (g/mole) = -
Density (g/cm3) = 1.700000 Total atom density (atoms/b-cm) = 5.876E-02
The above density is estimated to be accurate to 2 significant digits. Uncertainties are not addressed.
The following data were calculated from the input weight fractions.

Element	Neutron ZA	Photon ZA	Weight Fraction	Atom Fraction	Atom Density
H	1001	1000	0.007833	0.135405	0.007956
C	6000	6000	0.003360	0.004874	0.000286
O	8016	8000	0.536153	0.583890	0.034307
Na	11023	11000	0.017063	0.012932	0.000760
Al	13027	13000	0.034401	0.022215	0.001305
Si	14000	14000	0.365067	0.226483	0.013307
K	19000	19000	0.011622	0.005179	0.000304
Ca	20000	20000	0.011212	0.004874	0.000286
Fe	26000	26000	0.013289	0.004146	0.000244
Total			1.000000	1.000000	0.058756

9 Annex 2

9.1 Types of calorimeter for nuclear assay

In a very basic configuration, a calorimeter is composed by a measurement chamber (Figure 30), where the sample material is inserted and a temperature sensor to monitor the evolution of the sample temperature. The measurement chamber is coupled to the surrounding environment (thermostated heat sink) by walls characterised by a certain thermal resistance.

The heat flux $\frac{dQ}{dt}$ between the sample and the environment depends on the temperature difference T_s-T_e and the global heat transfer coefficient k.

$$\frac{dQ}{dt} = k(T_s - T_e)$$

A general classification of the different instruments for calorimetry measurements can be made according to the value of the thermal resistance between the measurement chamber and the heat sink.

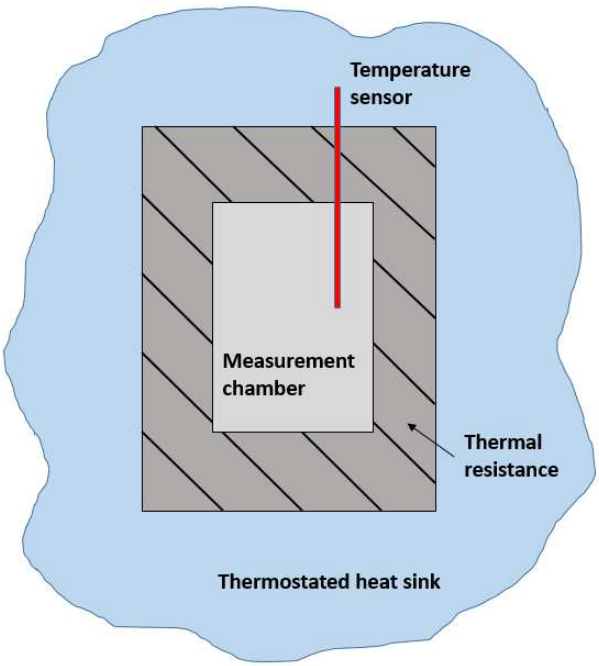

Figure 30: Setup of a basic calorimeter.

9.1.1 Adiabatic calorimeter

If the thermal resistance between the measurement chamber and the heat sink is infinitely large, the calorimeter is called adiabatic. In this configuration, the flow between the measurement chamber and the heat sink is zero and the whole heat generated by the sample under investigation is contained within the measurement chamber. The temperature of the sample, recorded by the temperature sensor, is related to the heat generation rate by the following equation:

$$\frac{dQ}{dt} = m\, c_p\, \frac{dT}{dt}$$

where $\frac{dQ}{dt}$ is the rate of thermal energy generation within the sample, m is the mass of the sample, c_p is the specific heat of the sample and $\frac{dT}{dt}$ is the time variation of the sample temperature.

Based on the sample temperature variation measured by the temperature sensor, estimation of the power generated by the process within the sample can be made according to the equation:

$$T_s(t) = T_s(0) + \frac{P_t}{C}$$

where P_t is the energy dissipated by the sample in the time t, $T_s(0)$ is the temperature of the sample at the time of the insertion in the calorimeter chamber and $T_s(t)$ is the temperature of the sample at the time t. In order to obtain the energy P_t from the temperature difference, the value of the total heat capacity C is needed, and this value is often obtained experimentally through a calibration of the equipment. Methods for calibration of calorimeters according to the ASTM C1458-16 standards (ASTM, 2016) will be presented in paragraph 3.

In reality, it is not possible to obtain an instrument with an infinite thermal resistance, thus another way is implemented in practice in order to cancel any heat flow between the chamber and the environment. In this technique, the temperature of the environment is maintained equal to the temperature of the chamber by means of an Adiabatic Control Unit (Figure 31). This technique, however, introduces perturbations on the measurement signal associated with the noise in the temperature control system. Adiabatic calorimeters are usually conceived with a single measurement chamber, and are therefore more vulnerable to thermal noise.

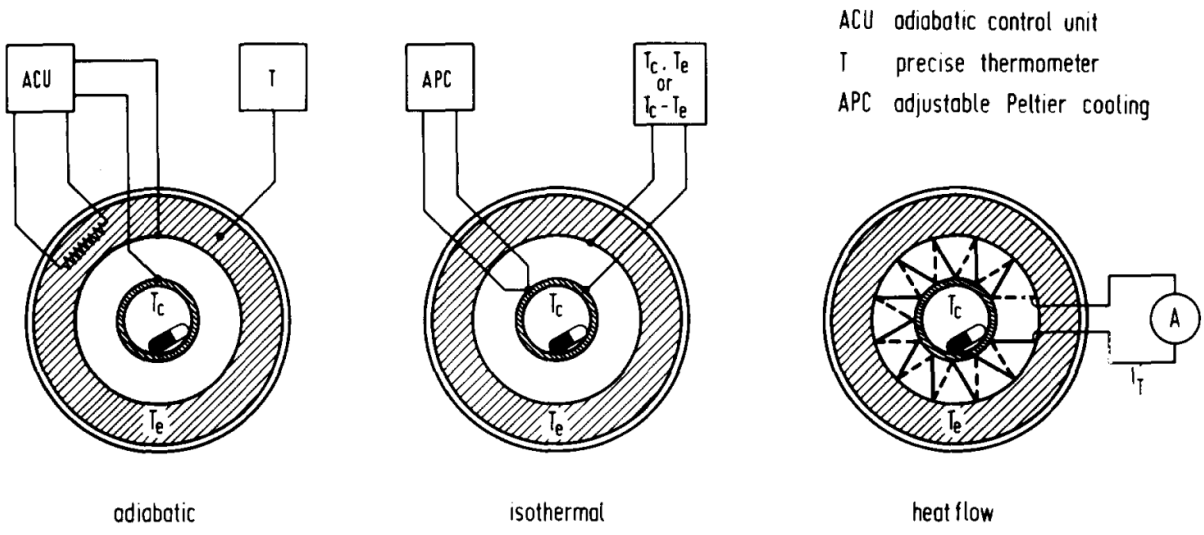

Figure 31: Principal types of calorimeters (from (Ramthun, 1973)).

If the sample has a finite source of heat, the internal temperature after raising will reach a steady state. If, like for nuclear matter, the sample features a constant rate of heat production, the temperature will rise at a constant rate. This is the reason why adiabatic calorimeters do not find many applications in the characterization of nuclear matter where the heat production rate is constant.

One example of adiabatic calorimeter is NETZSCH ARC 244 Adiabatic Reaction Calorimeter. This instrument is designed to measure the heat produced and consumed during exothermic or endothermic

processes. Adiabatic Reaction Calorimeters consist of a reaction chamber equipped with temperature probes and tubes for the introduction of the reactants. The chamber is placed inside a container that is controlled in temperature to follow the temperature of the reaction chamber. These instruments are usually designed for low volume samples (0.5-7 ml for the NETZSCH ARC 244 and up to maximum 1 L in other instruments) and for reactions with a discrete heat production.
These instruments are not adapted for nuclear material assay where the sample volumes can be important (up to 200 L) and where the heat production rate is constant.

9.1.2 Isothermal calorimeter

If the thermal resistance of the barrier between the calorimetric chamber and the heat sink is zero, the calorimeter is called isothermal. In this kind of calorimeters, the temperature of the chamber is constant, as any heat generated into the chamber is instantly evacuated to the heat sink. Since an apparatus with a zero thermal resistance cannot be realized, other techniques are implemented in the practice to achieve the isothermal condition. Since a certain thermal resistance will surround the measurement chamber, any heat flow through the chamber walls must be avoided, as it would result in a temperature increase due to the thermal resistance. For this reason, isothermal calorimeters require a compensation of the thermal energy generated by the sample. A first compensation technique is to remove the heat generated in the sample by phase transition in an opportune material surrounding the measurement chamber. Examples of this technique are the ice calorimeter, which exploits the melting of an ice film surrounding the measurement chamber, or calorimeters with liquid-gas phase transition. The most used technique nowadays is the compensation of the power produced by the sample by electric means. The first implementation of this technique was the Tian calorimeter (Tian, 1923) . In this solution, the calorimetric chamber is surrounded by two thermopiles that realize the thermal interface between the chamber and the surrounding. One thermopile is used to measure the temperature difference between the measurement chamber and the heat sink, while the second thermopile is used for compensating any exothermic process by means of the Peltier effect (Sarge, et al., 2014). Endothermic effects can also be compensated by reversing the current in the same thermopile.

9.1.3 Heat-flow calorimeter

When the thermal resistance between the sample and the heat sink has a finite value, the resulting instrument is called heat-flow calorimeter. In this configuration, heat can flow from the sample to the surroundings and it is measured in different ways. One of the most used techniques to measure the instantaneous thermal power $\frac{dQ}{dt}$ generated within the sample, is to use thermopiles installed between the sample and the heat sink but other techniques may also be employed.
The operation of a heat-flow calorimeter can be distinguished in three different modes according on how the temperature of the heat sink is controlled:

- The temperature of the surroundings is kept constant (Isoperibol mode)
- The temperature is changed linearly (Scanning mode)
- The temperature is changed stepwise or periodically (Modulated mode).

Due to the long time constants that characterise nuclear assay methods and because of the specific investigation, heat flow calorimeters are operated in the isoperibol mode.
Heat flow calorimetry is best suited for steady-state measurements, thus when the samples has a constant heating rate. As nuclear samples fall in this category, the heat-flow calorimeter configuration is one of the most used techniques for the characterization of these samples with calorimetry techniques.

Heat flow calorimeters are usually operated in one of the two following modes:

- **Passive mode:** in this operation method the heat flow produced by the sample is directly measured by heat flow sensors (e.g. thermoelectric modules) completely surrounding the measurement chamber. The output of the heat flow sensors is first measured without any heat production sample and the output curve obtained is called baseline. Once a sample is introduced in the measurement chamber, the output of the sensors increase in an exponential fashion until it reaches a plateau (Figure 32). The output voltage difference between the baseline and the new stabilization plateau is proportional to the thermal power generated by the sample via the instrument calibration factor which is experimentally obtain during the qualification phase of the equipment.

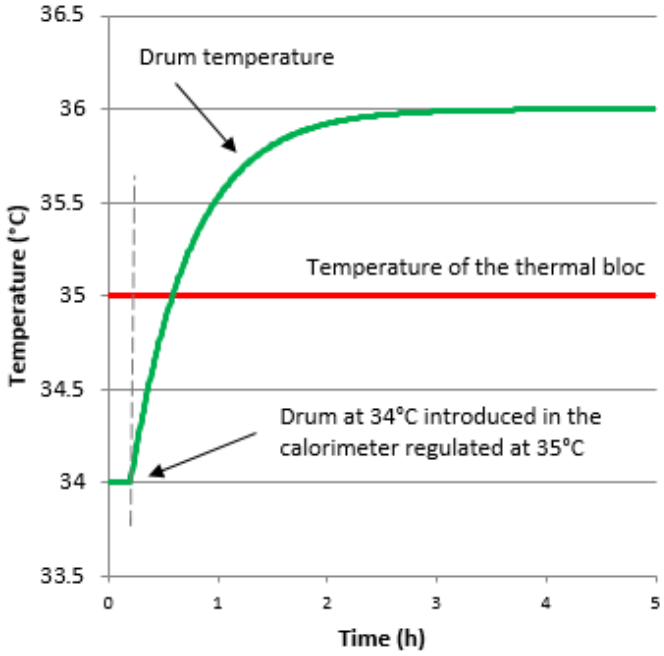

Figure 32: Typical output signal of a heat-flow calorimeter operated in the passive mode.

An example of a heat flow calorimeter operated in the passive mode is the KEP Nuclear LVC 1380 calorimeter (Mathonat, et al., 2015), based on the Calvet design (Calvet, 1948). The measurement cell is completely surrounded by thermoelectric modules that measure the heat flow from the measurement chamber to the external heat sink. The heat sink is composed by an aluminium block maintained at a constant temperature of 30°C by silicon heating elements. A thermal barrier, again composed by an aluminium block, is installed outside the heat sink and maintained at a constant temperature of 23°C. The heat sink is separated from the thermal barrier by a multi-layer insulation thickness that provides stabilization and homogenization of the heat flow. Another thickness of multi-layer insulation separates the thermal barrier from the thermal shield, an aluminium bloc maintained at a constant temperature of 20°C by means of Peltier modules. The temperature of the thermal block is measured by means of platinum probes in a four-wire connection and also with the SRFT method (see paragraph 9.4.5.2).

- **Power compensation mode:** in this mode of operation, a constant heat flux is maintained between the measurement chamber and the heat sink by maintaining both elements at a constant temperature, usually by delivering controlled values of thermal power by joule effect. This operation mode is often called isothermal because the measurement chamber is maintained at a constant temperature value. Once the sample is introduced in the chamber the variation of the

supplied power required to maintain the constant temperature is equal to the power generated by the sample. This operation mode usually features lower measurement time compared to the passive mode of operation because the calorimeter components are at equilibrium temperature and the instrument can supply heat actively to bring the item to equilibrium.

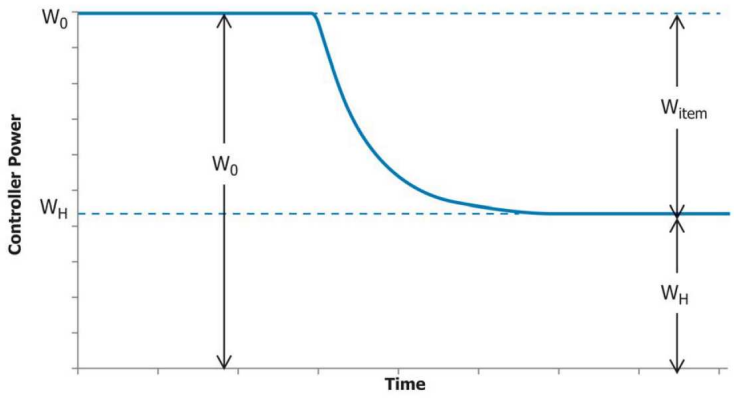

Figure 33: Typical output signal of a heat-flow calorimeter operated in the servo-control mode (from (ASTM, 2016)).

An example of heat flow calorimeter operated according to the servo control mode is the Antech CP264-0420 High sensitivity large sample isothermal calorimeter (Mason, 2003). This instrument consists of three concentric cylinders separated by a suitable insulating material. The three cylinders are maintained at three different constant temperature values decreasing outwards in order to create an outgoing controlled heat flow. The heat is then evacuated form the external cylinder by forced convection of air (air-bath configuration). The power delivered to maintain the inner cylinder at the set temperature value without any sample into the chamber is called the basepower P_0. Once a sample is introduced into the chamber, the servo control adjusts the power delivered to the inner cylinder in order to maintain a constant temperature on the cylinder surface. At equilibrium, the difference between the supplied power and the baseline power is equal to the power generated by the sample. The surface temperature is measured by nickel coils wound around the three cylinders but thermistors are also included for redundancy. Both sensors can be readout directly with a four-wire connection or through a Wheatstone bridge. Electrical coil heaters are used on each cylinder to provide the required thermal power.

Another example of isothermal calorimeter is the Large Volume Calorimeter developed by Bracken at colleagues (Bracken, 2004). This instrument is designed for measuring tritium and plutonium –bearing items in 208 L (55 gal) drums. The calorimeter consists of three concentric cylinders: the outer can, made of stainless steel, provides mechanical support to the system when lifted for the insertion of the test sample. The equipment is operated in the servo-control isothermal mode. The middle can and the sensor can, made of aluminium, are controlled in temperature by means of a silicon encapsulated wire heater. The middle can is maintained at 32°C while the sensor can is maintained at 36°C. This creates a constant heat flow between the sensor can and the surroundings. The temperature signal used to control the heating power is obtained by a four-wire resistance readout of a thermistor.

The sensor can is surrounded by 21 sensor bars featuring thermopile sensor assemblies. Every 50 mm a 50 mm by 50 mm thermoelectric module is installed, resulting in 50% of the can surface being active surface for measurement.

The calorimeter was characterised in different test conditions using National Institute of Standard and Technology (NIST) traceable ^{238}Pu heat sources. The results show no biases for tests performed with the heat source in different position and with different matrices. A sensitivity of 119.61 mW is declared and

a measurement precision of 0.3% was obtained with a source power of 1.2 W. An average measurement time of 14±5 h was recorded, but the value is strongly dependent on the final thermal capacity of the drum content.

Antech (ANTECH) developed a calorimeter that is capable of operating either as a single cell isothermal servo-control calorimeter or as a twin-cell passive calorimeter (Mason, et al., 2014). The measurement chamber consists of three concentric cylinders made from aluminium alloy. Copper heat coils wound around the outer surface of the three cylinders are used to control the temperature of the cylinders and nickel sense coils provide the temperature reading. The heat flow generated by the test sample is measured by means of double (two fixed together) thermopile sensors connecting the inner cylinder with the middle cylinder with a good thermal contact. An air gap of 10 mm is realized between the two cylinders to minimize heat losses between the two cylinders. With 32 sensor assemblies surrounding the inner cylinder, the estimated calorimeter sensitivity is 452.7 µV/mW when operated in single cell heat-flow mode, but this estimation is affected by errors for the approximation of the cylindrical geometry. The gap between the middle and the outer cylinders is filled with a silicon compound creating a stable thermal resistance between the two cylinders. The outer cylinder is equipped with a Peltier cooling system removing any excess of thermal power.

In isothermal operation mode, the middle and the outer cylinders are maintained at a fixed temperature by the nickel sense coil controlling the electrical power supplied by the copper heater winding. The thermopile sensor assembly controls the inner cylinder average temperature to maintain a constant temperature difference with respect to the middle cylinder temperature. Thermopile modules are more sensitive compared to nickel coils and this allows increasing the sensitivity of the calorimeter. Calibration of the calorimeter in isothermal operation mode is performed by supplying a controlled electrical power though a modified 3013 canister with an internal electrical resistance-heating element and the reading of the calorimeter is compared with the measured supplied power.

In heat-flow operation mode, a constant heat-flow is maintain from the middle to the outer cylinder and the thermal power generated by the test sampled is measured by the double thermopile assembly surrounding the inner cylinder. Calibration in this configuration involves comparing the output signal of the Peltier sensor of the inner cylinder and the measured supplied electric power. The results are presented in terms of thermopile assembly output voltage as a function of applied electrical power reporting a measured sensitivity of 341.6 µV/mW in single cell configuration. An improved performance is expected for the twin-cell configuration due to the reduction of thermal noise but this configuration was not tested in this occasion. The calorimeter shows an accuracy of 0.16% above 1 W of dissipated power and 0.2 % from 1 W to 0.6 W with maximum stabilization time below 10 h.

9.1.4 The twin-cell design

With the aim of reducing the measurement errors caused by the thermal noise in the heat sink, the twin design was introduced in calorimetry by (Calvet, 1948) in its heat flow calorimeter developed from the (Tian, 1923) compensation calorimeter based on thermopiles.

In the twin-cell design, two identical measurement cells are installed inside the same heat sink. One cell houses the sample to be measured while the other cell remains empty or houses an inert reference material. Being in contact with the same heat sink, the two cells experience the same thermal noise. The noise can be eliminated by operating the temperature sensors according to the difference principle. In this way, any fluctuation of the thermal block is automatically eliminated in the output signal, thus increasing the sensitivity of the instrument and reducing the thermal noise affecting the baseline (see Figure 34).

When thermoelectric modules are used as temperature sensors, the modules realize the thermal contact between the measurement cells and the heat sink. The thermoelectric modules are connected such to give as output the differential signal between the two cells, where the thermal noise is already eliminated.

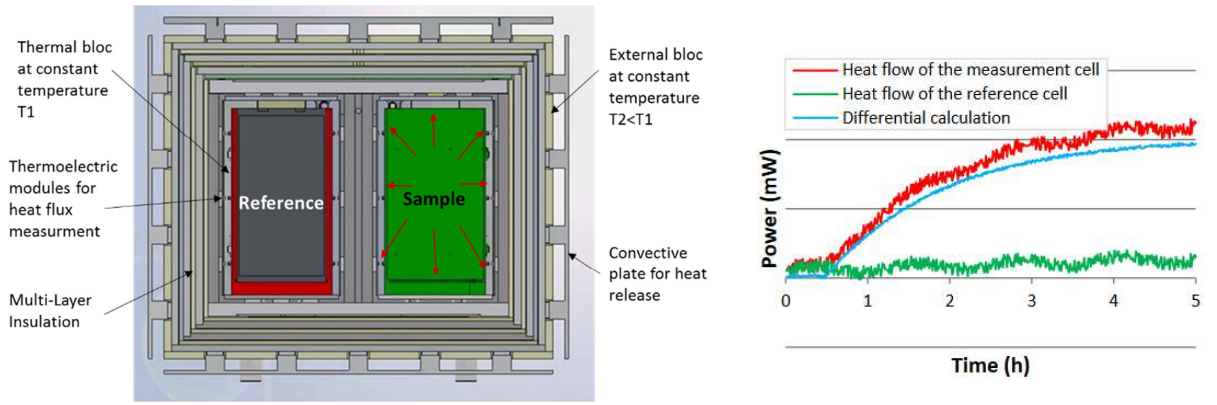

Figure 34: Twin-cell calorimeter (left) and effect of the differential signal on heat flow measurement.

The twin cell design provides the best precision, accuracy and sensibility thanks to the reduction of the thermal noise. However, the construction of the two cells must be identical and avoid any minimal difference in order to accurately cancel the thermal noise.
One important drawback of the twin design is the weight increase and the augmented space consumption. For large measurement chambers (>100 L) the twin design could become impractical or very difficult to implement.

9.1.5 The ghost twin-cell design (Setaram patent)

In calorimeters designed for the characterisation of large samples (>100 L), the implementation of the twin cell design could become challenging because of the significant weight increase and the unpractical dimensions. With the aim of benefiting from the noise reduction of the twin cell design also in large volume calorimetry, Setaram introduced the innovative concept of the ghost reference cell. In this concept, the reference cell is embedded into the measurement cell by providing:

- a reference plate replicating the mass of the measurement plate
- a compact reference sample placed below the measurement sample and with the same thermal capacity.

This solution allows the minimization of the distance between the measurement cell and the reference cell, thus providing that the two elements experience exactly the same thermal noise (Figure 35). This technology has been already implemented by Setaram in their large volume calorimeters and has been proven to be effective in the reduction of the thermal noise. In order to achieve this result, the reference cell was optimized to:

- accurately simulate the thermal capacity of the measurement cell
- ensure a good thermal contact with the thermal bloc
- minimize absorption of the thermal power form the sample
- provide the accurate measurement of the thermal noise from the regulation and the external perturbations.

Thanks to this innovation, a large volume calorimeter can benefit from the thermal noise reduction deriving from the twin cell design within the dimensions of a single cell calorimeter.

9.2 Calorimetry equipment calibration

According to (ASTM, 2016) the calibration procedure for heat flow calorimeters depends on the operation mode of the equipment. In the passive mode, calibration consists of determining the calorimeter sensitivity S, i.e. the conversion factor between the measured differential voltage and the thermal power of the item under investigation. In the power compensation mode, calibration consists in setting the sensor output setpoint voltage that corresponds to a specific base power.
Calibration is performed either with ^{238}Pu heat standards or with calibrated electrical standards spanning the power measurement range of the equipment.
For a passive heat-flow calorimeter, first a measurement of the baseline with the measurement chamber filled with conductive material and without heat sources is performed.
Then, the calorimeter can is removed and the standard is installed into the can. The can is reinserted into the measurement chamber and after reaching steady conditions, the output value is recorded. After the end of the measurement, the calorimeter is opened, the can is removed from the calorimeter, the standard is removed from the can and the void can is reinserted into the calorimeter for another baseline measurement. Then, an average baseline is calculated from the two baseline measurements as follows:

$$BP_0(ave) = \left(\frac{BP_0(1) + BP_0(2)}{2}\right)$$

Using the exact power of the heat standard W_{std}, and the calculated average baseline $BP_0(ave)$, the sensitivity of the calorimeter is calculated as:

$$S = \frac{BP_{std} - BP_0(ave)}{W_{std}}$$

The sensitivity S of a calorimeter is not usually a constant but changes slightly with the power rate. The sensitivity tends to decrease with the power rate because of the increased thermal conductivity of materials forming the primary thermal resistance. The change of sensitivity with the power is described by the following relation:

$$S = S_0 + k \cdot W_{std}$$

where S_0 is the mathematically determined sensitivity for zero power, and k is the slope of the varying sensitivity. For each power level, a minimum of three measurements must be performed following the above procedure.
The net sensor output BP_{std}-$BP_0(ave)$ variation with respect of the power rate is obtained from the following relation:

$$(BP_{std} - BP_0(ave)) = S_0 \cdot W_{std} + k \cdot W_{std}^2$$

The calibration of a heat flow calorimeter operated in the power compensation mode starts by selecting a an approximate basepower W, which should be 10-20% higher than the highest expected power rate in order to allow regulation of the power even at the highest power levels.
With the same procedure described for the passive mode of operation, the sensitivity S of the calorimeter is measured at a selected power value within the range of measurement of the instrument.
Then, the setpoint bridge potential (BP_{sp}) is calculated as:

$$BP_{sp} = BP_0(ave) + S \cdot W$$

The power of the heater is controlled to maintain the setpoint bridge potential BP_{sp} (this power value W_0 could be slightly different from the target value W because of the uncertainty associated in the measurement of the value S).
The calorimeter is charged with a can filled with conductive material but without heat sources and a test is performed. At equilibrium, the heater power is the basepower W_0 corresponding to BP_{sp}. The basepower measurement is performed at least three times with an empty measurement chamber removing and reinserting the can between each measurement. The standard deviation of the basepower measurements should be less than 1%.

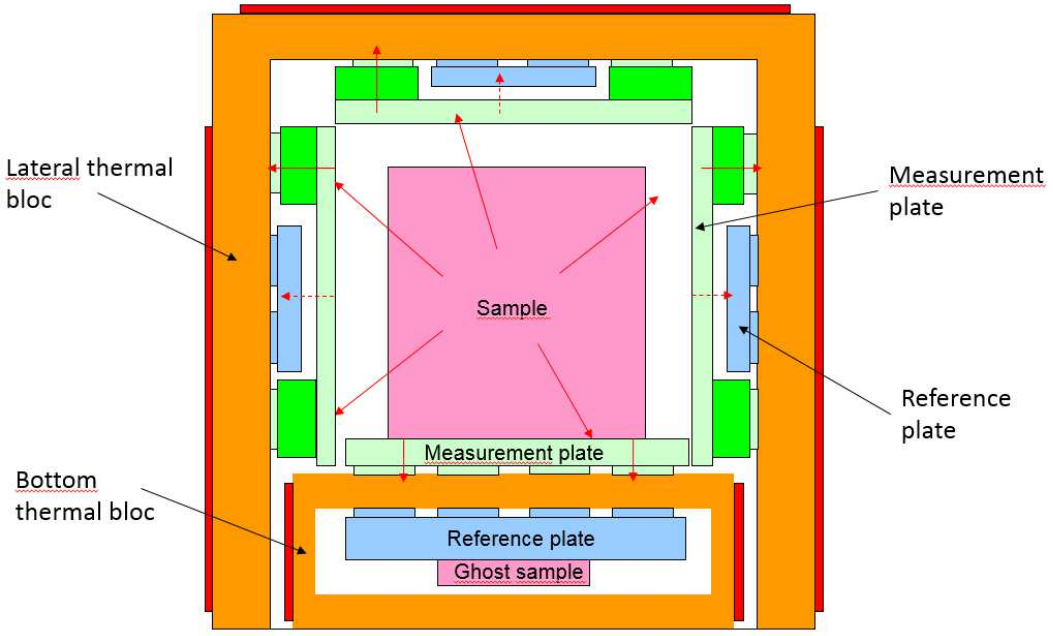

Figure 35: Sketch of the implementation of the ghost reference cell into a large volume calorimeter.

9.3 Assay time considerations

Compared with other NDA techniques for the characterisation of radioactive samples, in calorimetry the required time for the test is a very important factor to be considered as this technique involves quite long assay time depending on the characteristics of the matrix and the geometry of the sample (Likes, 1991). Assay of well packaged small samples could require less than one hour, while the characterization of large volume samples and samples including low diffusivity materials could last several days.
The time required for characterization depends on the following factors:

- Type of operation mode: as reported by the (ASTM, 2016), the servo-control mode requires less assay time compared to the passive mode of operation, as the components are at thermal equilibrium and the system can actively supply heat to achieve the equilibrium.
- Thermal diffusivity and the heat capacity of the materials used for the construction of the instrument and the materials composing the test sample. Heat transfer in materials with low thermal diffusivity, will require longer times compared to high diffusivity material. In addition, the higher the heat capacity of the instrument, the longer the time to reach thermal stabilization.
- The quality of construction: the minimization of the testing time but also the reach of a stable and reproducible heat flow requires the optimization of the construction features including thermal coupling of different layers, reduction of non-traceable thermal losses and stability of mechanical joints.
- The dimensions of the calorimeter and the diameter of the sample. The larger the diameter of the sample to be assayed, the larger will be the instrument required for the characterisation and thus larger the overall thermal capacity and longer the assay time.
- Sample packaging: the packaging of the sample to be assayed plays a very important role in the determination of the final assay time. However, often it is not possible to act on the sample packaging characteristics so it must be accepted as given. Another important parameter affecting assay time is the location of the heat source within the sample volume.
- Required assay accuracy: the achievement of the highest accuracy requires the equipment to reach a complete thermal equilibrium. If assay time is more important and a lower accuracy is acceptable, the test could be stopped before complete thermal equilibrium with significant save of time. This technique is used in mass attribute tests, where it is sufficient to know if the sample stays above or below a determined threshold for certain characteristics (Fiarman, et al., 1987).

Some techniques are available for the reduction of the assay time, in particular the thermal preconditioning of the sample and the use of end-point prediction techniques. Thermal preconditioning of the sample means to bring the temperature of the sample as close as possible to the set temperature inside the measurement chamber in order to reduce the time required for the temperature stabilization. The end-point prediction technique is an analytical estimate of the calorimeter response function that can be used instead of waiting the complete stabilization of the calorimeter. This technique can save up to 50% measurement time, provided that the mathematical description is sufficiently accurate (Croft, et al., 2010).

9.4 Heat sink temperature control techniques

During the operation of a calorimeter for nuclear assay applications, the stability of the surrounding temperature is paramount to achieve high performance and to push detection limits. Errors in the measurement of the heat sink temperature translates in error of the temperature regulation system and finally in oscillations of the reference temperature and thus errors in the measured heat flow. In calorimeters for nuclear applications, the surroundings are controlled by employing a heat sink with stable and controlled temperature.

The importance of the temperature stability of the calorimeter heat sink was clearly shown by (Hemmerich, et al., 1994) in the following analysis.

The thermal balance on a calorimeter of volume V, where conduction is the only heat transfer mode, gives the following balance equation:

$$\int_V \rho c_p \frac{\partial \vartheta}{\partial t} dv = \int_A \nabla \cdot (\lambda \nabla \vartheta) da + \int_V \sigma \, dv$$

$$\mathbf{\Delta} = \mathbf{\Pi} + \mathbf{\Sigma}$$

where the term on the left side represents the total increase of thermal energy **Δ** in the volume V per unit time, the first term in the right hand is the total heat flow **Π** exchanged by the volume V through the surface A and the last term **Σ** is the total thermal energy generated inside the volume V by the sum of heat sources σ.

In an ideal adiabatic calorimeter, the heat exchanged through the external surface is zero (Π=0) and the total heat generated inside the volume increases the thermal energy of the calorimeter volume:

$$\int_V \rho c_p \frac{\partial}{\partial t} dv = \Sigma \qquad or \qquad C_c \Theta = \Sigma$$

where C_c is the heat capacity of the volume and Θ is the derivative of the temperature with respect to time. As observed by Hemmerich, when a small heat source is tested in a large heat capacity volume, the temperature rise rate gets close to the temperature measurement accuracy and the heat sink temperature stability thus reducing the measurement accuracy.

In an ideal isothermal calorimeter, the volume of the calorimeter is thermostatically controlled so that all temperature derivatives with respect to time are zero. The heat flow is also cancelled by a continuous compensation of the heat generation effect. In this case, Σ is equal to the compensation power.

In the Isoperibol heat flow calorimeter, during the stabilization phase, part of the heat generated inside the volume is used to increase the temperature of the volume V and part is exchanged with the surrounding through the surface A. Once the steady-state condition is reached, no variation of the volume temperature with time is observed and the operation of the instrument is described by the following equation:

$$\Sigma = -\Pi$$

Since a perfect temperature control does not exists, some temperature variations could appear on the heat sink. In the presence of temperature variations, a parasitic heat flow appears and the measure signal is affected by this false value:

$$\Pi_{eff} = (C_c + C_s)\,\Theta - \Sigma_s$$

with the error $d\Sigma=(C_c+C_s)\Theta$ which is proportional to the temperature variation and the calorimeter and sample heat capacity.

Usually the heat capacity of the calorimeter is optimized to guarantee the desired heat flow between the measuring chamber and the surroundings, thus the effort is in the minimization of the temperature variation in the heat sink.

Using standard temperature control systems based on temperature sensors like Resistance Temperature Detectors (RTD), thermistors and thermocouples the maximum temperature control is around $|\Theta| \geq 1 \times 10^{-7}$ K/s (Hemmerich, et al., 1996). The effect of the regulation error on the calorimeter signal noise is strongly affected by the dimension of the calorimeter and consequently on the dimension of the sample to be tested. While a miniature calorimeter ($C_{CAL}+C_s \leq 10$ J K^{-1}) can achieve a resolution of ±1 μW, the same regulation error in a large volume calorimeter ($C_{CAL}+C_s \leq 1500$ J K^{-1}) often required in nuclear

calorimetry applications gives a resolution of ≥ 150 µW. The main direction towards the improvement of the measurement accuracy is then in the reduction of the temperature regulation error.
One solution to remove the effect of temperature oscillation from the measurement signal is the twin-cell configuration. Twin-cell calorimeters feature two identical measurement cells: one houses the sample to be measured and the other cell houses a reference sample with the same thermal characteristics. With this configuration, both cells experience the same temperature fluctuations of the surroundings, thus allowing subtraction of the thermal noise form the output signal. However, in order to achieve the highest accuracy, a good stabilisation of the calorimeter surroundings is required.
In the following section, the most used techniques to control the heat sink temperature are reviewed.

9.4.1 Resistance temperature detectors (RTDs)

A Resistance Temperature Detector (RTD) is a temperature probe based on the physical principle of the variation of the electrical resistivity of pure materials with changing temperature. The RTD is one of the most accurate temperature sensors. It provides good accuracy and it is also very stable in time. Thanks to these properties, it is progressively replacing thermocouples as the industrial standard for applications below 600°C.
The most used materials for the construction of RTDs are metals and in particular nickel, copper and platinum. Metal RTD elements have a positive temperature coefficient (PTC), meaning the resistance increases with increasing temperature. At the beginning, nickel wires were widely used because of the high temperature coefficient of resistivity. Nowadays platinum RTDs (Pt100, Pt1000 etc.) are the most common temperature sensors as they provide a more linear response at the highest temperature (**Figure 36**), and they feature a higher fusion point.

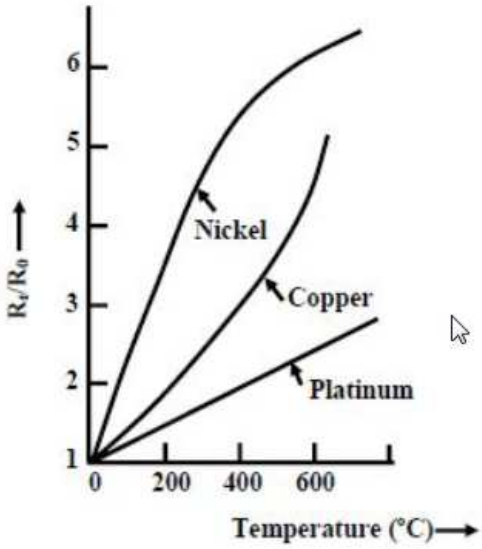

Figure 36: Variation of the coefficient of resistivity with respect of temperature for typical materials used in the fabrication of RTDs (from https://electricalstudy.sarutech.com/resistance-temperature-detector-or-rtd-construction-and-working-principle/index.html)

9.4.1.1 Nickel winding

This temperature measurement technique employs a nickel winding with a known positive resistance variation with temperature. Nickel is selected as the wire material having the highest temperature coefficient of resistivity. The Nickel wire is wound around the measuring chamber and the variation of

the temperature of the chamber is recorded by variation of the electrical resistance of the wire. This technology is used for example in (Mason, et al., 2003) where the nickel wire is wound around the measuring chamber in direct contact with the chamber external wall. In this application, a temperature measurement accuracy of 0.001°C is achieved. Another application of nickel sensing wire is in (Mason, et al., 2014) in the ANTECH CD285-3013 calorimeter. In this instrument, nickel sense coils wound around the middle and outer cylinders are used to control copper coil heaters also wound around the external surface of the two cylinders. Thermopile sensors are used in the inner cylinder containing the sample in order to have a direct measurement of the heat flow rate allowing the operation of the instrument also in the high sensitivity heat-flow mode.

9.4.1.2 Platinum sensors

Platinum has progressively become the reference material in the construction of RTDs because of the following characteristics:

- High Precision: the optimization of the manufacturing process and the accurate material selection allow minimizing deviations from the ideal resistance vs. temperature response, thus resulting in high measurement precision, stability in time and repeatability.
- High Signal Resolution: Platinum features a relatively high (approximately 3900 ppm) change in resistance vs. temperature. This characteristic provides good signal resolution. Elements with higher resistance further enhance resolution by increasing the Ohm/°C response to temperature variation. Platinum has the most stable resistance-temperature relationship over a large temperature range.
- Wide Operating Temperature Range: Platinum RTD elements are available for operation within the temperature range of -196 °C to 1000 °C as platinum is very stable to chemical and temperature stresses.
- Long-term Stability: The typical long-term drift of thin-film platinum RTD elements is 0.04 percent maximum after 1,000 hours at 500 °C.
- Standardization: The fabrication and calibration of platinum sensors is regulated by the IEC 60751 standard.

According to the IEC 60751 the sensors are grouped into four accuracy classes:

CLASS C = ± (0.6+0.01 T) (-50 to 500°C)
CLASS B = ± (0.3+0.005 T) (-50 to 500°C)
CLASS A = ±(0.15+0.002 T) (-30 to 300°C)
CLASS AA = ± (0.1+0.0017 T) (o to 150°C)

where T is the temperature in °C.

During the measurement, a small excitation current is passed across the sensor, and the voltage, which is proportional to resistance, is then measured and converted to temperature by a certain conversion factor. When very small amounts of heat are to be measured, attention must be paid that the thermal power by joule effect generated by the operation current circulating in the platinum element can interfere with the thermal power to be measured. This feature could decrease the detection limit of the device if appropriate remedies are not taken into account.
Platinum RTDs are fabricated in two different technologies: thin film and wire wound. In the thin film RTD a thin metal layer is deposited onto a ceramic substrate with a precise pattern. Then, connecting wires are provided and the assembly is protected with a thin glass layer. In the wire wound version, a

resistive coil is wound around a ceramic substrate and then protected with glass. If at the beginning wire wound sensors featured a much better accuracy, now thin film technology has achieved the same level of accuracy and thin film RTD have become the standard configuration for RTD sensors thanks to a higher vibration resistance, very small size and a good price/performance ratio.
Regulation by platinum RTDs is employed in most calorimeters from SETARAM. The platinum sensor is read out through a four-wire connection with a precision of 0.0005°C over a large temperature range from -200°C to +300°C.

9.4.2 Thermistors

Thermistors are resistance thermometers made in semiconductor materials. They feature a Negative Temperature Coefficient (this is the reason why they are also called NTCs) and they possess a higher temperature coefficient of resistivity when compared to metals. They have an exponential relation between the resistance and the temperature that can be described by the Steinhart-Hart equation. They have a poorer repeatability compared to RTDs as they tend to age and need frequent recalibration. Temperature changes around 0.01 K are readily available with sufficient accurate resistance measurements while rather sophisticated techniques are necessary to detect 10^{-6} temperature variations.
Thermistors are used for example in the vacuum-bottle solid-state calorimeter developed by (Bracken, et al., 1997). A first thermistor is used to measure the sample temperature while a second thermistor is used to monitor the reference temperature. A constant heat flux between the two sensors is guaranteed by a thermoelectric module operated in the servo-control mode. A third thermistor is used for feedback control of a thermoelectric cooling device used to maintain a constant reference temperature of 16.5°C. The resistance of the thermistors is measured with a precision of 0.1 Ω. The servo-controller maintain the thermistor resistance fluctuations to ±0.35 Ω at a setpoint of 2.9 x 10^4 Ω. This corresponds to temperature fluctuation of the order of ±0.26 x 10^{-3} °C. Higher performance were achieved operating the instrument in a water bath controlled at constant temperature to 0.5 x 10^3 °C. In this configuration the feedback resistance was controlled to the resolution of the multimeter (±0.1 Ω). Attaining higher performance in the control of the temperature setpoint by using a higher resolution meter for the measurement of the thermistor's resistance was not suggested by the authors because of limitations related to intrinsic noise inside the instrument.
Thermistors are also used in Large Volume Calorimeters for the control of the surrounding temperature. In the calorimeter developed by (Bracken, et al., 2004), thermistors are used to provide the temperature feedback signal to control the temperature on the cylindrical shells of the calorimeter by means of surface wire heaters encapsulated in silicon rubber. The reading of the resistance of the thermistor is obtained by a four-wire readout circuit and this signal is used to control the heating element through a servo-control system.

9.4.3 Electrical circuits

9.4.3.1 Wire connection

Connection of the Resistance Temperature Detector with only two wires is the simplest solution, but in this case, the resistance of the connecting wires is also included into the measurement thus degrading the accuracy of the temperature measurement. The error introduced acts as an offset, and could be removed from the signal, but since it is not constant, calibration it is not solving the problem. One solution would be to connect the temperature probe in a three-wire connection. In this solution, the third wire is used to measure the additional resistance caused by the lead and junctions. This contribution could be then

eliminated with a suitable electronic circuit. This would be true if the resistance of the two leads is exactly the same. As this is not always the case, in order to achieve the highest accuracy, a four-wire connection is needed. This solution enables the complete removal of the connecting wires resistance from the RTD measurement significantly increasing the measurement accuracy.

9.4.3.2 Wheatstone bridge circuit

Improved accuracy in the measurement of the resistance of the temperature probe is achieved by connecting the resistance into a Wheatstone bridge circuit. This is especially important when very small changes in resistance have to be measured. The electrical circuit of the Wheatstone bridge is reported in Figure 37.

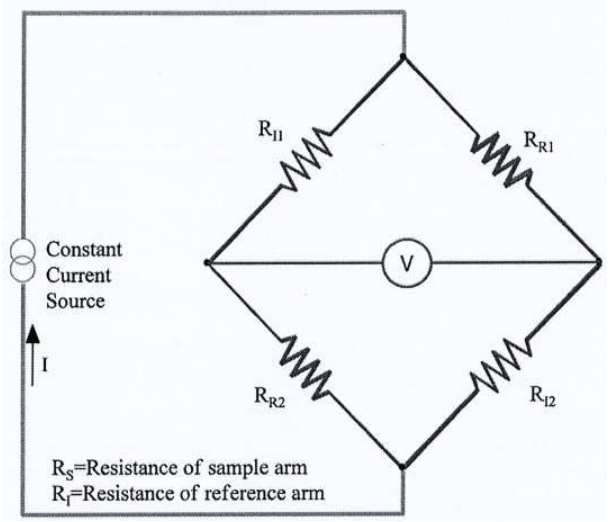

Figure 37: Layout of a typical Wheatstone bridge used in nuclear calorimeters (from (ASTM, 2016)).

The circuit is designed to accurately measure small imbalances of the two arms. When one of the resistors is replaced by a sensor, the circuit detects the variation of the measured parameters through the small variation of the electrical resistance. The circuit is excited by a small constant current and a digital voltmeter is used to measure the voltage difference between the two arms.
This technique is widely used for the readout of temperature sensors in nuclear calorimeters. The majority of the calorimeter developed by Mound Laboratory in US uses the Wheatstone bridge for reading the nickel wire temperature sensors in the equipment. The Wheatstone Bridge is positioned in a way that two arms of the bridge are positioned around the sample chamber while the other two arms are positioned around the reference chamber (Kasperki, et al., 1991). The two sides of the bridge are separated and placed in a thermostatic water bath regulated at 0.001°C. The bath acts as a reference for the temperature measurement and as a heat sink for the heat produced by the sample. The Wheatstone bridge is one of the arrangements for reading resistive temperature detectors that provide the best accuracy in the measurement.

9.4.4 Thermoelectric sensors

Thermoelectric sensors are based on the Seebeck effect: in a circuit composed by two different metals A and B in contact in two junctions, if the two junctions are maintained at different temperature T and T_0, an electromotive force is generated in the circuit equal to:

$$E = |\alpha_{AB}(T - T_0)|$$

where α_{AB} is the relative Seebeck coefficient between metals A and B. A thermometer based on this method is called thermocouple: a bimetallic thermoelectric circuit, where one junction is maintained at a known fixed temperature, produces an electromotive force that is function of the temperature of the second junction. In this technique, the measurement of the temperature is translated into the measurement of a voltage difference.

The main advantages of thermocouples compared to other temperature sensors are the largest working temperature range (-270 to 1800°C), the good ruggedness which make them suitable also in hostile environments. The sensing tip is very small (around x5 wire diameter) thus suitable for local temperature measurements. In addition, the very low mass of the probe provides a very fast response to temperature changes. Another main advantage is that thermocouples do not require an alimentation source, as they are self-powered. For the same reason, they do not suffer from self-heating errors like resistive temperature detectors. Also they are usually very cheap. On the other side, the output signal is quite low, this requiring a sophisticated measuring device for reading small voltage values. Thermocouple is the least sensitive and the least stable of the temperature sensors. Finally, as the thermocouple detects a temperature difference at its ends, a second measurement is needed for the reference temperature in order to obtain the thermocouple temperature.

The base accuracy of the sensors as provided by the supplier is ±0.5°C, but appropriate calibration with a reference probe could increase the sensor accuracy to ±0.1°C or even higher.

The output signal can be enhanced by connecting multiple thermocouples in series. In this way, the output signal is multiplied by the number of thermocouples in series. The resulting thermocouple chain is also called thermopile. Modules with several hundreds of junctions are readily available.

Thermopile modules are used in the Small Sample Calorimeter (SSCAL) developed by ANTECH for the European Commission's Joint Research Center (JRC) and described in (Thornton, 2001). In this calorimeter, the heat sink is composed by 25 kg aluminium cylinder housing two measurement cups. The cylinder is insulated on top and bottom while the external surface is surrounded by thermopile modules. The whole assembly is contained in an outer aluminium alloy cylinder equipped with two nickel windings, one for heating and one for sensing, that are used to control the cylinder in temperature. The thermal equilibrium of the calorimeter is achieved by maintaining a zero heat flow in the thermopile modules surrounding the heat sink. The output of the thermopile modules controls the active thermal system of the outer cylinder in order to suppress any heat flow from the heat sink to the surroundings.

Thermoelectric modules are also used in most of the calorimeters developed by Setaram, where the modules completely surround the measuring chamber thus ensuring a precise measurement of the thermal power generated by the sample.

9.4.5 Recent advance in temperature control

With the aim of further improving the stability in the control of the surrounding temperature in calorimetric instruments for nuclear assay, new techniques have been developed. We report here two techniques based on the thermal inertia. One is called Temperature Derivative Sensor (TDS) and was

developed by Hemmerich and colleagues at the JET Joint Undertaking and the second develop by Setaram based on the TDS, is called SRFT or Temperature Regulation System based on thermal Flux.

9.4.5.1 TDS (Temperature Derivative Sensor)

In this concept developed by (Hemmerich, et al., 1994), the stabilisation of the surroundings temperature is performed by adopting an inertial thermostat. As observed by Hemmerich in its analysis reported at the beginning of the chapter, in a calorimeter of volume V and heat capacity C_i without any heat source, form the thermal balance equation results:

$$\Theta C_i = \Pi_i$$

The calorimeter provide an output signal Π_i which is directly proportional to the fluctuations of the surrounding temperature Θ through the heat capacity C_i. Through this signal, it is then possible to control the temperature in order to maintain $\Theta = 0$ with a higher sensitivity. If with a conventional thermometer the electrical signal is around 0.001 V/K, with a suitable inertial mass system and thermopile array the signal can rises up to 1 V/K, thus improving the temperature stability by 1000 times if the same control system is adopted. The authors present two possible implementations of this solution in two calorimeter designs, CAL-I and CAL-II (Hemmerich, et al., 1996) where the performance of the TDS is further improved by placing the system in a vacuum chamber in order to reduce heat losses. While in CAL-I the complete assembly is housed inside the vacuum vessel, in CAL-II only the TDS system is inside the vacuum vessel and this greatly reduces stabilization time.

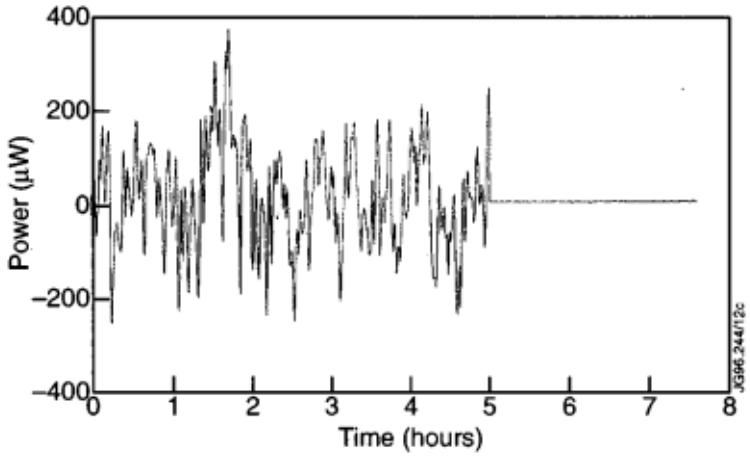

Figure 38: Baseline of a calorimeter using temperature control with conventional RTDs (±300 μW noise) and with the TDS control (±1.5 μW noise). (From [Hemmerich 1996]).

Characterization tests showed that the TDS techniques reduce the thermal noise from ±300 μW (using conventional thermometers) down to 1.5 μW.

9.4.5.2 SRFT (Flux Temperature Regulation System)

With the aim of improving the resolution of standard RTD probes used for the regulation of the temperature in their large volume calorimeters, Setaram adopted a modification of the TDS system developed by Hemmerich and called it SRFT (Système de Régulation Fluxmétrique de Température). This temperature control technique employs thermoelectric modules, which exhibit a much higher (up to

50 times) sensitivity compared to standard platinum sensors affected by a thermal noise around 0.0005°C.

In the SRFT, the temperature control technique is based on the measurement of the temperature difference between a high thermal capacity copper bloc maintained at constant temperature, and the thermal bloc of the calorimeter. The objective is to maintain the thermal bloc at the same temperature of the copper regulation bloc by guaranteeing a zero heat flow through the thermoelectric modules connecting the two blocks.

Setaram has implemented this technology in various calorimeters including the µLVC (Figure 39). The µLVC is an innovative differential heat-flow calorimeter based on a new design with twin cells, a new temperature regulation loop and a heat-flow measurement system inside a vacuum chamber (Patent deposit P005299 LA/VL). The SRFT system is composed by a large mass copper block coupled to the thermal block by means of three thermoelectric modules. The block is installed in a vacuum chamber to annul thermal losses to the surroundings. In reality, thermal losses are very small but not zero. For this reason, in order to avoid a temperature drift on the system, the thermal bloc is controlled to have a constant heat flux through the thermoelectric modules, and not a zero heat flux as in the ideal case (Galliez, et al., 2017).

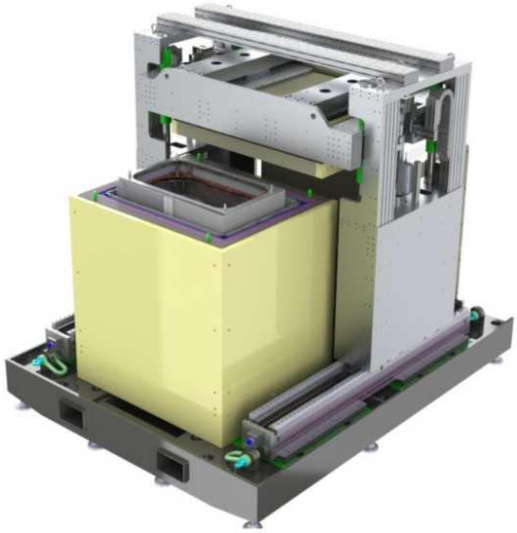

Figure 39: The Setaram µLVC calorimeter.

Qualification of SRFT regulation system by means of the Joule effect embedded cell, shows a significant reduction of the thermal noise of regulation if compared with a Wheatstone bridge (**Figure 40**). The short-term noise (< 1 h) decreases from 1 µW to 0.4 µW while the long-term noise (> 24 h) decreases from 10-20 µW to 1.5 µW.

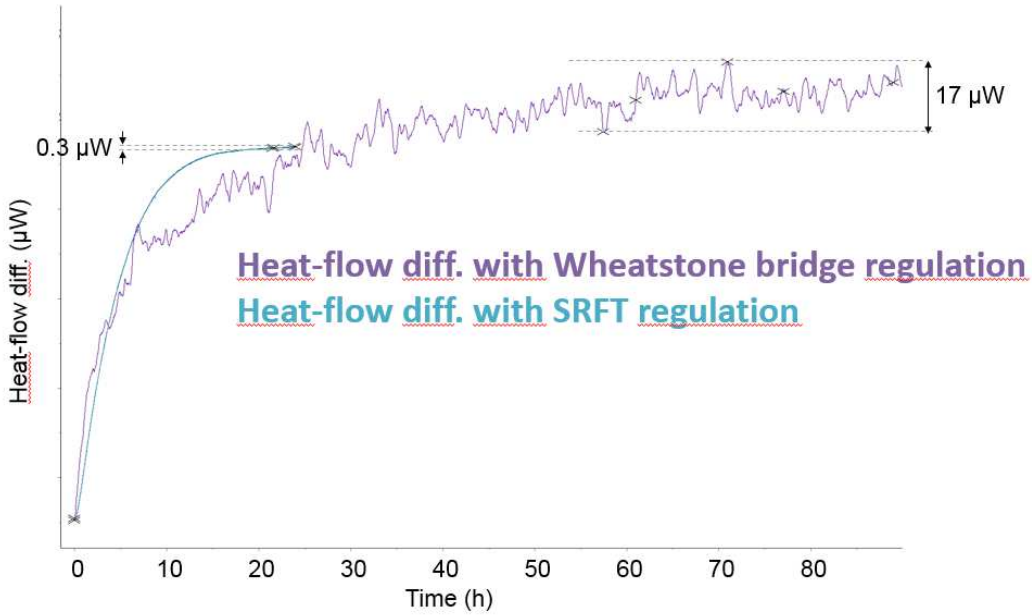

Figure 40: Comparison of the thermal noise with a Wheatstone bridge regulation and with the SRTF regulation after injection of 100 µW power by joule effect in the measurement cell.

9.5 Shielding from external temperature fluctuations

The insulation of the measurement cell form the environment is very important in order to filter the fluctuations of the external temperature. Different solutions to achieve this goal have been implemented and tested in nuclear assay calorimetry. This section reviews the most used techniques for the thermal shielding from the external temperature in calorimeters for nuclear applications.

9.5.1 Water bath

One of the most used solutions to screen the measurement chamber from the fluctuations of the external temperature is to place the chamber into a precision temperature controlled water bath, which provides a stable reference temperature and a quasi-infinite heatsink (negligible temperature variation during heat exchange). The bath temperature is maintained homogeneous within the bath volume using a stirrer or a circulation controlled by the signal from a feedback servo control. With this solution, the bath temperature is controlled within ±0.001°C. For large volume samples, the installation into a water bath would be impractical. In these cases, water circulation inside cooling plates is preferred.

9.5.2 Air bath

An alternative to water bath thermal screening is the use of an air bath. This is required when the risk of water contamination is not admissible or when the implementation of the water bath is on contrast with other technical solution envisaged for the realization of the calorimeter.
Shielding from external temperature fluctuations is achieved by circulating air inside a dedicated chamber surrounding the calorimeter's external envelope. The air flow is circulated either by forced convection using air at room temperature or inside a thermostatic closed loop.

9.5.3 Vacuum

Another approach for minimizing the influence of the external temperature fluctuations on the measurement chamber is to surround the measurement chamber with a vacuum envelope. The vacuum environment suppresses any convective effect and strongly reduces thermal exchanges by conduction.
This solution was adopted for example by (Dörr, et al., 2005) for their high-resolution vacuum calorimeter. In this equipment, the measurement chamber is placed inside a double walled vacuum chamber, continuously maintained at a pressure of $\leq 10^{-5}$ mbar. The gap of the vacuum chamber is then connected to a flow circulation loop that circulates water with temperature controlled to $\pm 10^{-4}$ K by means of RTD sensors and an air-to liquid heat exchanger with thermoelectric heat pumps

9.5.4 Peltier modules

Peltier modules can be used to control the temperature of the external surfaces of calorimetric equipment, thus shielding the measurement chamber for the external temperature fluctuations. This solution was adopted by Setaram in the LVC 3013, LVC F250 and LVC 1380 Large Volume Calorimeters and proved to be effective.
In this solution the external surface of the calorimeter is maintained at a constant temperature of 20±0.1°C by Peltier modules installed on the surface. A convection plate installed outside the external surface enhances the ejection of the thermal power evacuated by the Peltier modules and increases the exchange area for air convection. In addition, the gap between the cooling plate and the convection plate limits the heat backflow from the convection plate to the cooling plate. The number of Peltier modules and their positions within the cooling plate were optimized by numerical simulations in order to obtain a stable external temperature with the minimum temperature gradient.

9.5.5 Heating elements

Another way to maintain a stable temperature around the measurement chamber without the use of fluid baths is the use of heating elements positioned on the external walls of the calorimeter. This solution is adapted when water cooling is not allowed and the minimization of the global dimension of the instrument is not compatible with an air-bath system.
This technique was adopted for example by (Mason, et al., 2009) for the Antech 400HF-5300 calorimeter. In that case, low voltage surface heating pads were installed on the external surface of the calorimeter chamber. The power dissipation is controlled by a computer based control system which maintains a constant temperature on the external surfaces of the chamber.

9.6 Comparison of calorimeters for nuclear applications available in the market

In this section, a comparison of the instruments available in the market for the assay of nuclear matter is presented.

9.6.1 Antech

Antech is a company specialized in the design, development, construction and operation of a wide range of non-destructive nuclear measurement instruments for application in safeguard, nuclear plant

decommissioning, radiation detection etc. Founded in UK as A. N. Technology Ltd., it now includes a subsidiary in US under the name ANTECH Inc.

In the field of large volume calorimeters for nuclear material assay, Antech proposes two main products: a single cell isothermal calorimeter and a twin cell heat flow calorimeter.

The model CP264-0420 is a high sensitivity large sample calorimeter with a measurement chamber with a 190.5 mm diameter and 355.6 mm height. The instrument is a true isothermal "air bath" calorimeter. The complete equipment weighs around 300 kg making the calorimeter fully transportable without compromising measurement accuracy. The instrument can measure nuclear samples with power ranging from 0.005 to 20 W with an accuracy better than 0.5% over the operating range and better than 0.2% at 1 W.

The CHF400 series covers precision twin cell sample calorimeters with measurement chambers ranging from 7.8 L to 72 L. The instrument features a thermostatically controlled body housing two identical cells for the sample and the reference. The measurement technique is based on thermopile modules that thermally connect the measurement chamber with the thermal bloc and measure the heat flux between the two. Thanks to the optimized thermal insulation, the instrument features low detections levels down to 5 µW for the smallest cell (7.8 L) and 700 µW for the largest cell (72 L). The electrical noise is limited to 25 µW peak to peak and the measurement accuracy is typically less than 0.5% above 10 mW.

9.6.2 KEP Technologies

KEP Nuclear is the division of KEP Technologies that is devoted to the study, conception and construction of different instruments for nuclear measurements. Based on fifty years of experience in instruments for thermal analysis of the Setaram Company, Kep Nuclear proposes a large range of instrument completely dedicated to nuclear measurements. With the aim of achieving the highest measurement performance, all the instruments are heat flow calorimeters conceived in a twin-cell configuration and working in the passive mode of operation (**Figure 41**). Only the LVC-1380 is conceived as a single cell instrument because of the very large measurement cell (385 L) but innovative concepts were introduced in the designed in order to have ghost reference cells embedded into the measurement cell, thus providing an integrated reference. The KEP Nuclear products range is quite large providing instruments for different sample volumes ranging from 3.3 to 385 L. Every instrument features an optimized design for achieving the highest measurement accuracy at a low testing time.

The LVC-3013 was conceived for testing the 3.3 L samples of the DOE 3013 standard. It is a twin cell differential heat-flow calorimeter optimized for thermal power measurements in the range between 0.002 W and 20 W. It features a detection limit of 300 µW for an electric noise contribution of 10 µW. Shielding from the external temperature oscillation is provided by an air bath while standard electrical heaters are available for the calibration of the measurement cells.

The LVC-270 is designed for samples up to 15 L. It is available in two different versions optimized for different power ranges: the LVC-270-3W covers a thermal power range from 1.5 mW to 3 W while the LVC-270-15 W is optimized for power values from 3 mW to 15 W for a detection limit of 500 µW achieved thanks to the low electric noise contribution. Both versions feature a water-bath thermal insulation system and thermoelectric modules fully surrounding the two measurement cells.

The LVC-300 is a high-sensitivity twin cell heat-flow calorimeter featuring a measurement cell of 20 L. It can measure radioactive samples in the power range of 1.5 mW to 3 W with an accuracy of 0.4% and a precision of 0.15%. The thermal insulation is based on the air bath (no liquid cooling) and the equipment features embedded electrical heaters for calibration. The total weight is 1000 kg and the instrument can be installed in a trolley structure for displacement.

The LVC-580 is a high sensitivity twin cell heat-flow calorimeter for cylindrical samples up to 25 L. It can measure radioactive matter in a wide range of thermal activities from 10 mW to 25 W with 0.5% accuracy and 0.3% precision in the measurement range. It features a water bath for the screening of the external temperature oscillations and standard heating elements for calibration.

The LVC-390 can accept samples up to 60 L. It features a twin-cell design and can measure samples in the range of 1 mW -13 W with an accuracy lower than 1% and a precision better than 0.5% in the measurement range.

The LVC-680 is designed for testing samples up to 90 L in a double cell setup. The measurement range is within 1.5 mW and 26 W with a detection limit of 2.5 mW. The measurement accuracy is lower than 1% and the precision better than 0.5% in the measurement range.

The LVC-1380 is the instrument of choice for very large drums up to 385 L and it is the only calorimeters available in the market for measuring samples bigger than 200 L. Because of the very large measurement chamber, only one cell is included in the design but an innovative design was develop in order to embed small reference cell within each measurement plate. Thanks to these innovations, the instrument features a detection limit of 1.5 mW with an accuracy of 2.5% and a precision better than 2%. Because of the large dimensions of the instrument, the shielding from the surrounding environment is obtained with an air-bath.

KEP Nuclear	LVC 3013	LVC 270-3W	LVC 270-15W	LVC 300	LVC 580	LVC 390	LVC 680	LVC 1380
Calorimeter type	Isothermal Heat Flow Differential	Isothermal Heat Flow Differential	Isothermal Heat Flow Differential	Isothermal Heat Flow Differential	Isothermal Heat Flow Differential	Isothermal Heat Flow Differential	Isothermal Heat Flow Differential	Isothermal Heat Flow Differential Patented design
Number of cells	2	2	2	2	2	2	2	1
Volume of measurement cell (liters)	3.3	15	15	20	25	60	90	385
Measuring range (mW)	2 - 20000	1.5 - 3000	3 - 15000	1.5 - 3000	10 - 25000	10 - 13000	15 - 26000	10 - 3000
Measuring range (1 g T ~ 324 mW)	0.006 -62	0.005 - 9	0.3 - 46	0.005 - 9	0.03 - 77	0.03 - 40	0.045 - 80	0.03 - 9
Measuring range (1 g 239Pu ~ 1,93 mW)	1 - 10360	0.8 - 1550	33 - 5000	0.8 - 1550	5 - 12950	5 - 6736	7.8 - 13471	0.8 - 1550
RMS noise (µW)	10	5	15	10	35	25	45	10
Detection limit (µW)	300	250	500	250	1500	1500	2500	1500
Temperature range (°C)	25 -40	25 -40	25 -40	25 -40	25 -40	25 -40	25 -40	25 -40
Precision	< 0.15%	< 0.2%	< 0.2%	< 0.2%	< 0.3%	< 0.5%	< 0.5%	< 1%
Measurement time	3h (with predictive calculation)*	3 - 4h (with predictive calculation)*	3 - 4h (with predictive calculation)*	3 - 4h (with predictive calculation)*	3 - 4h (with predictive calculation)*	5 - 6h (with predictive calculation)*	5 - 6h (with predictive calculation)*	10h (with predictive calculation)*
Cooling system	Air bath	Water	Water	Air bath	Water	Water	Water	Air bath
Calibration system	Standard electrical heaters	Standard electrical heaters	Standard electrical heaters	Standard electrical heaters	Standard electrical heaters	Standard electrical heaters	Standard electrical heaters	Standard electrical heaters
External dimensions (Width/Depth/Height) (mm)	700 x 460 x 750	1040 x 780 x 850	1040 x 780 x 850	1230 x 1125 x 1230	970 x 830 x 1230	1500 x 1000 x 960	1500 x 1000 x 1260	4260 x 2400 x 3010
Weight (Kg)	300	500	500	1000	660	1000	1200	12000

* Depending on the sample mass, thermal conductivity, and shape

Figure 41: Comparison of Large volume calorimeters proposed by KEP Nuclear.

9.6.3 Tritium Laboratory Karlsruhe (TLK)

In this section, we describe the instruments for nuclear assay measurements installed at the Tritium Laboratory at the Karlsruhe Institute of Technology.
Amongst the instruments for calorimetric nuclear assay installed the Tritium Laboratory Karlsruhe, the IGC-V0.5 is the most accurate measurement device. The equipment was updated in 2012 for improving its performance (Bükki-Deme , et al., 2013). The instrument is based on the Inertial Guidance Control type proposed by (Hemmerich, et al., 1994) that can achieve an ultrasensitive temperature stability (±30 nK). The whole equipment is installed inside a double walled vacuum chamber with water circulation loop to limit the effect of the external temperature oscillation. The instrument covers a thermal power measurement from $5 \cdot 10^{-7}$ to 10 W and it features a very low detection limit down to 0.5 µW. Thanks to the upgrade program, the accuracy of the calorimeter was significantly improved in particular at low power values: at 1 µW the accuracy increased from 60 % to 17%.
The Tritium Laboratory Karlsruhe owns another calorimeter for larger samples, up to 20 L, the IGC-V25 (Büukki-Deme , et al., 2015). It is based on the same temperature control technique of the V0.5, the Inertial Guidance Control. The calorimeter body consists of a double walled vacuum chamber with a water circulation loop. The calorimeter features a thermal measurement range from $5 \cdot 10^{-6}$ to 5 W and a detection limit of 5 µW.

The following table presents the comparison of the detection limit of the different Large Volume Calorimeters presented in this document. The detection limit for different isotopic composition plutonium composition corresponding to PWR-type fuel {^{238}Pu; ^{239}Pu; ^{240}Pu; ^{241}Pu; ^{242}Pu} = {1.7 %; 56.0 %; 24.1 %; 12.8 %; 5.4 %} (Carlson, et al., 1997) and UNGG-type fuel {^{238}Pu; ^{239}Pu; ^{240}Pu; ^{241}Pu; ^{242}Pu } = {0.2 %; 70.0 %; 25.0 %; 1.0 %; 0.2 %} (Berthet, 1999) is calculated and with 10% of ^{241}Am.

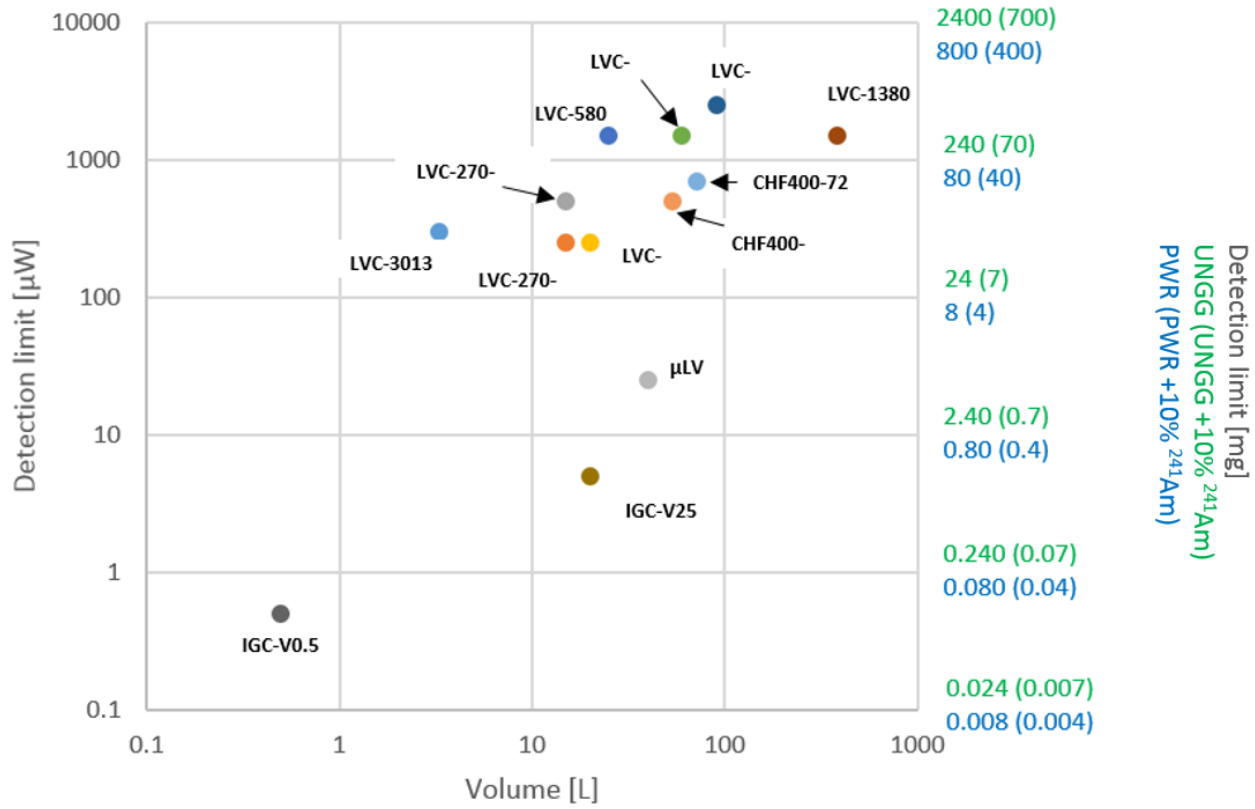

The following specific powers were used (Hafemeister, 2014):

$W(^{238}Pu) = 560$ W/kg
$W(^{239}Pu) = 1.9$ W/kg
$W(^{240}Pu) = 6.8$ W/kg
$W(^{241}Pu) = 4.2$ W/kg
$W(^{242}Pu) = 0.1$ W/kg
$W(^{241}Am) = 114$ W/kg
$W(^{234}U) = 0.2$ W/kg

Figure 42: Comparison of different Large Volume Calorimeters based on the volume of the measurement chamber and the detection limit.

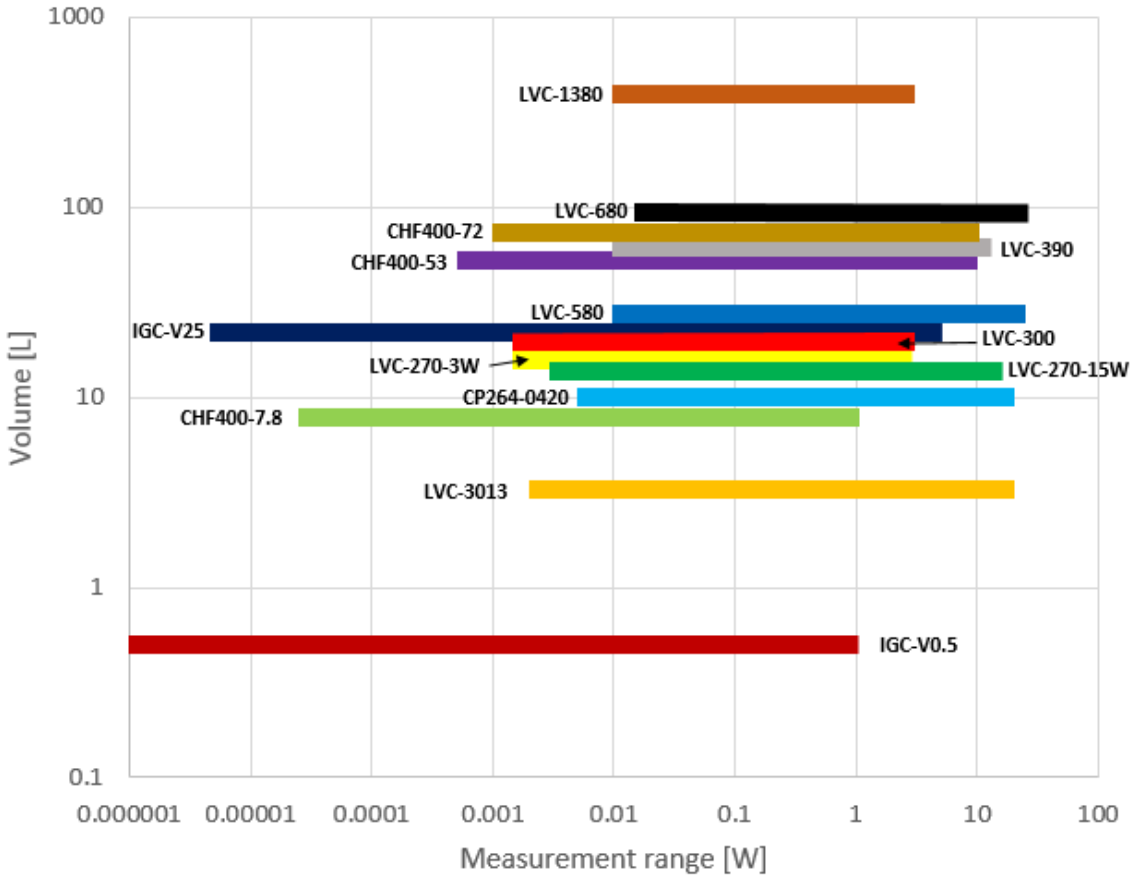

Figure 43: Comparison of different Large Volume Calorimeters based on the measurement range and the volume of the measurement chamber.